Università degli Studi di Torino

Scuola di Dottorato in Scienze della Natura e Tecnologie Innovative

Indirizzo in Fisica ed Astrofisica

Precision thermodynamics in non-Abelian gauge theories with non-equilibrium methods

Alessandro Nada

Tutor: Marco Billó

Relatore: Michele Caselle

Co-relatore: Marco Panero

Contents

List of Figures

List of Tables

Abstract

The computation of the equation of state of strongly-interacting matter at extreme temperatures and densities is a crucial endeavour in theoretical particle physics, being directly related to heavy-ion collision experiments, the evolution of the early Universe and the properties of neutron stars. In this thesis, several aspects of this matter have been studied, starting with a study of the thermodynamics of $SU(2)$ and $SU(3)$ pure gauge theories in the confining phase: first-principles computations from lattice simulations have been described in terms of a non-interacting glueball gas using a string-inspired model for the high-lying glueball spectrum. An alternative approach, which includes an effective description of repulsive interactions between glueballs, provides an even more precise description of the equation of state in the proximity of the transition.

In this thesis we report also recent findings on the use of the ξ/ξ_{2nd} ratio to test effective Polyakov loop models, as it may play an important role in the determination of the action that characterizes such models. This ratio is able to provide precious insight on the spectrum of excitations of the flux tube in non-Abelian gauge theories and thus it represents a simple and cheap way to understand if such effective models are able to capture fundamental properties of the original theory.

The last part of this thesis is focused on a new way of computing the equation of state in lattice gauge theories through the use of a well-known result in nonequilibrium statistical mechanics, called Jarzynski's equality, which relates fluctuations in the work performed during a nonequilibrium transformation to the free energy difference between two equilibrium ensembles. In this thesis, we will analyze how it is possible to implement this result in lattice gauge theories by using out-of-equilibrium transformations in Monte Carlo simulations, in particular for computationally challenging problems such as the calculation of interface free energies and of the pressure. Most importantly, this new technique has been tested on a large-scale determination of the equation of state of the $SU(3)$ non-Abelian gauge theory, and compared with recent determinations obtained with different methods, some of which proposed in the last few years.

Acknowledgements

Introduction

In the framework of the Standard Model, quantum chromodynamics (QCD) is the fundamental theory of the strong interaction, which is one of the four forces that govern our Universe along with gravity, electromagnetism and the weak interaction. The strong interaction exhibits two truly peculiar properties that have been extremely well tested over the years: confinement and asymptotic freedom. The fundamental particles that are involved in this interaction are quarks and gluons, which are characterized by a *color* charge. At low energies these particles display the so-called *color confinement*: in a nutshell, quarks and gluons cannot be isolated, but they must always be confined into *colorless* composite states called *hadrons*, which they cannot be separated from. Such states are classified into baryons (such as the nucleons that, in turn, make up nuclear matter), mesons (such as pions and kaons) and further, more exotic, states such as tetraquarks, pentaquarks and glueballs, the latter of which are states composed only by gluons and no quarks.

Conversely, at high energies the strong interaction features the so-called *asymptotic freedom* [1, 2]: at asymptotically large energy scales and, correspondingly, as the length scales decrease, the true nature of the fundamental constituents is shown, as the strength of the interaction becomes vanishingly small and perturbative calculations are made possible. One of the most relevant implications of asymptotic freedom is that, under extreme conditions, the dynamics of the theory is profoundly modified with respect to what we observe at hadronic energy scales, as a completely new behaviour of strongly-interacting matter emerges. In particular, a crucial prediction of QCD is that at extremely high temperatures, or at extremely high baryon densities, a new phase of matter exists, usually denoted as the *quark-gluon plasma* (QGP): under these conditions, quarks and gluons are thought to be asymptotically free. Understanding the *thermodynamics* of strongly-interacting matter is, thus, imperative: moreover, the study of an exotic new phase such as the QGP and, in general, of the phase diagram of QCD, has not purely theoretical motivations. In fact, extreme conditions of temperature are thought to have happened in the first moments of the Universe after the Big Bang, while extreme baryon density (that is, cold and dense QCD) is thought to characterize the crucial properties of neutron stars. In the last decades a huge experimental effort has been directed towards the study of the QCD phase diagram; in particular, heavy-ion collision experiments such as RHIC at Brookhaven National Laboratories, LHC (namely, the CMS, ATLAS and ALICE collaborations) at CERN are able to reproduce signatures of a new phase of strongly-interacting matter. Indeed, this long-lasting experimental programme will continue in the foreseeable future also in new facilities such as FAIR at GSI.

The study of the equation of state of strongly-interacting matter, that is the

relation between state variables such as temperature, pressure, energy or entropy, clearly plays a crucial role: indeed, its determination from first principles represents a crucial endeavour in theoretical particle physics. While the QCD equation of state is interesting by itself, it has direct, practical applications in different fields, such as nuclear physics and cosmology: it serves as an input for the analysis of thermal systems such as those created in heavy-ion collisions or for the study of the early phases of the Universe itself.

From the theoretical side, the most significant and reliable contribution to this effort comes undoubtedly from the lattice formulation of QCD, which represents a tool for first-principles numerical predictions with ever-increasing precision and accuracy. From its inception in the '70s [3], lattice gauge theory has provided an invaluable contribution in terms of quantitative predictions in several lines of research in QCD and QCD-like theories: however, there are very few analytical predictions, and Monte Carlo numerical simulations represent the main instrument at our disposal. Still, lattice QCD is *the* mathematically rigorous, gauge-invariant non-perturbative regularization of the theory, as it is well-defined for any value of the coupling constant. This is particularly appealing when studying thermodynamic observables: the quark-gluon plasma produced in experiments appears to be still strongly-coupled and, thus, intrinsically non-perturbative tools are required to study phenomena such as the deconfinement transition or the chiral symmetry restoration.

In the first chapter of this manuscript we will present a general overview of some crucial features of QCD at nonzero temperature and a brief introduction to the framework of lattice gauge theories, with a specific focus on thermodynamics. In particular, at the end of this chapter, we will try to present with some detail the most relevant methods that are routinely used to compute, via Monte Carlo simulations, equilibrium observables such as the pressure and the entropy.

In the last few years, thanks to constant progress in computational power and algorithmic sophistication, and also to a better understanding of all the systematic effects related to simulations with fermions, there have been major advancements in the computation of equilibrium thermodynamics for full QCD with $2 + 1$ (or even more) dynamical quark flavors. However, other QCD-like theories can still play a central role in the understanding of the mechanisms underlying the deconfinement transition and, more in general, of the thermodynamics of strongly-interacting matter. A typical example is that of pure gauge theories, in which no dynamical quarks are included: even if they have no physical counterpart in nature, they offer a theoretically cleaner setup with respect to QCD, without the technical complications due to the regularization of fermions on the lattice. Several studies analysed the thermodynamics of pure-glue theories, such as the SU(3) Yang-Mills theory [4–7], SU(N) theories in the large-N limit [8] and in $2 + 1$ space-time dimensions [9, 10]. Chapter 2 will be dedicated to the work of refs. [11, 12], in which the equation of state in the confined phase of the SU(2) and SU(3) pure gauge theories computed on the lattice has been described in terms of a non-interacting gas of glueballs with a string-inspired spectrum. The roots of this phenomenological approach are to be found in the work of Hagedorn in the '60s [13] on the statistical bootstrap model, and also in its more recent version, the hadron resonance gas model, both of which will be reviewed. Most importantly, we will analyse how the studies of refs. [11, 12] represent a perfect interplay between first-principles results from the lattice,

and the phenomenological description of a glueball gas, which is able to provide precious insight on the contributions to physical observables in the confining phase. Moreover, we will show how thermodynamic observables can be used to investigate the high-lying glueball spectrum, since, as we will see in detail, the non-interacting gas prediction is reliable provided that an Hagedorn-like spectrum for heavy glueballs is included.

Although lattice results are available for a very large set of thermodynamic variables, there are some fundamental limits: the most relevant example is that of the so-called "sign problem", which prevents numerical simulation from providing reliable results at nonzero baryon chemical potential. One possibility to avoid in large part this issue is through the study of effective Polyakov loop (EPL) models, which have been the object of several studies in recent years with different approaches [14–34]. Even if not strictly related to the equation of state, the third chapter of this thesis will be devoted to the study of the ratio between the correlation length ξ and the second moment correlation length ξ_{2nd} presented in [35]: we will see how this quantity is able to provide precious information on the spectrum of excitations of the flux tube. The measurement of this ratio in EPL models would be crucial in understanding if these proposals are able to capture essential features of the flux tube of non-Abelian gauge theories, and, if not, guiding what kind of additional terms EPL actions need, in order to recreate the same predictions of the original theory.

If we look again at high-precision determinations of the equation of state in the literature, we see that full QCD calculations still require an impressive numerical effort and many systematic effects have to be taken into account. Thus, recently there has been renovated interest in the study of new ways of computing the equation of state, in addition to techniques that are routinely used, such as the integral method [36]: among the latest advancements, we mention studies in a moving reference frame [7] and using the gradient flow [37].

The rest of this thesis is devoted to a novel proposal for the computation of the equation of state, based on a well-known result from nonequilibrium statistical mechanics, called *Jarzynski's equality*. This relation, discovered only 20 years ago [38, 39], relates the difference in free energy F between two equilibrium states A and B with the average of the exponential of the work W that is done on the system during transformations between A and B. Since there are no particular restrictions on how such transformations are performed, this is truly a result of thermodynamics *out of equilibrium.* This nonequilibrium work relation is to be considered as a generalization of a series of theoretical advancements previously developed during the '90s [40, 41] and deeply related with another crucial result in nonequilibrium statistical mechanics, Crooks' theorem [42]. When these discoveries were made, the experiments at the nanometer scale were also reaching full maturity, providing the possibility to test in the proper microscopic systems these theoretical results: this was the case for Jarzynski's equality, that was experimentally confirmed a few years after its discovery [43].

Besides its numerous applications in microscopic systems such as proteins and DNA/RNA filaments, Jarzynski's equality has been derived and successfully implemented also for stochastic processes and, in particular, for Markov processes and Monte Carlo simulations. However, this result has seen no applications in lattice

field theory until the work of ref. [44], where we proposed an implementation to the case of pure gauge theories. Thus, in the fourth chapter we will provide an in-depth analysis of Jarzynski's equality, with a particular focus on its relation with the second law of thermodynamics, its derivations for isolated Hamiltonian systems, Markov processes and Markov chains. Then, in the last part we will move from statistical mechanics to lattice gauge theory, with a detailed description of the results obtained in [44] for the free energy of an interface in the $\mathbb{Z}_2$ gauge model.

In lattice field theory, the computation of free-energy differences is related to a multitude of physically interesting quantities: thus, applications of Jarzynski's equality are in principle possible in many different lines of research. If we focus on thermodynamics, then the determination of the pressure is a perfect candidate, as it is equivalent to minus the free energy density: in chapter 5 we will analyse how to compute the pressure in a lattice gauge theory using Jarzynski's equality. Moreover, we will present some preliminary tests performed in the SU(2) pure gauge theory and reported in [44], aimed at providing a quantitative estimate of the efficiency of this technique, in particular with respect to the integral method. In the second part of this chapter, a large-scale determination for the equation of state of the SU(3) pure gauge theory will be presented: even if the thermodynamics of this theory can be considered as a solved problem, thanks to the seminal work of [4], recent high-precision determinations with different methods [6, 7, 45] displayed relevant discrepancies, which cannot be simply interpreted as due to statistical fluctuations. More in general, the revived interest in novel methods for the calculation of equilibrium thermodynamics may in principle be able to highlight systematic errors due to a specific methodology. In light of this, we will see how the novel method based on Jarzynski's equality is able to provide a very competitive and highly reliable determination of the SU(3) equation of state. Finally, the last chapter of this thesis is devoted to some concluding remarks and final observations.

Chapter 1

The equation of state of non-Abelian gauge theories

The study of the thermodynamic properties of quantum chromodynamics, and in particular of the equation of state, represents an ongoing effort of a large sector of the theoretical physics community, due to the far-reaching applications that the study of the QCD phase diagram has. The main tool at our disposal to investigate *from first principles* how strongly-interacting matter behaves under extreme temperatures are numerical simulations of the original theory regularized on the lattice. Indeed, the reliability of perturbative expansions in g^2 is severely limited because of the inherently nonperturbative nature of phenomena such as the deconfinement transition itself. The aim of this introductory chapter is, first, to introduce some of the most important concepts related to QCD at nonzero temperature and, second, to present the numerical methods and techniques that are routinely used in this field of research.

The present chapter is structured as follows: a short introduction to the phenomenology of quantum chromodynamics at finite temperatures and densities is presented in section 1.1, mainly focusing on the nature of the deconfinement transition and the relevant symmetries of the theory. Section 1.2 is devoted to the presentation of the lattice field theory framework used to perform the nonperturbative computations of equilibrium thermodynamics in non-Abelian gauge theories. Then, the observables related to the equation of state will be presented, and a set of common strategies used to compute them will be described and analysed with some detail in section 1.3. Finally, in section 1.4 some recent numerical results from the lattice will be presented, with a particular focus on the SU(3) pure gauge theory and cutting-edge results for full QCD with 2+1 and 2+1+1 dynamical quark flavors.

1.1   QCD at nonzero temperature and density

A complete understanding of the behaviour of strongly-interacting matter in a regime of extreme temperatures and densities is one of the most fascinating and important theoretical challenges in contemporary particle physics. Recent experimental advancements confirmed the theoretical prediction of the existence of a new phase of matter at high enough temperature and/or baryon density, commonly known as the "quark-gluon plasma" (QGP). In this new region hadrons are not

anymore the relevant degrees of freedom: the color charges, i.e. quarks as well as gluons, are said to be "deconfined". The quark-gluon plasma is never observed directly, but its existence has been confirmed by the observation of several phenomena which separately indicate the presence above around 160 MeV of a nearly ideal fluid which undergoes rapid thermalization. This new phase is separated from the confined, hadronic phase (where the QCD vacuum is located) by a deconfining change of state: a qualitative representation of the phase diagram of QCD is presented in fig. 1.1. The properties of the deconfinement transition depend strongly on the values of the temperature and baryon chemical potential: for small values of μ_B, the transition is a crossover, but if the baryon density increases it has been conjectured that a critical point with a second order transition is present; at even higher μ_B, the deconfinement transition may become of the first order type, even if strictly rigorous predictions are lacking. A thorough analysis on how the phase diagram changes as quark masses are varied (for example, in the chiral limit) is present in ref. [46]. Even more exotic phases of matter may be present at very high baryon densities, as reported in the rightmost region of fig. 1.1, characterized by color superconductivity and superfluidity.
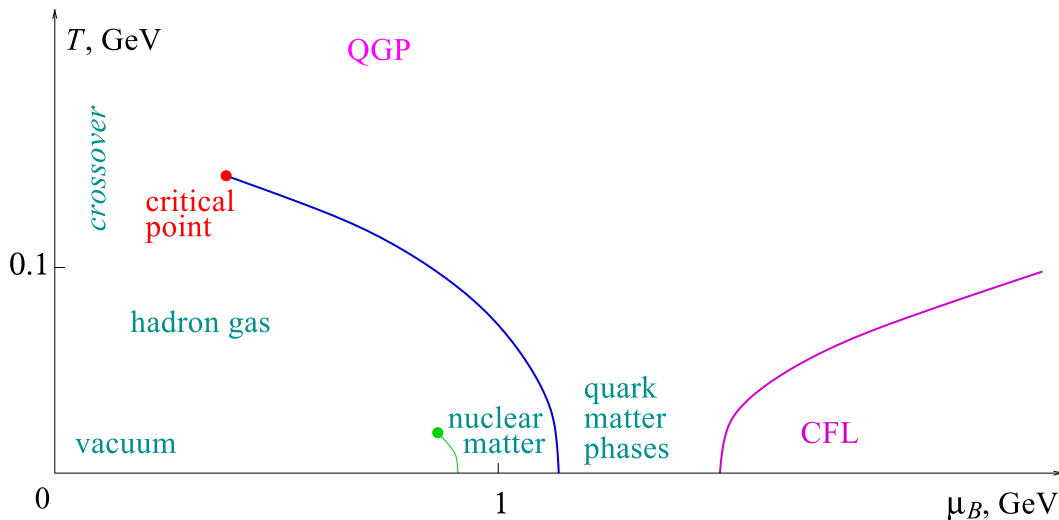
Figure 1.1: QCD phase diagram: on the lower left the QCD vacuum and the confined, hadronic phase; in the upper region the quark-gluon plasma (QGP); on the lower right, the color-flavor locked (CFL) phase. The blue line is the a first-order deconfinement transition line, the red point is the second-order critical point while the violet line denotes the entrance into the color-superconductivity region. Image from ref. [46].

A very successful phenomenological description of the properties of the quark-gluon plasma observed in experiments is provided by relativistic fluidodynamics, while the hadron resonance gas model has been very effective in the description of equilibrium properties in the confined phase. However, deriving a reliable description of the hot and dense strongly-interacting matter from first principles, i.e. from the Lagrangian of quantum chromodynamics, is not an easy task.

The perturbative approach based on the weak-coupling expansion in finite temperature QCD is highly problematic, as the deconfinement phase transition is an

intrinsically non-perturbative phenomenon whose properties cannot be fully captured by an expansion in the coupling. The best and most successful approach from first principles is without any doubt the lattice regularization of QCD: indeed, the framework provided by numerical simulations on the lattice is *the* non-perturbative way of studying QCD and it has provided an enormous amount of predictions for many physical quantities. However, before reviewing the lattice QCD framework in section 1.2, we will give a short review of the statistical mechanics of quantum chromodynamics at $T \neq 0$.

The grand partition function for QCD is

$$Z(V, T, \mu_f; g, m_f) = \hat{\mathrm{Tr}} \left[e^{-(H - \mu_f Q_f)/T} \right]$$

where Q_f is the conserved quark number and μ_f the corresponding chemical potential; the thermodynamic average of an observable O can be obtained using

$$\langle O \rangle = Z^{-1} \hat{\mathrm{Tr}} \left[O \, e^{-(H - \mu_f Q_f)/T} \right].$$

The path integral representation of the grand partition function can be written as

$$Z(V, T, \mu_f; g, m_f) = \int [\mathcal{D}A][\mathcal{D}\bar{\psi}][\mathcal{D}\psi] e^{-S_g[A_\mu]} e^{-S_f[\bar{\psi}, \psi, A_\mu]}, \tag{1.1}$$

where the Euclidean gauge action reads

$$S_g[A_\mu] = \int_0^{1/T} \mathrm{d}\tau \int_V \mathrm{d}^3 x \, \frac{1}{2} \mathrm{Tr} \left[F_{\mu\nu}(x) F_{\mu\nu}(x) \right]. \tag{1.2}$$

The Euclidean fermionic action is

$$S_f[\bar{\psi}, \psi, A_\mu] = \int_0^{1/T} \mathrm{d}\tau \int_V \mathrm{d}^3 x \sum_{f=1}^{N_f} \bar{\psi}_f(x) \left(\gamma_\mu D_\mu + m_f - \mu_f \gamma_0 \right) \psi_f(x), \tag{1.3}$$

where we stress that the compactified temporal direction with extent $1/T$ defines the inverse of the temperature; moreover the conserved quark number density for the flavor f is

$$Q_f = \bar{\psi}_f(x) \gamma_0 \psi_f(x).$$

As usual

$$D_\mu = \partial_\mu - ig A_\mu, \qquad A_\mu(x) = T^a A_\mu^a(x), \qquad F_{\mu\nu}(x) = \frac{i}{g} [D_\mu, D_\nu] \tag{1.4}$$

where the T^a are the generators of the $\mathrm{SU}(N)$ gauge symmetry algebra, with index $a = 1, ..., N^2 - 1$; the index f denotes the quark flavor: $f = u, d, s, c, b, t$. To ensure the correct Bose-Einstein and Fermi-Dirac statistics, the path integral of eq. (1.1) must be evaluated using periodic boundary conditions along the Euclidean-time direction for the gauge bosons

$$A_\mu(\tau, \mathbf{x}) = A_\mu(\tau + \frac{1}{T}, \mathbf{x}) \tag{1.5}$$

and antiperiodic ones for the quark spinors

$$\psi(\tau, \mathbf{x}) = -\psi(\tau + \frac{1}{T}, \mathbf{x}). \tag{1.6}$$

Besides the usual dependence on the macroscopic parameters (temperature T, volume V and chemical potentials μ_f) the partition function of eq. (1.1) depends also on the gauge coupling g and on the masses of the fermions m_f.

Having established the basics for the study of QCD properties at $T \neq 0$, we devote the following paragraphs to the analysis of some of the most important symmetries underlying the behaviour of hot and dense strongly-interacting matter.

1.1.1   Center symmetry

When the (Euclidean) temporal direction is compactified and the appropriate boundary conditions are imposed, a new kind of symmetry of the Yang-Mills theory emerges (we will see later what happens when quarks are included). Let's consider first a standard local gauge transformation of the fields, namely

$$g(x) : A_\mu(x) \rightarrow A_\mu^g(x) = g(x) \left(A_\mu(x) + \frac{i}{g} \partial_\mu \right) g^\dagger(x);$$

this holds if the gauge transformations satisfy $g(\tau, \mathbf{x}) = g(\tau + 1/T, \mathbf{x})$. Now, we can also define new transformations $h(x)$ which are periodic up to a global SU(N) matrix denoted as z

$$h(\tau, \mathbf{x}) = z\, h(\tau + \frac{1}{T}, \mathbf{x}) \tag{1.7}$$

and this transformation implies that the transformed fields now obey

$$A_\mu^g(\tau, \mathbf{x}) = z\, A_\mu^g(\tau + \frac{1}{T}, \mathbf{x}) z^\dagger. \tag{1.8}$$

This implies that $h(x)$ keeps the action invariant only if z is an element of the center of the group, which in the case of SU(N) gauge theories is an element of the cyclic group Z_N

$$z = \exp \left(\frac{2\pi i\, n}{N} \right) \mathbf{1}$$

with $n = 0, 1, ... N - 1$; these transformations take the name of *center* transformations and the action is invariant under the *center* symmetry. As we will see in detail in a moment, the center symmetry is truly the symmetry which is spontaneously broken in the deconfined phase; but before doing this, we have to identify the order parameter related to this phase transition.

Thanks to the periodicity of the temporal dimension, a new set of gauge-invariant observables can be computed: let us consider for example a Wilson line winding around the compactified dimension

$$W(\mathbf{x}) = \mathcal{P} \exp \left\{ ig \int_0^{\frac{1}{T}} \mathrm{d}\tau A_0(\tau, \mathbf{x}) \right\} \tag{1.9}$$

where $\mathcal{P}$ denotes the path-ordered exponential; under gauge transformations we have that

$$W^g(\mathbf{x}) = g(0, \mathbf{x}) W(\mathbf{x}) g(\frac{1}{T}, \mathbf{x})^\dagger;$$

the trace of this Wilson line is the so-called *Polyakov loop* $P(\mathbf{x})$

$$P(\mathbf{x}) = \mathrm{Tr}\, W(\mathbf{x}).$$

Under center transformations, due to the periodic property of eq. (1.7), the Polyakov loop becomes

$$h(x) : P(\mathbf{x}) \rightarrow P^h(\mathbf{x}) = \exp\left(\frac{2\pi i\, n}{N}\right) P(\mathbf{x}), \qquad (1.10)$$

i.e. it acquires a phase belonging to Z_N, while it is still invariant for a standard gauge transformation ($P^g(\mathbf{x}) = P(\mathbf{x})$). The physical interpretation of a Polyakov loop is related to the propagator of a static quark with coordinates $\mathbf{x}$ wrapping around the torus: its expectation value can be seen as

$$\langle P(\mathbf{x})\rangle \propto e^{-F_q/T}$$

where F_q is the free energy associated to the isolated static quark. The Polyakov loop is a crucial quantity for the study of Yang-Mills theory at nonzero temperature, as it is the order parameter of the deconfinement transition. In order to see this, we observe that at low temperatures the theory is confining and we expect the free energy of an isolated quark to be infinite. This is exactly what happens, as for $T < T_c$ we have that $\langle P(\mathbf{x})\rangle = 0$: indeed, the vacuum expectation value of the Polyakov loop is invariant under center transformations. Conversely, for $T \rightarrow \infty$ the expectation value becomes nonzero ($\langle P\rangle \neq 0$) and the vacua of the theory are not center-symmetric anymore. There are N different expectation values (connected with each other by center transformations) and when crossing the transition the system picks one of them.

We remind that the center symmetry is a true symmetry only for the pure gauge theory, or, in other terms, for QCD with infinitely heavy quarks. If the theory includes also dynamic quark flavors, then the situation is markedly different: first of all the center symmetry of the pure gauge action is broken explicitly by the fermionic degrees of freedom. Indeed, for gauge transformations of the kind of eq. (1.7) one has boundary conditions of the type

$$\psi(\tau, \mathbf{x}) = -z\,\psi(\tau + 1/T, \mathbf{x}) \qquad (1.11)$$

which are antiperiodic only for $z = \mathbf{1}$. In such cases (whenever the quark masses are finite) the center symmetry is broken explicitly and $\langle P\rangle \neq 0$ always holds.

1.1.2 Chiral symmetry

If we consider the full QCD Lagrangian with N_f massless quark flavors, we can identify an invariance under global transformation of the quark fields of the following symmetry:

$$\mathrm{U}(N_f)_R \otimes \mathrm{U}(N_f)_L = \mathrm{SU}(N_f)_V \otimes \mathrm{SU}(N_f)_A \otimes \mathrm{U}(1)_V \otimes \mathrm{U}(1)_A. \qquad (1.12)$$

The $\mathrm{U}(1)_V$ symmetry deals with transformations of the type

$$\psi_f \rightarrow \exp(i\alpha)\psi_f \qquad (1.13)$$

where the conserved charge is the baryon number B; from here one the index f denotes a massless quark flavor.

Instead, $SU(N_f)_V$ vector rotations mix the flavors under

$$\psi_f \to \exp(i\theta^a T^a)_{f'f}\psi_f \qquad \text{with } a = 0, 1, ..., N_f^2 - 1\,; \qquad (1.14)$$

for N_f degenerate (not necessarily massless) flavors the quark spinors can be thus written as an N_f-plet whose components transform under eq. (1.14). This symmetry is softly broken in nature when $N_f = 2$ by the not-perfectly degenerate up and down quark masses, leading to the approximate (but still very good) isospin symmetry in the light-hadrons spectrum. When considering also the strange quark ($N_f = 3$) this invariance leads to the approximate strangeness symmetry.

The $SU(N_f)_A$ symmetry corresponds to axial transformations of the kind

$$\psi_f \to \exp(i\theta^a T^a \gamma_5)_{ff'}\psi'_f \qquad \text{with } a = 0, 1, ..., N_f^2 - 1\,; \qquad (1.15)$$

it is spontaneously broken at zero and low temperatures and it gives rise to $N_f^2 - 1$ massless Goldstone bosons. For $N_f = 2$ the three Goldstone bosons are the pions (whose masses are indeed very small when compared to those of the nucleons and are generated by the fact that in nature $m_{u,d} \neq 0$); for $N_f = 3$ we have also the kaons and the η meson (which are even more massive due to the relatively large bare mass of the strange quark). However, for large enough temperatures the symmetry is restored: the correct order parameter is the so-called *chiral condensate*

$$\langle \bar{\psi}\psi \rangle_f = \frac{T}{V}\frac{\partial \ln Z}{\partial m_f} \qquad (1.16)$$

which has a nonzero expectation value in the QCD vacuum below the transition temperature; above T_c (whose value is very close to that of the deconfinement transition) it is zero.

Last, the $U(1)_A$ axial symmetry is indeed a symmetry of the QCD Lagrangian, but not of the quantum theory. Indeed, under the transformations

$$\psi_f \to \exp(i\alpha\gamma_5)\psi_f \qquad (1.17)$$

the measure of the path integral is modified

$$[\mathcal{D}\psi][\mathcal{D}\bar{\psi}] \to \exp\left(\frac{-i\alpha g^2 N_f}{32\pi^2}\int \mathrm{d}^4x\,\epsilon_{\mu\nu\rho\sigma}F^a_{\mu\nu}(x)F^a_{\rho\sigma}(x)\right)[\mathcal{D}\psi][\mathcal{D}\bar{\psi}]. \qquad (1.18)$$

Indeed there are gauge configurations for which the integrand of eq. (1.18) is nonzero and the current

$$j_5^\mu = \bar{\psi}\gamma^\mu\gamma^5\psi$$

is not conserved: this is the so-called *axial anomaly* [47, 48], a typically quantum effect because of which there is no conserved charge and no Goldstone boson.

1.2   Thermodynamics in lattice gauge theories

The lattice regularization of quantum field theories has proven to be the main tool in the investigation of the properties of quantum chromodynamics at nonzero temperature from first principles, being able to compute a large number of equilibrium

observables related to the QCD plasma. Many problems directly related to the quark-gluon plasma have been thoroughly analysed through lattice simulations, such as the nature of the deconfinement and of the chiral restoration, electromagnetic fields in the QGP, freeze-out conditions and, of course, the equation of state for vanishing baryon chemical potential, which will be analysed separately in section 1.3.

In the following paragraphs we will review the theoretical framework under which numerical simulations are performed: in section 1.2.1 the discretized version of the Yang-Mills action will be analyzed and the lattice counterparts of some observables introduced in section 1.1 will be presented. A short introduction to the discretization of fermions on the lattice has been included in section 1.2.2, leaving aside most of the details. Section 1.2.3 is dedicated to some crucial features of computations on the lattice, with particular attention to the setting of the scale. Further details and analyses, especially concerning fermionic actions and their improvements, can be found in ref. [49].

1.2.1 The gauge action and related observables

Lattice computations are usually performed in a finite hypercubic lattice (that we will generally denote as Λ) of spacing a and hypervolume $L_s^3 \times L_t = a^4(N_s^3 \times N_t)$, in which periodic boundary conditions for the gauge fields and antiperiodic ones for the quark variables are imposed along the compactified dimension. As described in the section 1.1, the temperature T of the system is taken to be the inverse of the temporal size, via the relation $T = 1/L_t$, while the sizes of the system in the other three "spatial" directions are usually taken to be much larger ($L_s \gg L_t$) to avoid finite-volume effects. In practice, (anti)periodic boundary conditions are imposed also in the spatial directions.

The simplest choice for the Euclidean Yang-Mills action of the lattice theory is the standard Wilson action, introduced by K. Wilson at the dawn of lattice field theory [3], that reads

$$S_W = -\frac{2}{g^2} \sum_{x \in \Lambda} \sum_{0 \le \mu < \nu \le 3} \text{Re} \, \text{Tr} \, U_{\mu\nu}(x) \tag{1.19}$$

where g denotes the (bare) lattice coupling and

$$U_{\mu\nu}(x) = U_\mu(x) U_\nu(x + a\hat{\mu}) U_\mu^\dagger(x + a\hat{\nu}) U_\nu^\dagger(x) \tag{1.20}$$

is the so-called *plaquette*, i.e. the smallest loop one can have on the lattice. The $U_\mu(x)$ is a SU(N) group element (in the defining representation): it represents a parallel transporter (in color space) from the site x to the site $x + a\hat{\mu}$. In the following, we also introduce the Wilson parameter $\beta = 2N/g^2$, which should not be confused with the inverse temperature.

In the continuum limit, the Wilson action differs from the Yang-Mills action by terms of order $\mathcal{O}(a^2)$; a common alternative to eq. (1.19) is the use of an improved action, which guarantees a better continuum extrapolation from nonzero lattice spacing results, in the sense that $\mathcal{O}(a^2)$ terms are eliminated and only corrections $\mathcal{O}(a^4)$ survive. One well known example is the Symanzik improved action [50, 51]:

$$S_{\text{imp}} = -\frac{2}{g^2} \left[c_0 \sum_{x \in \Lambda} \sum_{\mu < \nu} \text{Re} \, \text{Tr} \, U_{\mu\nu}^{1\times1}(x) + c_1 \sum_{x \in \Lambda} \sum_{\mu \ne \nu} \text{Re} \, \text{Tr} \, U_{\mu\nu}^{2\times1}(x) \right] \tag{1.21}$$

where $U_{\mu\nu}^{1\times1}$ is the standard 1×1 plaquette of eq. (1.20), while $U_{\mu\nu}^{2\times1}$ is the rectangular loop of size 2×1. The coefficients c_0 and c_1 are set in order to improve the scaling with a at tree level.

Naturally, the periodic boundary conditions for the SU(N) link variables

$$U_\mu(\mathbf{x}, 0) = U_\mu(\mathbf{x}, aN_t)$$

are imposed as in the continuum (see eq. (1.5)).

At the quantum level, the dynamics of the lattice pure gauge theory is defined by the partition function Z

$$Z(\beta) = \int [\mathcal{D}U] \exp\left(-S_{\mathrm{g}}(U)\right) = \int \prod_{x\in\Lambda} \prod_{\mu=0}^{3} \mathrm{d}U_\mu(x) \exp\left(-S_{\mathrm{g}}(U)\right), \qquad (1.22)$$

where $\mathrm{d}U_\mu$ denotes the SU(N) Haar measure and S_g the desired pure gauge action. In this way the expectation value of a generic, gauge-invariant quantity $\mathcal{A}$ is given by

$$\langle\mathcal{A}\rangle = \frac{1}{Z} \int \prod_{x\in\Lambda} \prod_{\mu=0}^{3} \mathrm{d}U_\mu(x) \mathcal{A} \exp\left(-S_{\mathrm{g}}\right). \qquad (1.23)$$

Expectation values of this form then can be estimated numerically via *dynamical* Monte Carlo integration. In a numerical lattice simulation large sets of configurations of the fields $U_\mu(x)$ are generated by appropriate algorithms following, in the case of the pure gauge theory, the Haar measure of eq. (1.23). Then, on each of these configurations the desired observable $\mathcal{A}$ is directly measured and, in the end, the vacuum expectation value of eq. (1.23) is computed simply by taking the average.

The reliability of any simulation on the lattice is closely related to the ability to sample the phase space with the correct Boltzmann weight: we will see in the next section one case in which this is not possible.

Among the observables of interest in this thesis we define the normalized, traced Polyakov loop through a spatial point $\mathbf{x}$

$$P(\mathbf{x}) = \frac{1}{N} \mathrm{Tr}\, L(\mathbf{x}), \qquad (1.24)$$

where

$$L(\mathbf{x}) = \prod_{0\leq\tau<N_t} U_0(\mathbf{x}, \tau a) \qquad (1.25)$$

which corresponds to the continuum definition given in section 1.1.1. Another related, crucial quantity is the two-point Polyakov loop correlation function

$$G(r) = \left\langle \frac{1}{3N_s^3} \sum_{\mathbf{x}\in\Lambda_s} P(\mathbf{x}) \sum_{1\leq\mathbf{i}\leq\mathbf{3}} P\left(\mathbf{x} + r\mathbf{i}\right) \right\rangle \qquad (1.26)$$

(with Λ_s being the spatial volume) which is related to the static interquark potential $V_{q\bar{q}}$, as we will see in section 2.2.1 in detail.

1.2.2 Fermions on the lattice

A generic lattice discretization of the fermionic action of QCD can be written as

$$S_{\text{f}} = a^4 \sum_{x,y \in \Lambda} \sum_f \bar{\psi}_f(x) D_{x,y}(m_f) \psi_f(y) \tag{1.27}$$

where the index f denotes the quark flavor (with the respective mass m_f) and D_{xy} is the Dirac operator; the usual antiperiodic boundary conditions

$$\psi(\mathbf{x}, 0) = -\psi(\mathbf{x}, aN_t)$$

are imposed to preserve Fermi statistics. The complete partition function is

$$Z(\beta, m_f) = \int [\mathcal{D}U] \prod_f [\mathcal{D}\psi_f][\mathcal{D}\bar{\psi}_f] \exp\left(-S_{\text{g}}(U) - S_{\text{f}}(U, \psi_f, \bar{\psi}_f) \right) \tag{1.28}$$

which becomes (under the rules for the integration of Grassmann variables)

$$Z(\beta, m_f) = \int [\mathcal{D}U] \prod_f \det [D(m_f)] \exp\left(-S_{\text{g}}(U) \right). \tag{1.29}$$

Now, before the actual discretization of fermions on the lattice, we can analyse a well-known problem of Monte Carlo numerical simulation: whenever a nonzero baryonic chemical potential μ_B is included in the theory (as in eq. (1.3)), the determinant of the Dirac operator becomes complex. This issue, known in the literature as the "sign problem" is truly fundamental, as a complex number cannot be interpreted in terms of a Boltzmann weight for importance sampling: the evaluation of the path integral via Monte Carlo simulations is, thus, impossible. Various solutions have been proposed in order to circumvent this problem, with varying degrees of success. In chapter 3 we will analyse one possibility, based on the use of effective Polyakov loop (EPL) models to obtain reliable predictions on finite-density QCD and QCD-like theories.

The simplest attempt to put fermions on the lattice is via the *naïve* discretization of the Dirac operator: in the non-interacting case one simply substitutes the derivative with the finite difference

$$\partial_\mu \psi(x) \to \nabla_\mu \psi(x) = \frac{\psi(x + a\hat{\mu}) - \psi(x - a\hat{\mu})}{2a}$$

which gives $\partial_\mu \psi(x)$ in the $a \to 0$ limit with $\mathcal{O}(a^2)$ corrections. Similarly, the covariant derivative $D_\mu \psi$ becomes

$$D_\mu \psi(x) \to \frac{U_\mu(x)\psi(x + a\hat{\mu}) - U_\mu^\dagger(x - a\hat{\mu})\psi(x - a\hat{\mu})}{2a}$$

that gives the correct result in the continuum limit with $\mathcal{O}(a)$ corrections. Thus, we can write down the naïve discretization of D as

$$S_{\text{naive}} = a^4 \sum_{x,y \in \Lambda} \sum_f \bar{\psi}_f(x) D_{x,y}^{\text{naive}}(m_f) \psi_f(y) \tag{1.30}$$

$$D_{x,y}^{\text{naive}} = m_f \delta_{x,y} + \sum_{\mu=0}^3 \gamma_\mu \left(\frac{U_\mu(x)\delta_{x+a\hat{\mu},y} - U_\mu^\dagger(x - a\hat{\mu})\delta_{x-a\hat{\mu},y}}{2a} \right). \tag{1.31}$$

where we have made the color and Dirac indices explicit. It is a well-known fact that this discretization suffers from a serious problem: if one computes the (discrete) Fourier transform of D_{xy}^{naive} and computes the propagator $D^{-1}(p)$, 2^D poles appear in the chiral limit ($m_f = 0$). Thus, there are $2^D - 1$ unwanted modes which go by the name of *doublers* and that survive the continuum limit: the naïve lattice Dirac operator actually describes 16 (in $D = 4$) different quark flavors.

Different solutions have been proposed in the literature to deal (at least to some extent) with the presence of fermion doublers in the lattice regularization: among the most used and relevant ones for the calculation of thermodynamical observables (and in particular for the equation of state) we mention *Wilson fermions* and *staggered fermions*.

The solution proposed by Wilson [52] gets rid of fermion doublers by including an irrelevant, dimension-five operator which is proportional to the lattice version of the Laplacian. The new Dirac operator now reads

$$D_{x,y}^{\mathrm{Wilson}}(m_f) = m_f \delta_{x,y} + \sum_{\mu=0}^{3} \gamma_\mu \left(\frac{U_\mu(x)\delta_{x+a\hat{\mu},y} - U_\mu^\dagger(x-a\hat{\mu})\delta_{x-a\hat{\mu},y}}{2a} \right) \qquad (1.32)$$

$$- r \sum_{\nu=0}^{3} \left(\frac{U_\nu(x)\delta_{x+a\hat{\mu},y} - 2\delta_{x,y} + U_\nu^\dagger(x-a\hat{\nu})\delta_{x-a\hat{\nu},y}}{2a} \right) \qquad (1.33)$$

and now the coefficient of the $\bar{\psi}\psi$ term (i.e. the bare mass of the quark) is $m_f + 4r/a$.

It is customary to introduce the *hopping* parameter

$$\kappa_f = \frac{1}{2a(m_f + 4r/a)}$$

and rewrite the Dirac operator as

$$D_{x,y}^{\mathrm{Wilson}}(\kappa_f) = \delta_{x,y} - \kappa_f \sum_{\mu=0}^{3} (r-\gamma_\mu)U_\mu(x)\delta_{x+a\hat{\mu},y} + (r+\gamma_\mu)U_\mu^\dagger(x-a\hat{\mu})\delta_{x-a\hat{\mu},y} \quad (1.34)$$

The main effect is that the mass degeneracy between the fermion doublers is lifted and in the continuum limit the $2^D - 1$ unwanted modes acquire an infinite mass and are effectively decoupled from the theory. Please note that this operator is not invariant anymore under transformations of eq. (1.15): it breaks chiral symmetry explicitly and there is no spontaneous breaking of it, even in the massless quarks limit.

More possibilities have been proposed in the literature since the one by Wilson. We mention here in particular an extremely popular discretization of the fermionic action put forward by Kogut and Susskind [53, 54], which goes by the name of *staggered fermions*. We refer to [55] for an introductory analysis of this approach and others, such as domain wall fermions, while for further information on their use in lattice thermodynamics we refer to [49].

1.2.3   Features of lattice simulations at nonzero temperature

In order to obtain precise results for the thermodynamics in lattice gauge theories an accurate tuning of the temperature to the desired value is essential. We recall

that the temperature is the inverse of the extent of the compactified dimension (usually chosen to be the "time" direction), i.e.

$$T = \frac{1}{L_t} = \frac{1}{a(\beta)N_t}.$$

On the lattice, it can be varied both by increasing or decreasing the number of lattice sites N_t in the temporal compactified dimension, or by changing the lattice spacing a itself. Most importantly, both a and N_t can be varied in a complementary manner in order to extrapolate the results to the continuum; moreover we will see in detail in section 1.3 that both ways are viable options when computing the equation of state.

If the lattice spacing $a(\beta)$ is used to tune the temperature T to the desired value, it is crucial to have an accurate functional relation between the spacing and the inverse coupling $\beta = 2N/g^2$. Such a relation is given by the renormalization group: in perturbation theory we can define the Callahan-Symanzik β-function β_{LAT} via the renormalization group equation

$$-a\frac{\partial g}{\partial a} = \beta_{LAT} = -b_0\, g^3 - b_1\, g^5 + ... \tag{1.35}$$

where the first two coefficients b_0 and b_1 of the expansion of β_{LAT} are independent of the renormalization scheme; they are known in perturbation theory and are

$$b_0 = \frac{11\,N}{48\pi^2}, \qquad b_1 = \frac{34}{3}\left(\frac{N}{16\pi^2}\right)^2 \tag{1.36}$$

respectively. Eq. (1.35) yields the relation between a and g^2 (in units of the integration constant Λ_{LAT})

$$a\Lambda_{LAT} = \left(\frac{1}{b_0 g^2}\right)^{b_1/2b_0^2} \exp\left(-\frac{1}{2b_0 g^2}\right)(1 + \mathcal{O}(g^2)); \tag{1.37}$$

similar relations hold for the quark masses.

However, the range of lattice spacings a that are interesting for studying thermal properties of Yang-Mills theory is not usually accessible by perturbation theory and thus eq. (1.37) cannot be used as a reliable relation between a and β for thermodynamics. A different, non-perturbative way of setting the scale is obtained by expressing each of the observables of interest in units of physical quantities that can be computed separately on the lattice and whose experimental value is known. One possibility is for example to compute non-perturbatively on the lattice the mass of the pion am_π (in units of the spacing), and then use it to express all other observables. Namely, for the temperature we would have that

$$\frac{T}{m_\pi} = \frac{1}{am_\pi N_t} \tag{1.38}$$

and then we would use the experimental value of m_π to give a physical value in MeV to the temperature.

Another viable way of setting the scale for lattice simulations is through the calculation of the static potential of a quark-antiquark pair, $V_{q\bar{q}}$, or of the interquark

force, $F_{q\bar{q}}$. These observables are easily accessible on the lattice by the computation of Wilson loops or Polyakov loop correlators: the relevant dimensionful quantities are in particular the string tension σ or the Sommer scale r_0 (and its variant r_1). Such quantities cannot be directly observed and measured easily in an experiment though: because of this, the lattice spacing and all other observables are usually expressed adimensionally, either in the proper units of σ or r_0 (e.g. $a\sqrt{\sigma}$ or a/r_0). A practical determination of the scale will be showed later more in detail in section 2.2.1.

In pure gauge theories, once the scale setting relation $a(\beta)$ is known, we are able to perform the continuum extrapolation: the limit $a \to 0$ (or equivalently $\beta \to \infty$) is taken by keeping the temperature T in physical units fixed by using a sequence of larger and larger values of N_t. On the other hand, when considering the full theory with dynamical quarks, the situation is somewhat more complicated by the fact that *physical* quark masses must also be kept fixed (along with the temperature T) when varying the lattice spacing. In practice, this means that also the bare quark masses am_f must be tuned in order to keep the physical masses constant. A concept which is useful for the correct calculation of continuum-extrapolated thermodynamic observables in lattice QCD is that of "lines of constant physics". A line of constant physics is a curve in the parameter space of the theory, along which the renormalized quark masses are kept constant by tuning the bare masses and the inverse coupling:

$$m_f^R(am_{u,d}(\beta), am_s(\beta), \beta) = \text{const.}$$

In practice, one chooses other physical observables which are computed more straightforwardly than m_f^R, such as hadron masses or decay constants. As we have just seen, the determination of the lines of constant physics and the setting of the scale play a crucial role for thermodynamics, even if they are computed in zero temperature simulations.

When performing lattice simulations there are some intrinsic physical constraints related to how fine and how large the lattice has to be that must be taken into account. On one hand, the spacing must be small enough to accommodate all the relevant energy scales: this means that in the confining phase

$$a \ll m_H^{-1}$$

where m_H is the mass of the physical states that one wishes to study. On the other hand the spatial size of the lattice must be larger than the Compton wavelengths of the pions, which are proportional to the inverse of their mass; this leads to

$$aN_s \gg m_\pi^{-1}.$$

This explains why simulating physical pion masses is extremely expensive on the computational side, as very fine and very large lattices are needed: it has been made possible only recently, and initially only with staggered fermions.

In the high-temperature, deconfined phase the screening masses go as $m \sim T$: if we take the constraints for the low-temperature phase

$$a \ll m^{-1} \ll aN_s$$

they become

$$1 \ll N_t \ll N_s$$

that means that the spatial size must be significantly larger than the temporal one, limiting the range of temperature that can be reached at fine lattice spacing. Actually, screening masses at $T > T_c$ go as $m \sim gT$ or $m \sim g^2 T$ (g being the coupling), which, especially at very high temperatures, are rather different from T, and must be taken into account in lattice simulations.

One last word must be spent for what concerns the multiple extrapolations that may be needed for the results of the simulations. As we have seen, lattice computations are usually affected by systematic uncertainties related to the finite size of the lattice volume and to finite lattice spacing effects: because of them we need careful extrapolations to an infinite volume and to the continuum, respectively. Another source of systematic errors is due to choosing unphysically heavy pions for the simulations, whose contribution to the fermionic action is computationally cheaper to evaluate. The resulting values then must be extrapolated (using, for example, chiral perturbation theory) to the physical point or, alternatively, to the chiral limit, depending on the desired observable. It is important to stress that one has to extrapolate first to the infinite-volume limit $V \to \infty$, then to the continuum limit $a \to 0$ and finally to the physical pion mass.

1.3 Computing the equation of state on the lattice

The determination of the equation of state represents an extremely important theoretical prediction which is not only in principle accessible by heavy-ion collision experiments, but has also a highly relevant role for the quantitative description of the state of the early Universe. Indeed, one of the main goals of lattice calculations at nonzero temperature and quark density has been the precise determination of the equilibrium properties of QCD and QCD-like theories. By means of Monte Carlo lattice simulations one can obtain accurate results for observables such as pressure, energy density and entropy density.

The "equation of state" is the set of relations between the thermodynamic parameters (pressure, volume, temperature ...) that is valid when the system is at equilibrium. We start with the pressure p, which in statistical mechanics is defined as

$$p = \frac{\partial(T \ln Z)}{\partial V}$$

where Z is the partition function of the system under analysis. In the thermodynamic limit $V \to \infty$ we can rewrite it as the opposite of the free energy density $f = F/V$

$$p = -\lim_{V \to \infty} f = \lim_{V \to \infty} \frac{T}{V} \ln Z. \tag{1.39}$$

Next, we consider the energy E

$$E = T^2 \frac{\partial \ln Z}{\partial T}$$

and the entropy S

$$S = \frac{\partial(T \ln Z)}{\partial T}.$$

The entropy density s can be written as

$$s = \frac{S}{V} = \frac{1}{V}\frac{\partial(T\ln Z)}{\partial T} = \frac{1}{V}\ln Z + \frac{T}{V}\frac{\partial\ln Z}{\partial T} = \frac{p}{T} + \frac{\epsilon}{T} \tag{1.40}$$

where we also introduced the energy density ϵ:

$$\epsilon = E/V = \frac{T^2}{V}\frac{\partial\ln Z}{\partial T}. \tag{1.41}$$

A useful quantity is also the trace of the energy-momentum tensor $T^{\mu\nu}$ (also known as "trace anomaly"), which we write as $\Delta(T) = \epsilon - 3p$. It is immediate to prove that it can be conveniently expressed as

$$\Delta(T) = \epsilon - 3p = T^5\frac{\partial}{\partial T}\left(\frac{p(T)}{T^4}\right). \tag{1.42}$$

In the following we will often refer to these quantities via the adimensional ratios p/T^4, ϵ/T^4, s/T^3 and Δ/T^4. Last, we define the "speed of sound" in the thermal medium as

$$c_s^2 = \frac{\mathrm{d}p}{\mathrm{d}\epsilon}. \tag{1.43}$$

Several methods have been proposed in the last decades to compute these quantities on the lattice: we will devote this section to an overview of these methodologies with a particular focus on those that are most relevant and have been used the most. We will take into consideration primarily how the computation is performed in Yang-Mills theories, while adding in some cases a few examples for the generalization to the full theory with dynamical fermions.

1.3.1   The integral method

The so-called "integral method" has been introduced for the first time many years ago in ref. [36]: the starting point is rewriting the pressure, eq. (1.39), adimensionally in units of T^4

$$p = \frac{T}{V}\ln Z = \frac{1}{N_s^3 N_t}\frac{1}{a^4}\ln Z \quad\Rightarrow\quad \frac{p(T)}{T^4} = \frac{N_t^3}{N_s^3}\ln Z(T). \tag{1.44}$$

Now, instead of computing directly the partition function, we want to take its derivative with respect to some parameter and then integrate it to obtain again the pressure. In practice, the derivative is taken with respect to the inverse coupling β and the integration is performed between two values of the Wilson parameter that correspond to two different temperatures. Thus, this operation allows us to compute the difference of the pressure (in units of T^4)

$$\frac{p(T)}{T^4} - \frac{p(T_0)}{T_0^4} = \frac{N_t^3}{N_s^3}\int_{\beta(T_0)}^{\beta(T)}\mathrm{d}\beta'\frac{\partial\ln Z}{\partial\beta'}\quad; \tag{1.45}$$

the lower limit, that is $\beta(T_0)$, can be set to a value such that the corresponding physical pressure $p(T_0)/T_0^4$ is practically zero and can be safely neglected, or it can be fixed using a different theoretical input such as the contribution of a glueball gas, as we will see in chapter 2.

The positive aspect of this procedure is that now the integrand of eq. (1.45) can be readily computed from plaquette expectation values, namely

$$\langle U_{\mathrm{p}} \rangle_T = \frac{1}{6 N_t N_s^3} \left\langle \frac{\partial \ln Z}{\partial \beta} \right\rangle_T \tag{1.46}$$

where the factor 6 comes from the number of plaquette associated with each site of a four-dimensional lattice (it is 3 in $D = 3$ and 1 in $D = 2$).

We still have to renormalize the pressure to get rid of a quartic divergence, and we do it by explicitly subtracting the vacuum expectation value at $T = 0$ from the integrand for each value of β. The pressure thus becomes

$$\frac{p(T)}{T^4} - \frac{p(T_0)}{T_0^4} = 6 N_t^4 \int_{\beta(T_0)}^{\beta(T)} \mathrm{d}\beta' \left(\langle U_{\mathrm{p}} \rangle_T - \langle U_{\mathrm{p}} \rangle_0 \right) . \tag{1.47}$$

The first plaquette expectation value is computed on the usual $N_t \times N_s^3$ lattice (keeping N_t constant) while the second term is evaluated on a symmetric lattice of sizes $N_{s,0}^4$, which are large enough so that it is effectively at zero temperature for that value of β.

The primary quantity that is computed in this procedure is actually the trace of the energy-momentum tensor of eq. (1.42), that was indeed a derivative of the pressure. It is simply proportional to the aforementioned difference in plaquette expectation values

$$\Delta(T) = -\frac{6}{a^4} \frac{\partial \beta}{\partial \ln a} \left(\langle U_{\mathrm{p}} \rangle_T - \langle U_{\mathrm{p}} \rangle_0 \right) \tag{1.48}$$

where the $\partial \beta / \partial \ln a$ factor can be computed via the scale setting relation $a(\beta)$. It is easy to rewrite the pressure using eq. (1.42) and eq. (1.48) as

$$\frac{p(T)}{T^4} - \frac{p(T_0)}{T_0^4} = \int_{T_0}^T \mathrm{d}T' \frac{\Delta(T')}{T'^5} \tag{1.49}$$

while ϵ and s are readily computed with the usual linear combinations, namely eqs. (1.40) and (1.42).

In the presence of dynamical fermions the relation of eq. (1.47) is easily generalized: in this case the derivative of the partition function with respect to the inverse coupling β adds a term which depends on the mass of the fermions. Namely, for the trace of the energy-momentum tensor we have that

$$\frac{\Delta(T)}{T^4} = -N_t^4 \frac{\partial \beta}{\partial \ln a} \left[6 \left(\langle U_{\mathrm{p}} \rangle_T - \langle U_{\mathrm{p}} \rangle_0 \right) - \frac{\partial m_f(\beta)}{\partial \beta} \left(\langle \bar{\psi}\psi \rangle_{f,T} - \langle \bar{\psi}\psi \rangle_{f,0} \right) \right] \tag{1.50}$$

where $m_f(\beta)$ is the renormalized quark mass (which depends non-trivially on the lattice spacing a) and $\langle \bar{\psi}\psi \rangle_f$ is the chiral condensate for the f quark flavor, see eq. (1.16). For each quark flavor that is added to the system under analysis one has to consider one more term in eq. (1.50) containing the respective mass m_f and chiral condensate $\langle \bar{\psi}\psi \rangle_f$. Now, besides the derivative already present in eq. (1.48), we have to determine also $m_f(\beta)$.

Among the drawbacks of this procedure we want to stress the necessity of performing simulations on symmetric $T = 0$ lattices to subtract the divergence from the trace anomaly and the pressure for each desired temperature. Moreover

the continuum extrapolation at low temperatures is hindered by the rather coarse lattices (at reasonable N_t) one has to introduce to set T to the desired value.

A possible but somewhat limited turnaround to these issues is the so-called "fixed-scale" approach (for a recent example, see ref. [56]), in which the number of sites in the temporal, compactified direction is varied while keeping β (i.e. the lattice spacing a) fixed. In this way the temperature is tuned in discrete steps only by changing N_t: first one computes the trace anomaly using eqs. (1.48) and (1.50) and then integrates over the desired temperatures (see eq. (1.49)). Of course one has to numerically interpolate first the limited number of values of $\Delta(T)$ before proceeding with the numerical integration. This approach needs only one value for the subtraction (since only one lattice spacing is used) and allows for rather fine lattices at low temperatures; conversely large discretization effects appear at high temperatures. Finally, the continuum limit is taken simply by repeating the simulations for a set of different lattice spacings a. A full-scale determination of thermodynamic observables using this approach has been performed in ref. [57]; for a recent development with shifted boundary conditions see ref. [58].

1.3.2   The derivative method

An interesting way to compute directly pressure and energy density is by formulating the theory on an anisotropic lattice of temporal size $L_t = a_t N_t$ and spatial size $L_s = a_s N_s$ [59, 60]. Temperature and volume are defined as

$$T = \frac{1}{a_t N_t}, \qquad V = (a_s N_s)^3,$$

respectively. We define the ratio of the two lattice spacings as $\xi \equiv \frac{a_s}{a_t}$, while the corresponding generalized Wilson action is

$$S_g[U] = \beta_s \sum_{sp} \left(1 - \frac{1}{N}\mathrm{Re\,Tr}U_{sp}\right) + \beta_t \sum_{tp} \left(1 - \frac{1}{N}\mathrm{Re\,Tr}U_{tp}\right) \tag{1.51}$$

where $\beta_s \equiv \frac{2N}{\xi g_s^2}$ and $\beta_t \equiv \frac{2N\xi}{g_t^2}$ are the anisotropic inverse couplings. Using simply the usual statistical mechanics definition of pressure and energy density one gets

$$\epsilon = \frac{T^2}{V}\frac{\partial \ln Z}{\partial T} = T^4 \left(\frac{N_t}{\xi N_s}\right)^3 \langle a_t \frac{\partial S}{\partial a_t}\rangle \tag{1.52}$$

$$p = \frac{T}{V}\ln Z = -\frac{T^4}{3}\left(\frac{N_t}{\xi N_s}\right)^3 \langle a_s \frac{\partial S}{\partial a_s}\rangle \tag{1.53}$$

The quantity inside $\langle ... \rangle$ in eq. (1.52) can be directly calculated:

$$a_t \frac{\partial S}{\partial a_t} = \left(1 + g_s^2 a_t \frac{\partial g_s^{-2}}{\partial a_t}\right)\beta_s \sum_{sp}\left(1 - \frac{1}{N}\mathrm{Re\,Tr}U_{sp}\right)$$

$$+ \left(-1 + g_t^2 a_t \frac{\partial g_t^{-2}}{\partial a_t}\right)\beta_t \sum_{tp}\left(1 - \frac{1}{N}\mathrm{Re\,Tr}U_{tp}\right) \tag{1.54}$$

and the same for the one in eq. (1.53)

$$a_s \frac{\partial S}{\partial a_s} = \left(-1 + g_s^2 a_s \frac{\partial g_s^{-2}}{\partial a_s}\right) \beta_s \sum_{sp} \left(1 - \frac{1}{N} \mathrm{ReTr} U_{sp}\right)$$
$$+ \left(1 + g_t^2 a_s \frac{\partial g_t^{-2}}{\partial a_s}\right) \beta_t \sum_{tp} \left(1 - \frac{1}{N} \mathrm{ReTr} U_{tp}\right) \tag{1.55}$$

So eqs. (1.52) and (1.53) become finally (in units of T^4)

$$\frac{\epsilon}{T^4} = \frac{3N_t^4}{\xi^3} \left[\left(1 + g_s^2 a_t \frac{\partial g_s^{-2}}{\partial a_t}\right) \beta_s P_\sigma + \left(-1 + g_t^2 a_t \frac{\partial g_t^{-2}}{\partial a_t} s\right) \beta_t P_\tau\right] \tag{1.56}$$

$$\frac{p}{T^4} = -\frac{N_t^4}{\xi^3} \left[\left(-1 + g_s^2 a_s \frac{\partial g_s^{-2}}{\partial a_s}\right) \beta_s P_\sigma + \left(1 + g_t^2 a_s \frac{\partial g_t^{-2}}{\partial a_s}\right) \beta_t P_\tau\right]. \tag{1.57}$$

Here P_σ and P_τ are the expectation values of spacelike and timelike plaquettes respectively:

$$P_{\sigma,\tau} = \langle 1 - \frac{1}{N} \mathrm{ReTr}\, U_{sp,tp}\rangle. \tag{1.58}$$

If we fix $\xi = 1$ (that is, $a_s = a_t$) we find eq. (1.48), as expected. As usual at this point, the pressure and the other thermodynamic quantities have non-vanishing vacuum contributions which must be eliminated by subtraction. Moreover, the dependence of g_s and g_t on the respective lattice spacing has to be studied independently (see for example [61]).

Even if this methodology has not been used often in the literature, recent works exploited it extensively for precision calculations (see for example ref. [62]).

1.3.3 The equation of state from a moving frame

A radically different method for the computation of the equation of state based on the use of shifted boundary conditions has been proposed in a series of recent papers [7, 63–67]. The underlying idea is that in relativistic thermal theories the entropy is proportional to the total momentum of the system as measured by a moving reference system: the Euclidean path integral formulation is indeed quite simple. On the temporal direction, whose physical size is $L_t = aN_t$, the following boundary conditions are imposed:

$$U_\mu(L_t, \vec{x}) = U_\mu(0, \vec{x} - L_t \vec{\xi})\,, \tag{1.59}$$

where the spatial shift vector $\vec{\xi}$ characterizes the moving frame in the Euclidean spacetime [65]; namely, $i\xi$ corresponds to the imaginary velocity of the system. In a system with such boundary conditions the free energy density is

$$f(L_t, \vec{\xi}) = -\frac{1}{L_t V} \ln Z(L_t, \vec{\xi}) \tag{1.60}$$

and it can be proved (see for example ref. [65]) that the invariance under SO(4) rotations implies that

$$f(L_t, \vec{\xi}) = f(L_t \sqrt{1 + \vec{\xi}^2}, \vec{0}). \tag{1.61}$$

Thus, one effect of the shifted boundary conditions is that the actual temperature of the system is no longer the inverse of the temporal extent of the lattice, but

$$T = \frac{1}{L_t \sqrt{1 + \vec{\xi}^2}} \tag{1.62}$$

and thus it is decreased with respect to a system with periodic boundary conditions and temporal extent L_t.

By repeatedly deriving eq. (1.61) with respect to both L_t and $\vec{\xi}$ it is possible to generate new interesting Ward identities. In particular the relation (no summation over k indices)

$$\langle T_{0k} \rangle_{\vec{\xi}} = \frac{\xi_k}{1 - \xi_k^2} \left(\langle T_{00} \rangle_{\vec{\xi}} - \langle T_{kk} \rangle_{\vec{\xi}} \right) \tag{1.63}$$

holds, where $T_{\mu\nu}$ is the energy-momentum tensor in Yang-Mills theory. It is defined starting from the usual field strength $F_{\mu\nu}^a$ as

$$T_{\mu\nu}(x) = \frac{1}{g^2} \left[F_{\mu\rho}^a(x) F_{\nu\rho}^a(x) - \frac{1}{4} \delta_{\mu\nu} F_{\rho\sigma}^a(x) F_{\rho\sigma}^a(x) \right]. \tag{1.64}$$

Since parity symmetry is softly broken by the presence of such boundary conditions, the off-diagonal terms T_{0k} are not necessarily zero anymore. From eq. (1.63) one can extract the entropy density $s(T)$

$$s(T) = -\frac{L_t (1 + \vec{\xi}^2)^{\frac{3}{2}}}{\xi_k} \langle T_{0k} \rangle_{\vec{\xi}} Z_T \tag{1.65}$$

where Z_T is a renormalization constant that has to be computed separately.

In order to compute both $s(T)/T^3$ and $Z_T(g_0^2)$ on the lattice, one has to give a definition of the energy-momentum tensor: one such possibility is using the so-called "clover" definition [68] for the field strength $F_{\mu\nu}^a$:

$$F_{\mu\nu}^a(x) = -\frac{i}{4a^2} \text{Tr} \left[(Q_{\mu\nu}(x) - Q_{\nu\mu}(x)) T^a \right] \tag{1.66}$$

with

$$Q_{\mu\nu}(x) = U_{\mu\nu}(x) + U_{\nu-\mu}(x) + U_{\mu\nu}(x) + U_{-\mu-\nu}(x) + U_{-\nu\mu}(x). \tag{1.67}$$

For details on the determination of the renormalization constant $Z_T(g_0^2)$, see ref. [67]; once $Z_T(g_0^2)$ is known, one can compute $\langle T_{0k} \rangle$ and use eq. (1.65) to obtain the entropy density $s(T)$, using only a single simulation for each temperature. Indeed, unlike in the integral method (see eq. (1.48)) where also $T = 0$ simulations are performed to get rid of the quartic divergence, no further subtraction is needed.

In the end, the entropy in units of T^3 is computed using

$$\frac{s(T)}{T^3} = -\frac{L_t^4 (1 + \vec{\xi}^2)^3}{\xi_k} \langle T_{0k} \rangle_{\vec{\xi}} Z_T \tag{1.68}$$

while the pressure requires the numerical integration

$$p(T) = \int_0^T \mathrm{d}T' s(T') \tag{1.69}$$

Recent high-precision results are reported in ref. [7] and a generalization to fermionic degrees of freedom is ongoing.

1.3.4 Using the gradient flow

In principle many different thermal properties of the theory could be extracted by studying directly the energy-momentum tensor $T_{\mu\nu}$: however, in order to do so a proper definition is needed, which is correctly normalized and conserved in the continuum limit. The integral method avoids this problem by computing not the tensor $T_{\mu\nu}$ itself, but its trace, and then obtaining p, ϵ and s afterwards. The use of shifted boundary conditions tackles this issue more directly, through the derivation of new Ward identities valid on a moving frame, that allow for the calculation of both the entropy $s(T)$ and the necessary renormalization constants.

Recent theoretical developments that make use of the Yang-Mills gradient flow [69–71] allow for a definition of the energy-momentum tensor that can be used to practically compute thermodynamic observables on the lattice: this line of research has been carried forward in the last few years both in the pure-gauge theory [45, 72–74] and in full QCD [37, 75].

The Yang-Mills gradient flow is a deformation of the gauge fields $A_\mu(x)$ along a fictitious "flow time" t; the new field at $t > 0$ is denoted as $B_\mu(t, x)$ and defined by the diffusion-like differential equation

$$\partial_t B_\mu(t, x) = D_\nu G_{\nu\mu}(t, x) \tag{1.70}$$

with the condition $B_\mu(t = 0, x) = A_\mu(x)$. The positive flow time field strength $G_{\mu\nu}$ is

$$G_{\mu\nu} = \partial_\mu B_\nu(t, x) - \partial_\nu B_\mu(t, x) + [B_\mu(t, x), B_\nu(t, x)] \tag{1.71}$$

and the covariant derivative of the flowed field is

$$D_\nu G_{\nu\mu}(t, x) = \partial_\nu G_{\nu\mu} + [B_\nu(t, x), G_{\nu,\mu}(t, x)]. \tag{1.72}$$

An important property of the gradient flow is that correlation functions of the $B_\mu(t, x)$ fields are ultraviolet finite for flow times $t > 0$ [70]; this is due to the fact that the diffusion in t introduces a natural regulator in the theory.

The next step concerns the definition of the correct operator at nonzero flow-time t: in particular we have that a generic local operator $\tilde{O}(t, x)$ of the flowed fields $B_\mu(t, x)$ can be written in the small-t limit as

$$\tilde{O}(t, x) \sim \sum_i c_i(t) O_i^R(x)$$

where the $O_i^R(x)$ are the renormalized operators in the $t = 0$ original gauge theory and the $c_i(t)$ are coefficients that are calculable in perturbation theory. Two such operators are

$$\tilde{U}_{\mu\nu}(t, x) = G_{\mu\rho}^a(t, x) G_{\nu\rho}^a(t, x) - \frac{1}{4} \delta_{\mu\nu} G_{\rho\sigma}^a(t, x) G_{\rho\sigma}^a(t, x) \tag{1.73}$$

$$\tilde{E}(t, x) = \frac{1}{4} G_{\mu\nu}^a(t, x) G_{\mu\nu}^a(t, x) \tag{1.74}$$

which are UV finite for $t > 0$. Most importantly they can be expanded in terms of renormalized local operators of increasing dimensions; namely we have

$$\tilde{U}_{\mu\nu}(t, x) = \alpha_{\tilde{U}}(t) \left(T_{\mu\nu}^R(x) - \frac{1}{4} \delta_{\mu\nu} T_{\rho\rho}^R(x) \right) + O(t) \tag{1.75}$$

$$\tilde{E}(t, x) = \langle \tilde{E}(t, x) \rangle_0 + \alpha_{\tilde{E}}(t) T_{\rho\rho}^R(x) + O(t) \tag{1.76}$$

where $T^R_{\mu\nu}$ is the renormalized energy-momentum tensor in the original gauge theory, the higher-dimensions operators are suppressed for small flow time t and the expansion coefficients $\alpha_{\tilde{U}}(t)$ and $\alpha_{\tilde{E}}(t)$ can be computed perturbatively (see ref. [72]). We can then rearrange eqs. (1.75) and (1.76) so that we can finally define a consistent energy-momentum tensor at finite t

$$T_{\mu\nu}(x,t) = \frac{1}{\alpha_{\tilde{U}}(t)}\tilde{U}_{\mu\nu}(t,x) + \frac{\delta_{\mu\nu}}{4\alpha_{\tilde{E}}(t)}\left(\tilde{E}(t,x) - \langle\tilde{E}(t,x)\rangle_0\right) \qquad (1.77)$$

which has the desired property

$$T^R_{\mu\nu} = \lim_{t\to 0} T_{\mu\nu}(x,t). \qquad (1.78)$$

Since $T_{\mu\nu}(x,t)$ is UV-finite and does not depend on the regularization scheme, it can be computed on the lattice. The actual computation follows this procedure: firstly the gauge configurations are created on the lattice, then the gradient flow equations are solved up to flow times in the window $a \ll \sqrt{8t} \ll T^{-1}$ or $\Lambda^{-1}_{\mathrm{QCD}}$. These values of t are chosen as to suppress finite lattice spacing, finite volume and nonperturbative corrections, respectively. The operators of eqs. (1.75)-(1.76) are constructed and evaluated on the flowed field configurations and finally the extrapolations first to $a \to 0$ and then to $t \to 0$ are performed.

The thermal observables can be easily extracted from the renormalized energy-momentum tensor: for example the trace anomaly (1.42) is

$$\Delta(T) = \epsilon - 3p = -\langle T^R_{\mu\mu}(x)\rangle \qquad (1.79)$$

and the entropy density (1.40) times the temperature is

$$sT = \epsilon + p = -\langle T^R_{00}(x)\rangle + \frac{1}{3}\sum_{i=1}^{3}\langle T^R_{ii}(x)\rangle \qquad (1.80)$$

where the expectation value includes also the average over all lattice sites x.

1.4 A review of lattice results for the equation of state

Nowadays several research groups are continuously improving the results for the equation of state not only in QCD, but in a variety of QCD-like theories too. A lot of attention is still focused on results from the pure gauge sector, which is the object of high-precision studies that are able to reach increasingly high temperatures well above T_c. The large scale study of ref. [6] presented results with small errors for the SU(3) theory equilibrium thermodynamics on very large set of temperatures, thus improving considerably from the seminal work of ref. [4]; data for the trace anomaly is presented in fig. 1.2.

In this work the integral method [36] was used to compute the pressure; the only difference with respect to the usual methodology is in the way the trace of the energy-momentum is computed. Instead of simply computing the plaquette difference of eq. (1.48), one takes

$$\left(\frac{\Delta(T)}{T^4} - \frac{1}{16}\frac{\Delta(T/2)}{(T/2)^4}\right) + \left(\frac{1}{16}\frac{\Delta(T/2) - \Delta(0)}{(T/2)^4}\right) \qquad (1.81)$$
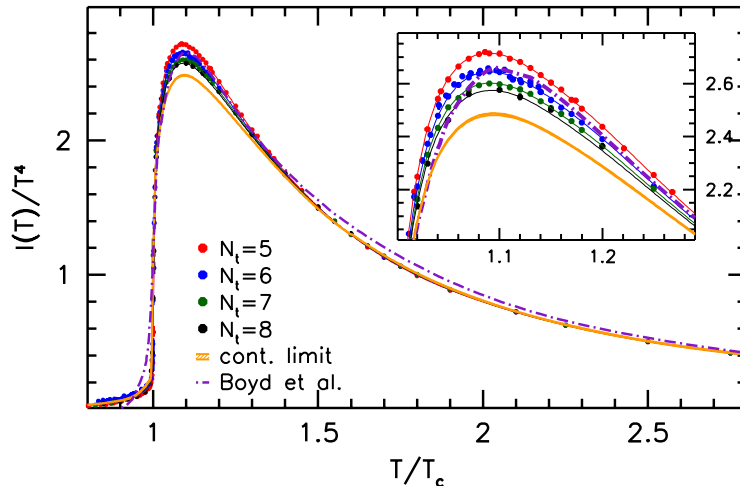
Figure 1.2: Results for the trace of the energy-momentum tensor in units of T^4 from ref. [6] computed with a variant of the integral method (see section 1.3.1). The yellow solid line represents the continuum extrapolation, the violet dash-dotted line indicates older results of ref. [4]; the complete set of results goes up to temperatures $T \sim 1000 T_c$.

in which the term on the left is computed at a certain β on $(2N_s)^3 \times N_t$ and $(2N_s)^3 \times 2N_t$ lattices, respectively; the term on the right is computed instead on $N_s^3 \times N_t$ and N_s^4 lattices at another β', such that the lattice spacing is twice the one associated with β. In this way the physical spatial volume is always the same in all simulations: the reason for this methodology lies in the fact that the trace anomaly depends on the volume in the vicinity of T_c and in this way one can avoid simulating enormous lattices of size $(2N_s)^4$ at zero temperature.

More recently, a new determination in a slightly smaller temperature range has been presented in ref. [7] using shifted boundary conditions (see section 1.3.3), again with high accuracy; the results are presented in fig. 1.3.

We note that these two calculations agree quite well with each other with a notable exception: in the region corresponding to the peak in the trace anomaly a relevant discrepancy can be observed, as well represented in fig. 1.4; similar discrepancies are also present in related equilibrium observables such as pressure, energy density and entropy density. Here, the Padè interpolation of results obtained with shifted boundary conditions (green line) agrees well with the well-known determination of ref. [4] but not with the more recent one of ref. [6].

While we will not attempt in this section a thorough discussion on the reason underlying this non-negligible disagreement, we merely observe that the determination of the SU(3) equation of state, albeit not strictly an open problem anymore, may still be subject to some systematic errors which, in turn, might depend on the methodology used to compute it. Thus, we stress the fact that the equation of state of the SU(3) pure gauge theory is a perfect benchmark for any new proposals of methods for the computation of thermodynamic equilibrium observables: indeed, it could also be used to understand if potential systematics are present in other methods. We will return on the thermodynamics of the SU(3) Yang-Mills theory in chapter 5, where a novel determination of the equation of state, performed with a
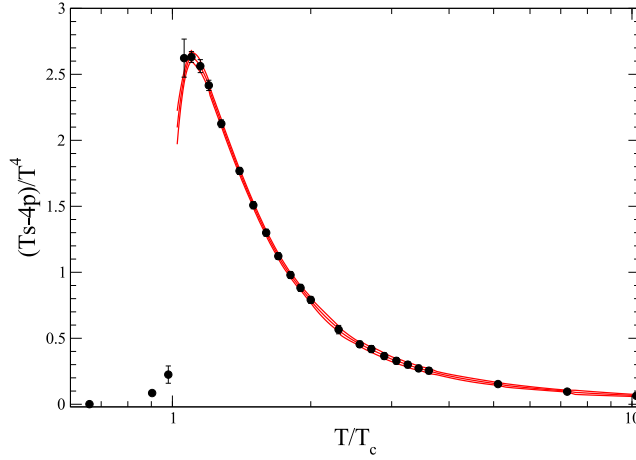
Figure 1.3: Continuum-extrapolated results for the trace anomaly Δ/T^4 (black points) obtained in ref. [7] using shifted boundary conditions (see section 1.3.3). Results are available up to $T \sim 250T_c$.
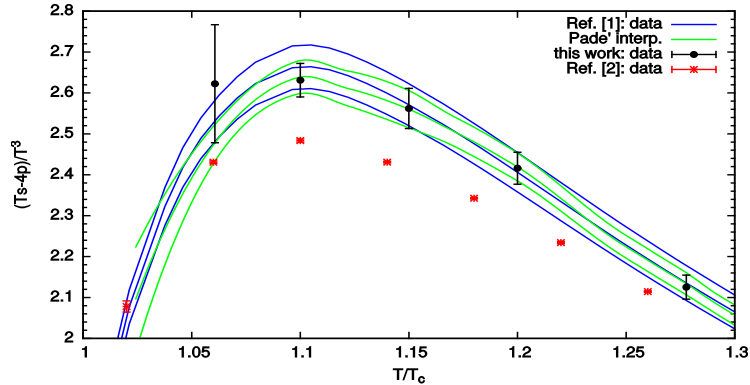
Figure 1.4: Continuum-extrapolated results in the $T_c < T < 1.3T_c$ region for the trace of the energy-momentum tensor Δ/T^4 obtained in ref. [6] (red points), ref. [7] (black points) and ref. [4] (blue line). Image taken from ref. [76].

method based on nonequilibrium transformations, will be presented.

Finally, we would like to mention some cutting-edge results in the computation of the equation of state for full QCD, with 2+1 and 2+1+1 dynamical quark flavors such as the work of ref. [77] and ref. [78], the latter of which is also reported in fig. 1.5.

Enormous progress has been achieved in the last 20 years, both in terms of computational power and of algorithmic advancements: this has led to an incredible push to overcome apparently insurmountable obstacles, such as the inclusion of the charm quark as a dynamical degree of freedom in the simulations. We refer to the respective papers for a thorough discussion of statistical errors, systematic effects

(a) Trace anomaly

(b) Pressure
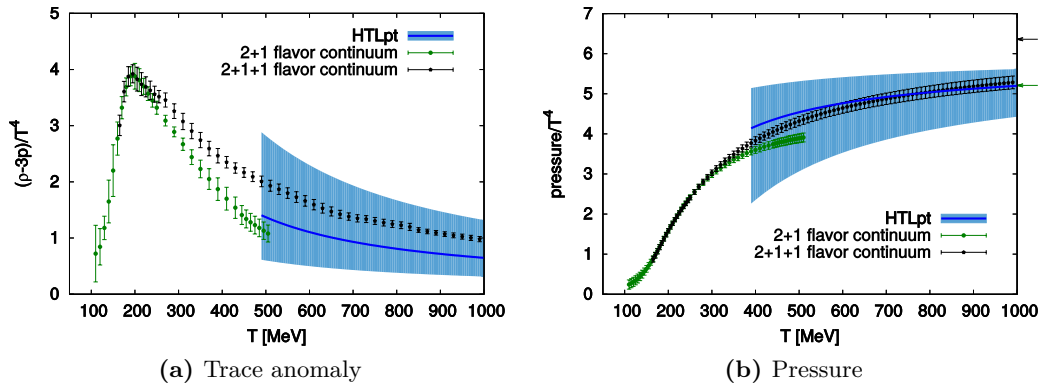
Figure 1.5: Lattice results of the equation of state in QCD with 2+1+1 quark flavors from ref. [78], along with a comparison with the prediction of hard thermal loop (HTL) resummed perturbation theory. Left: results for the trace of the energy-momentum tensor in units of T^4 for 2+1 (green dots) and 2+1+1 (black dots) dynamical quark flavors and the HTL prediction (blue line), up to temperatures of $T \sim 1000$ MeV. Right: same as left figure, but presenting results for the pressure p in units of the temperature to the fourth; the arrows on the right side indicate the Stefan-Boltzmann limit.

and comparison with hard thermal loop (HTL) predictions.

Chapter 2

Hagedorn spectrum in the $SU(2)$ and $SU(3)$ gauge theories

Numerical simulations on the lattice have proven to be an invaluable tool in the investigation of the thermodynamic properties of strongly-interacting theories: recent results of the last decade reached a high degree of precision, allowing for accurate comparisons with other approaches, such as phenomenological models and effective theories. In particular, the determination of the equation of state provides precious information on several aspects of the theory under analysis: the study presented in this chapter, based on the work of refs. [11, 12], will show how recent progress for the thermodynamics of pure gauge $SU(2)$ and $SU(3)$ theories in the confining phase is a perfect tool for the investigation of the glueball spectrum for large masses. Indeed, the numerical results will be described through the use of a non-interacting glueball gas, provided that, in addition to the glueball spectrum computed on the lattice, the heavier states are included with the use of a string-inspired Hagedorn spectrum.

This approach has actually a very long history, since its roots must be searched in the work of R. Hagedorn in the '60s: in the first part of this chapter, contained in section 2.1, we will review the original statistical bootstrap model and its more modern counterpart, the hadron resonance gas (HRG) model. In particular section 2.1.2 will be devoted to a short review of recent comparisons of HRG model predictions with cutting-edge lattice results. The second part of this chapter will be entirely focused on the work of ref. [11] with several in-depth analyses of many different aspects of this study. Firstly, in section 2.2.1, we will review the scale setting computation for the $SU(2)$ pure gauge theory, which serves as a preliminary work needed also for the accurate determination of the temperatures; then the numerical results from nonzero temperature lattice simulations will be presented in section 2.2.2. In section 2.2.3 we will analyse the description of Yang-Mills thermodynamics in terms of a non-interacting glueball gas, comparing analogies and differences with respect to the HRG model. Then the string-inspired model needed for the glueball spectrum will be reviewed (also from a historical point of view) in sections 2.2.4 and 2.2.5 and used to describe the thermodynamics of $SU(2)$ in the vicinity of the deconfinement transition. Eventually, in section 2.2.6 the results for the $SU(2)$ and $SU(3)$ gauge theories will be compared and the full predictive power of the model will be tested.

The last part of this chapter (section 2.3) will be focused on the excluded-volume approach for the study of Yang-Mills thermodynamics, presented in ref. [12], which represents an alternative approach for an high-precision description of the lattice results of the equation of state.

2.1   Statistical bootstrap and the HRG model

Before the advent of the quark model and, later, of quantum chromodynamics, a truly novel approach for the description of the strong interaction was proposed by the German physicist R. Hagedorn more than 50 years ago [13, 79–82]; a recent review of the most important results by Hagedorn can be found in ref. [83]. His model was introduced to provide a quantitative description of the production of the huge number of heavy hadronic particles that were first observed in particle accelerators during the '50s and '60s. The basic idea was extremely simple: any of the heavy hadrons is nothing but a resonant particle of lighter particles, which in turn were composed of even lighter particles, until one reaches the lightest one, i.e. the pion. This is best explained by Hagedorn himself in his famous words [13]

> "a fireball consists of fireballs, which in turn consist of fireballs, and so on..."

The concept that Hagedorn had in mind can be tackled in a quantitative way by first analyzing a similar mathematical problem, namely looking at how many ways can be used to partition an integer number n into ordered partitions. Paraphrasing Hagedorn, we want to think of "large integers, made of smaller integers..."; indeed, a way of solving this basic problem can be found in a recursive way:

$$\rho(n) = \delta(n-1) + \sum_{k=2}^{n} \frac{1}{k!} \prod_{i=1}^{k} \rho(n_i) \, \delta\left(\sum_i n_i - n\right)$$

this goes by the name of *bootstrap equation* and immediately shows the idea of *self-similarity*, i.e. how the structure of $\rho(n)$ is explained by $\rho(n)$ itself.

The physical system Hagedorn wanted to describe was one with lighter particles in motion and with a total energy that corresponds to the mass of the heavy particle. The bootstrap equation for a particle of mass m in this case becomes

$$\rho(m, V_0) = \delta(m - m_0) + \sum_N \frac{1}{N!} \left(\frac{V_0}{(2\pi)^3}\right)^{N-1} \int \prod_{i=1}^{N} \mathrm{d}m_i \, \mathrm{d}^3 p_i \, \rho(m_i) \, \delta\left(\sum_i p_i - p\right)$$

$$(2.1)$$

that is the basis of the *statistical bootstrap model*. V_0 is the "composition volume", that indicates the intrinsic range of strong interactions. The statistical bootstrap equation was solved analytically shortly afterwards by Nahm [84], giving

$$\rho(m, V_0) \sim m^{-3} e^{m/T_\mathrm{H}} \tag{2.2}$$

which highlights the typical exponential-like behaviour that will be ubiquitous throughout this chapter. The T_H parameter is the well-known *Hagedorn temperature*, given by

$$\frac{V_0 T_\mathrm{H}^3}{2\pi^2} \left(\frac{m_0}{T_\mathrm{H}}\right)^2 K_2\left(\frac{m_0}{T_\mathrm{H}}\right) = 2\ln 2 - 1 \tag{2.3}$$

where K_2 is a modified Bessel function of the second kind of index 2; we will analyze the physical meaning of T_{H} later in this section. Let us simply add that if V_0 scales like the inverse of the pion mass, namely $V_0 \simeq 4\pi/(3m_\pi^3)$, then an approximate estimate of the Hagedorn temperature is $T_{\mathrm{H}} \simeq 150$ MeV.

The self-similar picture painted by the statistical bootstrap model implies that the spectrum of hadronic particles is composed by heavier and heavier states, whose number grows exponentially with the mass and is approximately given by the density $\rho(m, V_0)$. This peculiar behaviour has clearly huge implications in the thermodynamics of strong interacting particles: in order to see this we consider a gas of identical scalar particles of mass m, whose grand partition function is

$$\mathcal{Z}(T, V) = \sum_N \frac{1}{N!} \left[\frac{V}{(2\pi)^3} \int \mathrm{d}^3 p \, e^{-\sqrt{p^2 + m^2}/T} \right]^N$$

that after some manipulation becomes

$$\ln \mathcal{Z}(T, V) = \frac{VTm^2}{2\pi^2} K_2 \left(\frac{m}{T} \right);$$

note that V is the physical volume and is not to be confused with V_0. The next crucial step is to consider a gas of hadronic resonances of mass m_i, in which all the interactions are included in processes of resonance formation: this means approximating a strongly-interacting gas with a *non-interacting* gas that contains all possible hadronic species of a certain mass m with the respective degeneracies. If we put this consideration in a more mathematical form we have that

$$\ln \mathcal{Z}^{\mathrm{TOT}}(T, V) = \sum_i \rho(m_i) \ln \mathcal{Z}_i(T, V) = \sum_i \frac{VTm_i^2}{2\pi^2} \rho(m_i) K_2 \left(\frac{m_i}{T} \right) \qquad (2.4)$$

where the index i represents a specific hadronic mass. The weight $\rho(m_i)$ indicates how many resonance states of mass m_i exist and it is here where the statistical bootstrap model enters. Indeed, if we start from eq. (2.2), then we approximate the modified Bessel function with

$$K_2 \left(\frac{m}{T} \right) \sim \sqrt{\frac{T}{m}} e^{-m/T}$$

and finally we replace the sum $\sum_i$ of eq. (2.4) with an integral, we will have at the end the following partition function

$$\ln \mathcal{Z}^{\mathrm{TOT}}(T, V) = \frac{VT}{2\pi^2} \int \mathrm{d}m \, m^2 \rho(m) K_2 \left(\frac{m}{T} \right)$$

$$\sim VT^{3/2} \int \mathrm{d}m \, m^{-3/2} \exp \left(\frac{m}{T_{\mathrm{H}}} - \frac{m}{T} \right). \qquad (2.5)$$

This grand partition function is clearly divergent for $T \to T_{\mathrm{H}}$: in the original interpretation of Hagedorn, T_{H} was a limiting temperature dictated by the strong interaction. The physical meaning of this apparent behaviour lies in the fact that the average energy of the constituents of the resonance gas (i.e., the ratio between the energy density and the number of constituents) does not increase with T. This is

because the increase in energy is not used to increase the momenta of the constituents, but the number of species instead.

However, this interpretation of the Hagedorn temperature has been surpassed at the beginning of the '70s after the advent of QCD as the theory of strong interactions: indeed, T_{H} is not anymore a limiting temperature, but it signals the presence of a phase transition instead. In ref. [85] N. Cabibbo and G. Parisi proposed a generalized version of the statistical bootstrap model, in which the solution of eq. (2.1) was slightly different, namely

$$\rho(m, V_0) \sim m^{\alpha-3} e^{m/T_{\mathrm{H}}};$$

indeed, they showed that at T_{H} the model has a second order phase transition for $\alpha < 1$. For temperatures higher than T_{H}, the thermodynamic quantities still have finite values, but the physical representation provided by eq. (2.5) is not valid anymore. Indeed, nowadays we have solid evidence that at extremely high temperatures or densities a new state of matter, usually denoted as quark-gluon plasma, appears. This does not mean that the model elaborated by Hagedorn has been forgotten though: it will be shown in section 2.1.1 that the original intuition has been recovered and reformulated, albeit in a somewhat different manner, in the form of the hadron resonance gas model.

2.1.1   The hadron resonance gas model

In the previous paragraphs we have seen how the statistical bootstrap model had great influence in the description of the hadronic state of matter in the '60s, but was substantially obsolete by the time QCD was established as the correct theory of strong interactions. However, in the last decades great advancements in the nonperturbative computation of the QCD equation of state on the lattice produced high-precision results for a variety of thermodynamic quantities and in general for the phase diagram of strongly-interacting matter. This provided an opportunity to bring the original intuition of Hagedorn alive again, since the resonance gas allows for a simple and solid framework that can be compared to lattice data in the confining phase and even used to describe them. This more modern approach, which in the literature goes by the name of hadron resonance gas (HRG) model, is somewhat different from the statistical bootstrap model, since there is no need of a density of states as the one of eq. (2.2) to describe most of the hadronic resonance spectrum. In fact, since thousands of mesonic and baryonic resonances have been discovered and studied with great detail in multiple particle accelerator experiments, their masses are well known and their single contribution to thermodynamic quantities can be computed exactly. Still, the original approach of considering a *non-interacting* gas of hadrons is intact and it has been used with great success to describe numerical lattice results obtained from first principles.

As in the idea of Hagedorn (see eq. (2.4)), the pressure of the HRG model can be written as a sum of independent contributions from non-interacting hadron resonances:

$$p^{\mathrm{HRG}}(T) = \sum_{M \in \mathrm{mesons}} p_M(T, V, \mu_{X^a}, m_M) + \sum_{B \in \mathrm{baryons}} p_B(T, V, \mu_{X^a}, m_B) \qquad (2.6)$$

where in principle one takes into account not only the contribution of mesons and

baryons, but also from other states such as glueballs, tetraquarks and further exotic resonances. In particular, the pressure of a meson M or of a baryon B is

$$p_{M,B}(T, V, \mu_{X^a}, m_{M,B}) = \frac{T}{V} \log Z_{M,B}(T, V, \mu_{X^a}, m_{M,B}). \qquad (2.7)$$

The partition function of a single non-interacting particle i can be written in $d = 3$ spatial dimensions as

$$\log Z_i(T, V, \mu_{X^a}, m_i) = \frac{V g_i \eta_i}{2\pi^2} \int_0^\infty dp\, p^2 \log\left(1 + \eta_i z_i e^{-E_i/T}\right) \qquad (2.8)$$

where V is the volume of the system and T its temperature, m_i is the mass of the particle i, g_i its degeneracy factor and η_i distinguishes between mesons (bosons, $\eta = -1$) and baryons (fermions, $\eta = 1$). E_i is the energy of the species i

$$E_i = \sqrt{m_i^2 + p^2}$$

and z_i its fugacity

$$z_i = \exp\left(\frac{\sum_a X_i^a \mu_{X^a}}{T}\right); \qquad (2.9)$$

X_i^a represent all the possible conserved charges associated to the species i, including baryon number B, electric charge Q and strangeness S and μ_{X^a} represents the respective chemical potential. The resulting prediction for the pressure (eq. (2.6)) has a direct dependence only on the temperature T and on the chemical potential μ_{X^a} associated to the conserved charge X^a.

2.1.2 Comparison with lattice data

The HRG model has been very successful in describing thermodynamic quantities in the confining regime, as reported in a variety of papers in the last few decades [86–91]. The values for the masses of hadron states and resonances are taken from the experimental results (i.e. from the particle data group) and hundreds of hadron resonances are usually included in the total prediction. The exact number depends on the mass cut, that is the threshold above which no further resonances are taken into account in the HRG prediction and that is usually put at very high energies.

Very recent comparisons between high-precision data for the equation of state of QCD with dynamical quarks and the HRG model include those in refs. [77, 92]. In fig. 2.1 two different determinations of the equation of state for 2+1 quark flavors are presented along with the prediction of the HRG model: excellent agreement is found up to very high temperatures of the order of the pseudo-critical temperature $T_c \sim 155$ MeV. For the determination of ref. [77] all states below 2.5 GeV were included.

We also mention that in recent years the hadron resonance gas model has been used successfully for precision studies of the fluctuation of conserved charges in the hot QCD matter. We refer to refs. [89, 93–96] for more details and recent advancements.

The excellent agreement between lattice results and the resonance gas on a variety of thermodynamic observables provides clear evidence that hadronic resonances are

(a) Wuppertal-Budapest collaboration [92]

(b) HotQCD collaboration [77]
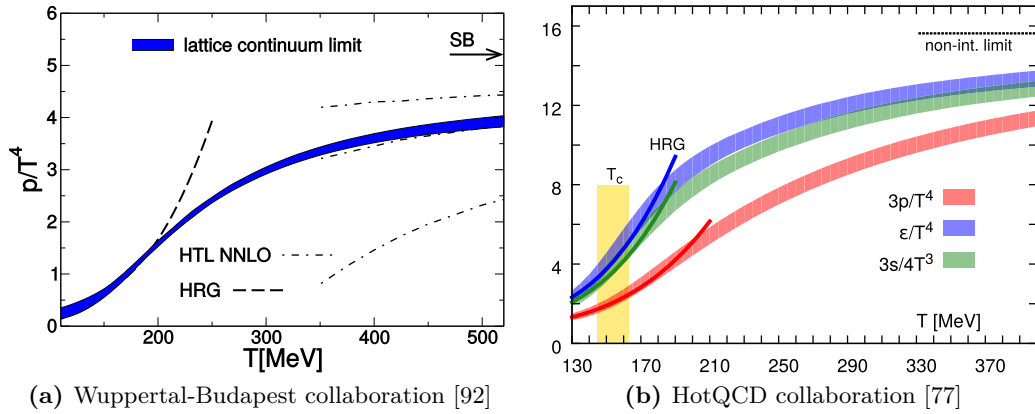
Figure 2.1: Comparison between the lattice results of the equation of state in QCD with 2+1 quark flavors and the hadron resonance gas (HRG) model prediction by two different collaborations. Left: results for the pressure in units of T^4 (blue band) and the HRG prediction (dashed line) from ref. [92]. Right: results for pressure p (red band), energy density ϵ (blue band) and entropy density s (green band), with the respective HRG predictions (solid lines), from ref. [77].

essential degrees of freedom near the deconfinement phase transition. On the other hand, it is an excellent question to ask if lattice results can give any hints on the composition of the high-lying hadronic states of the spectrum when compared with the HRG model prediction. Indeed, several papers (see for example refs. [97–102]) already put forward the possibility of including the contribution of still undiscovered states (which can be non-negligible very close to T_c) via an interpolation of high-precision lattice results. We also point out the work of refs. [103, 104] on the value of T_{H} in QCD.

As we will see in the section 2.2, a similar analysis, albeit on a larger scale, can be done for the pure gauge theory with no quarks: in this case the spectrum of the relevant states in the confining phase (i.e. glueballs) is much less known than the mesonic or baryonic one. In such case the original idea of a Hagedorn spectrum will be derived from a string model perspective and extensively used in the comparison with lattice data.

2.1.3 Ideal relativistic Bose and Fermi gases

We end this section by briefly reviewing the computation of thermodynamic quantities in the framework of an ideal relativistic Bose or Fermi gas, which are crucial in calculating HRG predictions and which will be extensively used later in this chapter. We start by considering the partition function Z of an ideal relativistic Bose or Fermi gas in d spatial dimensions

$$\log Z = V g \, \eta \frac{\Omega_d}{(2\pi)^d} \int_0^\infty \mathrm{d}p \, p^{d-1} \log \left(1 + \eta e^{-\sqrt{m^2+p^2}/T} \right) \qquad (2.10)$$

where as before $\eta = -1$ for bosons and $\eta = +1$ for fermions, m is the mass of the bosonic/fermionic particle, g is its degeneracy factor and Ω_d is the $d-$dimensional

solid angle

$$\Omega_d = \frac{2\pi^{\frac{d}{2}}}{\Gamma\left(\frac{d}{2}\right)} \tag{2.11}$$

and for simplicity the fugacity has been set to 1. Integrating by parts and expanding using the geometric series yields

$$\log Z = \frac{V g \eta}{d T} \frac{\Omega_d}{(2\pi)^d} \sum_{n=1}^{\infty} \int_0^{\infty} \mathrm{d}p \, \frac{p^{d+1}}{\sqrt{m^2 + p^2}} (-\eta)^n e^{-n\sqrt{m^2+p^2}/T}$$

and setting $\cosh u = \sqrt{1 + \frac{p^2}{m^2}}$ gives

$$\log Z = \frac{m^{d+1} V g}{d T} \frac{\Omega_d}{(2\pi)^d} \sum_{n=1}^{\infty} \int_0^{\infty} \mathrm{d}u \, (-\eta)^{n+1} \exp\left(-n\frac{m}{T} \cosh u\right) \sinh^{d+1} u$$

$$= \frac{2V g}{T} \left(\frac{m^2}{2\pi}\right)^{\frac{d+1}{2}} \sum_{n=1}^{\infty} \left(\frac{T}{n\,m}\right)^{\frac{d+1}{2}} (-\eta)^{n+1} K_{\frac{d+1}{2}}\left(n\frac{m}{T}\right) \tag{2.12}$$

where $K_\nu(z)$ is the modified Bessel function of the second kind of index $\nu = \frac{d+1}{2}$ and argument $z = n\frac{m}{T}$:

$$K_\nu(z) = \frac{\sqrt{\pi}\left(\frac{z}{2}\right)^\nu}{\Gamma(\nu + 1/2)} \int_0^{\infty} \mathrm{d}u \, e^{-z\cosh u} \sinh^{2\nu} u. \tag{2.13}$$

The pressure p can now be calculated: from eq. (1.39) we have

$$p = \frac{T}{V} \log Z = 2g \left(\frac{m^2}{2\pi}\right)^{\frac{d+1}{2}} \sum_{n=1}^{\infty} \left(\frac{T}{n\,m}\right)^{\frac{d+1}{2}} (-\eta)^{n+1} K_{\frac{d+1}{2}}\left(n\frac{m}{T}\right) \tag{2.14}$$

while for the (internal) energy density ϵ of eq. (1.41) we have

$$\epsilon = \frac{T^2}{V} \frac{\partial \log Z}{\partial T} = d \cdot p + 2g \left(\frac{m^2}{2\pi}\right)^{\frac{d+1}{2}} \sum_{n=1}^{\infty} \left(\frac{T}{n\,m}\right)^{\frac{d-1}{2}} (-\eta)^{n+1} K_{\frac{d-1}{2}}\left(n\frac{m}{T}\right) \tag{2.15}$$

obtained using the property

$$\frac{\partial K_\nu(z)}{\partial z} = -K_{\nu-1}(z) - \frac{\nu}{z} K_\nu(z). \tag{2.16}$$

The trace of the energy-momentum tensor Δ (see eq. (1.42)) can then be easily written as

$$\Delta = \epsilon - d \cdot p = 2g \left(\frac{m^2}{2\pi}\right)^{\frac{d+1}{2}} \sum_{n=1}^{\infty} \left(\frac{T}{n\,m}\right)^{\frac{d-1}{2}} (-\eta)^{n+1} K_{\frac{d-1}{2}}\left(n\frac{m}{T}\right) \tag{2.17}$$

and remarkably the trace Δ in d dimension is related to the pressure in $d - 2$ dimensions via

$$\Delta_d = \frac{m^2}{2\pi} p_{d-2}. \tag{2.18}$$

Using an asymptotic expansion of the functions K_ν, which is valid for large z we have that

$$K_\nu(z) \simeq \sqrt{\frac{\pi}{2z}} e^{-z} \left[1 + \frac{4\nu^2 - 1}{8z} + O\left(\frac{1}{z^2}\right) \right] \tag{2.19}$$

and the pressure p and the trace anomaly Δ become respectively

$$p = Tg \left(\frac{T\,m}{2\pi}\right)^{\frac{d}{2}} \sum_{n=1}^{\infty} \frac{(-\eta)^{n+1}}{n^{\frac{d}{2}+1}} \exp\left(-n\frac{m}{T}\right) \left[1 + \frac{d(d+2)}{8n} \frac{T}{m} + \mathcal{O}\left(\frac{T^2}{n^2 m^2}\right) \right] \tag{2.20}$$

and

$$\Delta = mg \left(\frac{T\,m}{2\pi}\right)^{\frac{d}{2}} \sum_{n=1}^{\infty} \frac{(-\eta)^{n+1}}{n^{\frac{d}{2}}} \exp\left(-n\frac{m}{T}\right) \left[1 + \frac{d(d-2)}{8n} \frac{T}{m} + \mathcal{O}\left(\frac{T^2}{n^2 m^2}\right) \right]. \tag{2.21}$$

2.2   The $\mathrm{SU}(2)$ and $\mathrm{SU}(3)$ equation of state in the confining regime

The study via lattice simulations of the equation of state of $\mathrm{SU}(N)$ pure gauge theories (both in $D = 2+1$ and $3+1$ spacetime dimensions) has been the object of several works in recent years [5, 6, 9–12, 105, 106], also for what concerns the investigation of the confining phase. In particular in its seminal paper [5] Meyer provided the first consistent description of thermodynamic observables of the $\mathrm{SU}(3)$ pure gauge theory in proximity to T_c in terms of a gas of glueball with a string-inspired Hagedorn spectrum. This kind of approach was very successful and indeed it was followed and expanded by further studies: in particular the work of ref. [9] examined the thermodynamics of $\mathrm{SU}(N)$ theories (with $N = 2, 3, 4, 6$) in $D = 2+1$ dimensions, showing once again the efficacy in describing the equation of state of several gauge models within this simple framework.

In this section we will analyse the recent work of ref. [11] which focuses on the $\mathrm{SU}(2)$ and $\mathrm{SU}(3)$ gauge theories in $3+1$ dimensions. It is of the utmost importance to stress that this work is not simply meant as a refinement of the original analysis by Meyer: in fact, even if the analysis of the $N = 3$ case is a crucial and essential part of this work, the most important aspect is devoted to the comparison with the $N = 2$ Yang-Mills theory. Indeed the theory with $\mathrm{SU}(2)$ gauge symmetry presents some crucial properties which are instrumental when using a string-inspired Hagedorn spectrum to describe its thermodynamics, as it will be shown in detail later. In particular, since the representations of the $\mathrm{SU}(2)$ group are (pseudo-)real, only glueball states with charge-conjugation quantum number $C = +1$ exist; on the other hand $\mathrm{SU}(3)$ allows also $C = -1$ states: this will have crucial repercussions in the proximity of the transition. Moreover, the deconfinement transition itself is first order for $\mathrm{SU}(3)$, while it is second order for $\mathrm{SU}(2)$: again, this will significantly change the estimate of the Hagedorn temperature T_H, that is a crucial parameter of the model.

2.2.1 Setting the scale

As already mentioned in section 1.2.3, knowing the precise physical value of the lattice spacing a (in units of some physical quantity) used in Monte Carlo simulations is of the utmost importance: in particular for nonzero temperature calculations, it allows for an accurate scan of the temperatures simulated on the lattice. The spacing a can be computed in different ways: one possibility is to do so non-perturbatively via the interquark potential $V(r)$, which can be computed on the lattice using

$$V(r) = -\frac{1}{L_t} \ln G(r); \tag{2.22}$$

where $L_t = aN_t$ is the physical extent of the compactified ("temporal") dimension and $G(r)$ is the Polyakov loop correlator, as defined in eq. (1.26). A physical quantity which can be used to link a to its value in physical units is the string tension σ: it can be extracted via a fit of the potential $V(r)$ using the following functional form:

$$aV(r) = a\sigma r + aV_0 - \frac{\pi a}{12r} \tag{2.23}$$

where the string tension σ is the coefficient of the linear term in r and the aV_0 term is an additive constant which takes into account an overall renormalization. Eq. (2.23) is in the form of the phenomenological Cornell potential [107] (that is, $V \sim \sigma r + \alpha/r$), but it is actually justified by a slightly more modern approach. Indeed, the interquark potential can be described in the framework of the effective string theory for the flux tube and in particular in an expansion in the low-energy, long-string limit. It was realized long ago [108] that the coefficient of the $1/r$ term, which is usually denoted in the literature as the "Lüscher term", is fixed unambiguously by the transverse fluctuations of the flux tube. Further terms in the $1/r$ expansion can be fixed using the underlying symmetries of the effective string action (see for example [109, 110]).

Another way which can be pursued to set the scale and which is more appropriate for intermediate distances (as opposed to the potential V, which requires larger interquark distances r) was introduced in ref. [111] and extensively applied in ref. [112] for the SU(3) Yang-Mills theory. This method is based on the calculation of the interquark force $F(r)$, which at finite lattice spacing it is defined as

$$F(r_{\mathrm{I}}) = \frac{V(r) - V(r-a)}{a} \tag{2.24}$$

in which r_{I} is an improved distance chosen such that the force of eq. (2.24) corresponds to the one in the continuum at tree level; for further details on the computation of r_I we refer to ref. [112], in which the methods of ref. [113] were generalized to three dimensions. In order to connect the spacing a we need a new scale that is directly related to the interquark force. In the literature two such possibilities have been proposed and extensively used, these being the length scales r_0 and r_1, which are defined as

$$r_0^2 F(r_0) = 1.65 \tag{2.25}$$

and

$$r_1^2 F(r_1) = 1. \tag{2.26}$$

The limit of large r which was needed for the computation of σ is not necessary anymore, and this makes this method a viable possibility for the scale setting in QCD with dynamical quarks, where string breaking hampers the computation of σ.

In ref. [11] the string tension σ was used to set the scale. The interquark potential $V(r)$ was computed from Polyakov loop correlators on lattices with $L_t = 32a$ up to distances of $r = 16a$, using the improved distances r_I of ref. [112]. The results of the fit for simulations performed with several values of the Wilson parameter $\beta = 4/g^2$ are presented in table 2.1 and showed on fig. 2.2 along with lattice data.

Table 2.1: Results for the string tension (in units of the inverse squared lattice spacing, third column) σa^2 at different values of the inverse coupling $\beta = 4/g^2$ (first column), calculated in ref. [11] by fitting the quark-antiquark potential $V(r)$ as a function of the tree-level improved interquark distance r_I [112] to eq. (2.23). The potential was extracted from Polyakov loop correlators on lattices of temporal extent $L_t = 32a$. The minimal distances (reported in the second column, in units of a) for the fits to eq. (2.23) follow the prescription $r\sqrt{\sigma} > 1$. The "perimeter-like" term aV_0 (fourth column) and the χ^2_{red} values of the fit (fifth column) are also reported.

β	$r_{\min}/a$	σa^2	aV_0	χ^2_{red}
2.27	2.889	0.157(8)	0.626(14)	0.6
2.30	2.889	0.131(4)	0.627(30)	0.1
2.32	3.922	0.115(6)	0.627(32)	2.3
2.35	3.922	0.095(3)	0.623(20)	0.2
2.37	3.922	0.083(3)	0.621(18)	1.0
2.40	4.942	0.068(1)	0.617(10)	1.4
2.42	4.942	0.0593(4)	0.613(5)	0.1
2.45	4.942	0.0482(2)	0.608(4)	0.4
2.47	4.942	0.0420(4)	0.604(5)	0.3
2.50	5.954	0.0341(2)	0.599(2)	0.1
2.55	6.963	0.0243(13)	0.587(11)	0.2
2.60	7.967	0.0175(16)	0.575(16)	0.3

Finally, in order to accurately set the scale in a non-perturbative way, one needs an appropriate functional form which relates the string tension (in units of the inverse lattice spacing squared) and the Wilson parameter β. In the work performed in ref. [11], the interpolation of the values of the logarithm of σa^2 was done using a cubic polynomial fit. Namely, following ref. [112], the functional form

$$\log(\sigma a^2) = \sum_{j=0}^{n_{\mathrm{par}}-1} a_j(\beta - \beta_0)^j \qquad (2.27)$$

was used, where $n_{\mathrm{par}} = 4$ represents the number of free parameters to be determined from the fit and $\beta_0 = 2.4$. The resulting parameters are $a_0 = -2.68$, $a_1 = -6.82$, $a_2 = -1.90$ and $a_3 = 9.96$ respectively, while the reduced χ^2 of the fit yields $\chi^2_{\mathrm{red}} = 0.01$; the final scale setting function is represented in fig. 2.3 along with the lattice results for σa^2. We recall that eq. (2.27) is not the only possibility, as other functional forms, such as that proposed in ref. [114], have been used in the past. Now, using the scale setting relation of eq. (2.27) we are able to give a correct estimate of
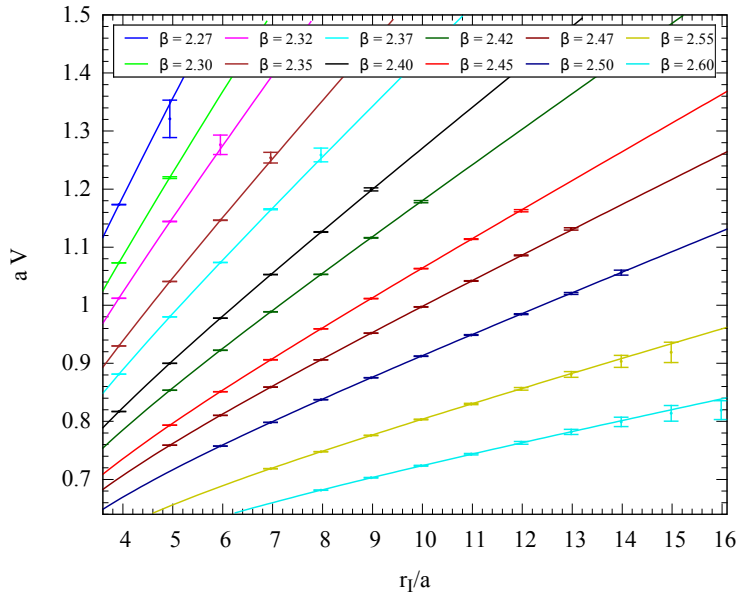
Figure 2.2:   Results for the interquark potential computed in ref. [11] are showed for different values of the improved distance r_I and for several values of the Wilson parameter β (different colors). The corresponding fits to the functional form of eq. (2.23) are also presented.

the lattice spacing a in units of $\sqrt{\sigma}$; thus we can also express the temperature as

$$\frac{T}{\sqrt{\sigma}} = \frac{1}{a\sqrt{\sigma}N_t} \tag{2.28}$$

and change the lattice spacing to tune T with great accuracy.

2.2.2   Numerical results for the SU(2) equation of state

Most of the computational effort of ref. [11] was devoted to the non-perturbative computation of the equation of state in the confining region of the SU(2) pure gauge theory. In order to do so, the integral method (for more details we refer to section 1.3.1) was used: the primary observable is the trace of the energy-momentum tensor (eq. (1.48) which is computed starting from plaquette expectation values at finite and zero temperature at the same value of the lattice spacing. A comprehensive review of the details of the runs performed for the studies of ref. [11] and ref. [12] is presented in table 2.2.

In order to express the results in terms of the temperature in units of the critical (deconfinement) temperature, the value

$$\frac{T_c}{\sqrt{\sigma}} = 0.7091(36) \tag{2.29}$$

computed in ref. [115] was used.
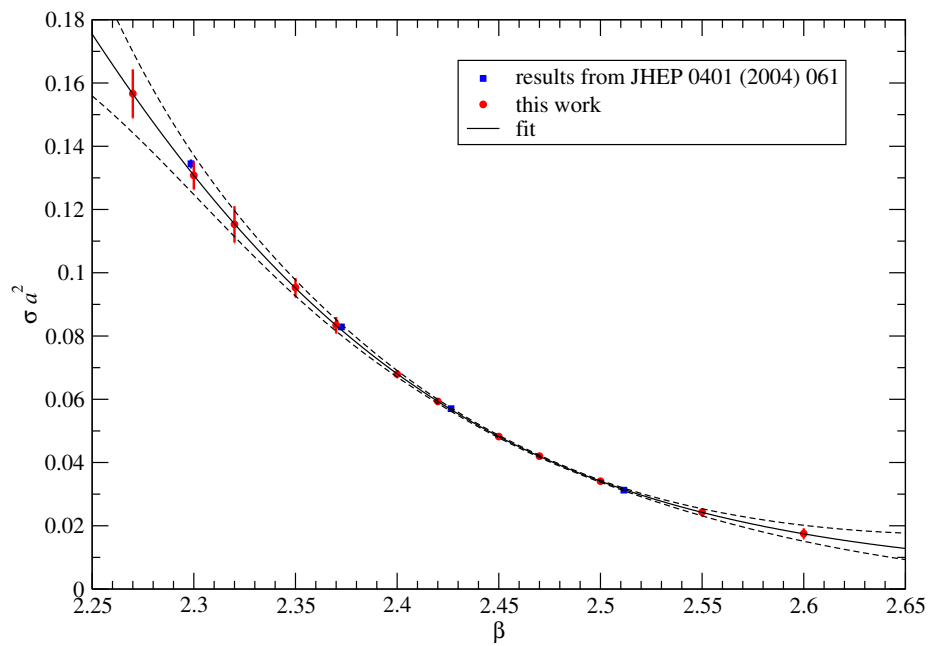
Figure 2.3: Values of the string tension in lattice units obtained in ref. [11] (red circles) are showed along with those reported in ref. [115] (blue squares). The solid black curve represents the interpolation to the functional form of eq. (2.27); associated uncertainties are shown by the dashed black lines.

Table 2.2: Setup of lattice simulations performed in ref. [11] and ref. [12]. Nonzero-temperature plaquette expectation values are evaluated on lattices of sizes $N_t \times N_s^3$ (first two columns), while those at $T = 0$ are obtained from simulations on lattices of sizes $\widetilde{N}^4$ (third column), at the same β values. This is done for n_β (fourth column) values of the inverse coupling β, in the interval reported in the fifth column. The total number of the thermalized configurations created in these runs is reported in the last two columns. The sample measured at $N_t = 5, 6, 8$ has been used in ref. [11], while $N_t = 7, 10$ and additional $N_t = 8$ results have been presented in ref. [12].

N_t	N_s	$\widetilde{N}$	n_β	β range	n_{conf} at finite T	n_{conf} at $T = 0$
5	60	32	17	$[2.25, 2.3725]$	1.5×10^5	1.5×10^5
6	72	40	25	$[2.3059, 2.431]$	1.5×10^5	1.5×10^5
7	80	40	12	$[2.38, 2.476]$	1.5×10^5	10^5
8	80	40	14	$[2.42, 2.516]$	1.5×10^5	10^5
10	96	40	12	$[2.51, 2.58]$	6×10^4	10^5

The results for the trace of the energy-momentum tensor at finite lattice spacing for temporal sizes $N_t = 5, 6, 7, 8, 10$ in the low-temperature confined phase are showed in fig. 2.4.
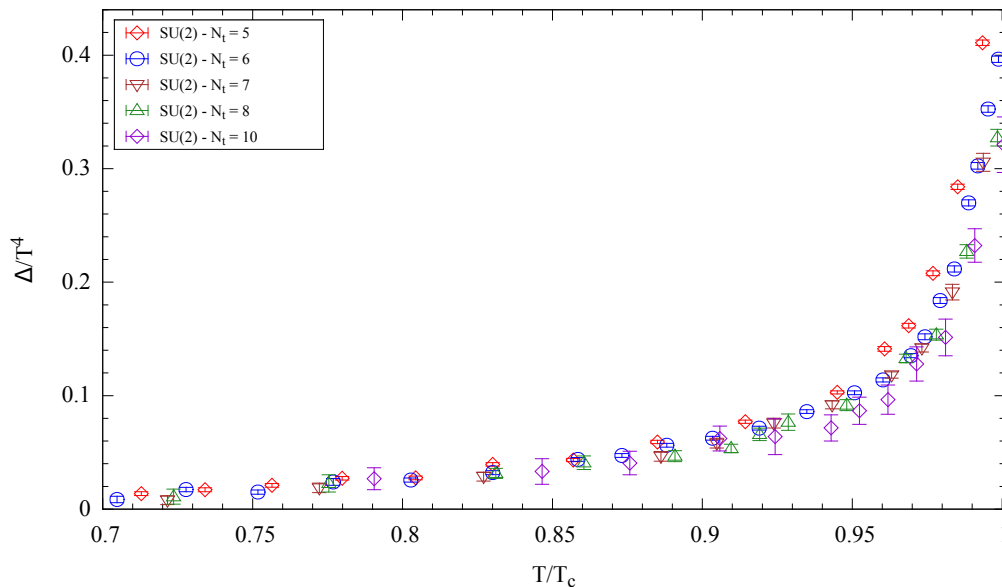
Figure 2.4: Complete lattice results for the trace of the energy-momentum tensor in the SU(2) Yang-Mills theory in units of T^4 from simulations with $N_t = 5, 6, 8$ from ref. [11] and $N_t = 7, 10$ (plus further $N_t = 8$) results from ref. [12].

2.2.3 The glueball gas prediction

The hadron resonance gas model has been widely successful in describing several thermodynamic observables computed non-perturbatively on the lattice, as reviewed

in section 2.1 in some detail. Thus, it is reasonable to think that a similar kind of approach applies for pure gauge theories, albeit with a completely different spectrum and at different temperatures. Since no mesons or baryons are present in Yang-Mills theory, the only states contributing to the thermodynamics of the confining phase are the so-called *glueballs*. As in the case of the HRG model for mesons and baryons, we are under the assumption that such states are weakly interacting with each other and so we will examine the case of a non-interacting gas of glueballs: this consideration is supported by both theoretical [116] and experimental [117] arguments. A possible generalization of this approach that includes some sort of interaction between glueball states has been proposed in ref. [12] and it will be discussed in section 2.3.

From an experimental point of view, the search for glueballs is still an open issue and these states remain elusive: thus, there is no experimental input for their masses, in contrast to what happens for the rich hadronic spectrum of full QCD. However, the very existence of glueball states is a typical non-perturbative prediction of QCD and indeed the glueball spectrum can and has been studied on the lattice with great detail for decades. Recent computations in unquenched QCD include those performed in refs. [118–120]. The masses computed from Monte Carlo simulations will be used as an input for the prediction of a non-interacting glueball gas described in terms of a free relativistic Bose gas (see section 2.1.3).

In practice, taking eqs. (2.14) and (2.17) and setting $d = 3$ we can write down the pressure as

$$p = \frac{m^2 T^2}{2\pi^2} \sum_{n=1}^{\infty} \frac{1}{n^2} K_2 \left(\frac{nm}{T} \right) \tag{2.30}$$

and the trace of the energy-momentum tensor as

$$\Delta = \frac{m^3 T}{2\pi^2} \sum_{n=1}^{\infty} \frac{1}{n} K_1 \left(\frac{nm}{T} \right). \tag{2.31}$$

Using eq. (2.19) and rewriting p and Δ adimensionally in units of T^4 we have that

$$\frac{p}{T^4} = \left(\frac{m}{2\pi T} \right)^{3/2} \sum_{n=1}^{\infty} \frac{1}{n^{5/2}} \exp\left(-\frac{nm}{T} \right) \left[1 + \frac{15T}{8nm} + \mathcal{O}\left(\frac{T^2}{n^2 m^2} \right) \right] \tag{2.32}$$

and

$$\frac{\Delta}{T^4} = \frac{m}{T} \left(\frac{m}{2\pi T} \right)^{3/2} \sum_{n=1}^{\infty} \frac{1}{n^{3/2}} \exp\left(-\frac{nm}{T} \right) \left[1 + \frac{3T}{8nm} + \mathcal{O}\left(\frac{T^2}{n^2 m^2} \right) \right]; \tag{2.33}$$

we observe that the expansion in T/m is justified by the fact that for SU(N) theories $T_c \ll m_{0^{++}}$, that is, the glueball masses are much larger than any of the temperatures of interest in the confining phase. We remark that the subleading terms of the sum over the index n appearing in eqs. (2.32) and (2.33) are exponentially suppressed and the series will be truncated accordingly.

The spectrum used to calculate the glueball gas prediction for the SU(2) pure gauge theory is the one computed in ref. [121], which we report in table 2.3. The prediction for the trace of the energy-momentum tensor $\Delta(T)$ of the first, lightest state with quantum numbers $J^{PC} = 0^{++}$, for temperatures in the range between $0.65 T_c$ and T_c, is showed in fig. 2.5 (dotted line). If we include all the glueball states

with masses smaller than $2m_{0^{++}}$, i.e. all the states below the so-called *two-particle threshold*, the total contribution is the one showed with a dashed line in fig. 2.5. In practice, the contribution to a certain quantity (in this case, Δ) is the sum of the contribution of the single states, i.e.

$$\frac{\Delta(T)}{T^4} = \sum_{m_i < m_{th}} (2J_i + 1) \frac{\Delta(m_i, T)}{T^4} \qquad (2.34)$$

where J_i is the spin of the i-th glueball and $2J_i + 1$ its spin degeneracy. In ref. [11] the mass threshold was set to $m_{\mathrm{th}} = 2m_{0^{++}}$: this somewhat arbitrary choice will be discussed later in detail. Suffice it to say that including also the remaining states of table 2.3 would induce a change in $\Delta(T)$ that would be hardly relevant and essentially negligible both at low ($T \ll T_c$) and high ($T \sim T_c$) temperatures.

Table 2.3: SU(2) glueball spectrum computed via lattice simulations in ref. [121]. Note the absence of $C = -1$ states.

J^{PC}	$m/\sqrt{\sigma}$
0^{++}	3.74(12)
2^{++}	5.62(26)
0^{-+}	6.53(56)
2^{-+}	7.46(50)
1^{++}	10.2(5)
3^{++}	9.0(7)

Table 2.4: SU(3) glueball spectrum below the two-particle threshold, computed on the lattice in ref. [122]. In this case, there is no degeracy between $C = +1$ and $C = -1$ states.

J^{PC}	$m/\sqrt{\sigma}$
0^{++}	3.347(68)
0^{++*}	6.26(16)
2^{++}	4.891(65)
2^{++*}	6.54(22)
0^{-+}	5.11(14)
2^{-+}	6.32(11)
1^{+-}	6.06(15)

From a qualitative analysis of the glueball gas prediction it emerges that this phenomenological approach works rather well at relatively low temperatures, i.e. around $0.7T_c$, where the dominant contribution of the 0^{++} state can describe well the lattice results. With the inclusion of the states below the two-particle threshold the glueball gas prediction can be considered acceptable at higher temperatures, up to $T \sim 0.8T_c$. When approaching the transition, the glueball gas clearly fails to properly account for the sudden increase in the value of the trace anomaly: this is to be contrasted to what happens when the HRG model is used to describe QCD thermodynamics up to temperatures very close to the pseudo-critical one (for details see section 2.1.2). Still, we can observe how the contribution from the heavier states included in the dashed line of fig. 2.5 becomes more and more relevant when the temperature increases, when compared with the contribution of the lightest state only, which is increasing very slowly. This is the first hint that we are missing the contribution of heavy glueball states in our analysis, whose contribution could be the dominant one when describing thermodynamic quantities up to T_c.

The crucial observation is that, for a gas of non-interacting bosons, observables of interest like the pressure and the trace anomaly possess an exponentially-like decreasing behaviour in m/T coming from the modified Bessel functions K_ν. This explains why including also the states computed on the lattice which are heavier
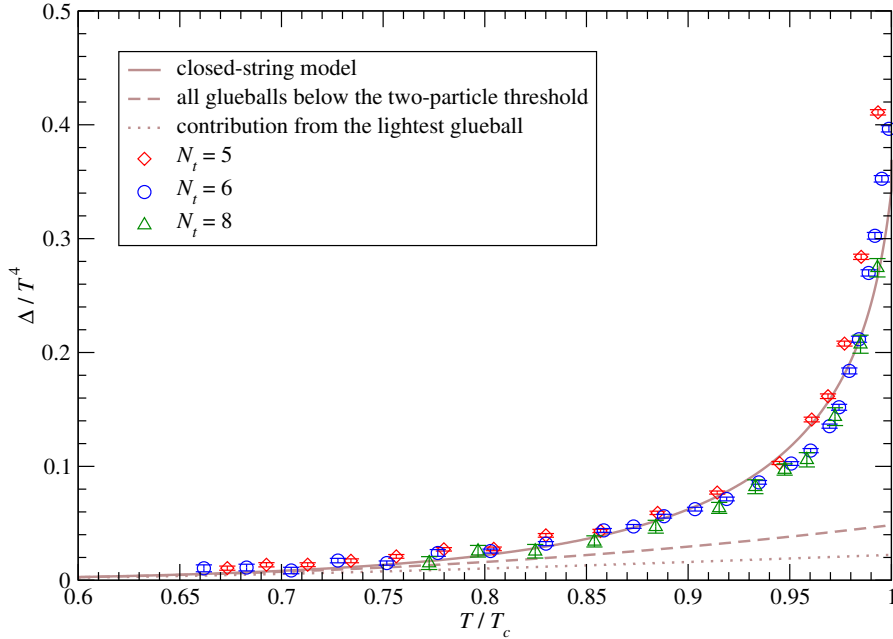
Figure 2.5: Comparison between lattice results for the trace anomaly in SU(2) Yang-Mills theory from simulations with $N_t = 5$, 6 and 8 of ref. [11] and the behavior expected for a gas of non-interacting massive glueballs in the confining phase ($T < T_c$). The dotted line corresponds to the contribution of the lightest state only, which has quantum numbers $J^{PC} = 0^{++}$. The dashed line includes all the low-lying glueballs whose masses are smaller than the threshold associated to the appearance of two 0^{++} glueballs (taken from [121]). The solid line corresponds to the case in which we included also the contribution from high-lying states, described by a bosonic string model. The trace of the energy-momentum tensor Δ is displayed in units of the fourth power of the temperature, and is plotted as a function of T/T_c.

than the mass threshold $2m_{0^{++}}$ (and that are not reported in tables 2.3 and 2.4) have a negligible contribution to the equation of state: the reason lies in the fact that there are simply too few of them to make an overall relevant contribution. Thus, the only hope of describing the sharp increase in the lattice data for $\Delta(T)$ is to have a glueball spectrum in which the number of states increases *exponentially* with m.

This kind of spectra goes generally by the name of *Hagedorn* spectra, since they are of the same form of the solution of the statistical bootstrap equation, eq. (2.2). As we will see in the section 2.2.5, such a spectrum arises naturally if an effective string theory for the flux tube is used to describe heavy glueball states. More generally, a Hagedorn-like spectrum arises whenever (heavy) hadrons are described in terms of long, thin and string-like color flux tubes: mesonic states are modeled in terms of *open* bosonic strings while glueballs by *closed* bosonic strings. In section 2.2.4 we

will briefly review previous attempts to describe the glueball spectrum using closed string models.

2.2.4 Closed string models for glueballs

In the past there have been many attempts to describe the full glueball spectrum with different phenomenological models: among the most relevant and successful ones there are bag-type models [123, 124] and string-inspired models [125, 126]. In this section we will briefly review a few qualitative aspects of the latter: in particular, the original model [125] by Isgur and Paton aimed at modeling glueball states as "rings of glue", that is tubes of chromoelectric flux which close on themselves. Then, such flux tubes can be described in terms of closed bosonic string states: more precisely, each phononic configuration corresponds to a particular glueball state.

The starting point is a closed string of flux, that is a loop of fundamental color flux, whose thickness is neglected: the glueball spectrum is obtained by finding its energy eigenstates after quantization. If we take a circular flux string of radius ρ and bare string tension σ_b, its bare energy is

$$E_b = 2\pi\sigma_b\rho; \tag{2.35}$$

fluctuations of the string are decomposed into phonons of frequency m/ρ, whose contribution depends on their total number M

$$E_{\text{phonons}} = \frac{M}{\rho} = \frac{1}{\rho} \sum_{m=2} m\left(n_m^+ + n_m^-\right) \tag{2.36}$$

where n_m^+ and n_m^- are the number of phonons with angular momentum $J = \pm m$ respectively. After renormalization the energy corresponding to left-moving and right-moving modes can be written as

$$E(n_m^+, n_m^-) = 2\pi\rho\sigma - \frac{13}{6\rho} + \frac{1}{\rho} \sum_{m=2} m\left(n_m^+ + n_m^-\right) \tag{2.37}$$

where the divergent contribution to vacuum energy has been partly absorbed in the renormalized string tension σ and the rest makes up the second term of eq. (2.37).

The first correction to this approach concerns the finite width of the flux tube: it is not a one-dimensional object but rather a tube of width of the order of $1/\sqrt{\sigma}$. This implies that phononic excitations for small closed string radii are suppressed: one way to incorporate this in the model is by a "fudge factor" $F(\rho)$ that multiplies the energy contribution of the string excitations. Putting all together we have

$$E_M(\rho) = 2\pi\rho\sigma + \frac{M+\gamma}{\rho}F(\rho) \tag{2.38}$$

where $\gamma = -13/6$, M is the total phonon number and in the original model $F(\rho) = 1 - e^{-f\rho}$.

We recall that flux tubes (for $N > 2$) carry an arrow, that is they have an orientation which indicates their charge conjugation number C: in the original model these two sectors do not mix and thus the $C = \pm 1$ spectra are perfectly degenerate (contrarily to what is observed in spectra computed on the lattice, see table 2.4).

More recently, there have been some attempts at improving the original Isgur and Paton model [126, 127] by including a set of modifications that is able to replicate with good success the glueball spectrum computed on lattice (such as that of table 2.4), in particular in $D = 2 + 1$ dimensions. Among the possible generalizations of this model we mention: closed strings not in the fundamental representation, an effective elasticity for the flux tube, a more elaborate suppression of phonons at small distances (that is, a different fudge factor $F(\rho)$) and also mixing mechanisms to split the $C = \pm 1$ degeneracy in the spectrum.

Crucially, the consequence which is most relevant for what concerns the high-lying glueball spectrum (and thus, as we will see, thermodynamics) is the following: as we will see, the string model indicates that there exist an infinite tower of radially excited states of increasing mass for each phonon combination. In the next section we will analyse how to extract a good description of the glueball density of states in the framework of the Nambu-Gotō bosonic string action.

2.2.5   A Hagedorn spectrum from effective string theory

The starting point of the simple approach that has been used in ref. [11] (and, previously, in refs. [5, 6, 9]) is the consideration that glueballs can be described, in the limit of large masses, by the Nambu-Gotō action for closed bosonic strings. This is not an arbitrary assumption, as the Nambu-Gotō action provides an excellent approximation of the actual effective string action, up to small corrections in the long-string limit; this has been confirmed by a large body of works in recent years [109, 110, 128–133].

In this context, the spectrum of closed bosonic strings in D spacetime dimensions reads

$$m^2 = 4\pi\sigma \left(N_L^\perp + N_R^\perp - \frac{D-2}{12} \right) \tag{2.39}$$

where σ is the string tension, and $N_{L,R}^\perp$ are integer numbers which account for the contribution of left- and right-moving transverse excitations ("phonons") along the string. The $-(D-2)/12$ term arises from the zero-point energy and it can be neglected in the large masses limit. We recall also that $N_L^\perp = N_R^\perp \equiv N^\perp$ for closed strings.

A crucial aspect of the closed string spectrum is that the degeneracy of these states is given by the number of *partitions* $\pi(N_{L,R}^\perp)$ (similarly to what happens in the original statistical bootstrap model, section 2.1). In our case, we have also to generalize the number of partitions for excitations on $D - 2$ transverse directions, which we denote by $\pi_{D-2}(N_{L,R}^\perp)$. For a pedagogical derivation of these results and of string thermodynamics in general we refer to Chapter 22 of ref. [134]. In the case of closed strings, the density of states is expressed through the product of the partitions of left-moving and right-moving phonons:

$$\rho_D(N_L^\perp, N_R^\perp) = \pi_{D-2}(N_L^\perp)\pi_{D-2}(N_R^\perp) \tag{2.40}$$

but, since $N_L^\perp = N_R^\perp \equiv N^\perp$, we have

$$\rho_D(N^\perp) = \left[\pi_{D-2}(N^\perp) \right]^2. \tag{2.41}$$

Now, using the Hardy-Ramanujan asymptotic formula for $\pi_b(n)$ [135], suitably generalized for b transverse directions

$$\pi_b(n) \simeq \sqrt{\frac{1}{2n}} \left[\frac{b}{24\,n} \right]^{\frac{b+1}{4}} \exp\left(2\pi\sqrt{\frac{bn}{6}} \right) \tag{2.42}$$

we can derive the explicit result for the spectral density as a function of the number of excitations $N^\perp$:

$$\rho_D(N^\perp) = \frac{1}{2\,N^\perp} \left[\frac{D-2}{24\,N^\perp} \right]^{\frac{D-1}{2}} \exp\left(4\pi\sqrt{\frac{(D-2)N^\perp}{6}} \right). \tag{2.43}$$

In the end we want $\hat{\rho}(m)$, i.e. the spectral density as a function of the mass m. It is simply defined via

$$\hat{\rho}_D(m)\mathrm{d}m = \rho_D(N)\mathrm{d}N \tag{2.44}$$

where the relation between $\mathrm{d}m$ and $\mathrm{d}N$ is found differentiating eq. (2.39). We have

$$\mathrm{d}N = \frac{m}{4\pi\sigma}\mathrm{d}m \tag{2.45}$$

so that now eq. (2.43) becomes

$$\hat{\rho}_D(m) = \frac{m}{4\pi\sigma} \frac{4\pi\sigma}{m^2} \left[\frac{(D-2)\pi\sigma}{3m^2} \right]^{\frac{D-1}{2}} \exp\left(\sqrt{\frac{\pi(D-2)}{3\sigma}}m \right). \tag{2.46}$$

When studying string thermodynamics, a peculiar behaviour appears: if we consider a system of closed bosonic string and we increase its (internal) energy we reach a regime in which the temperature of the system does not increase anymore. This is quite similar to what happens in the statistical bootstrap model we reviewed in section 2.1, and indeed this temperature goes by the name of *Hagedorn temperature* and is defined as

$$T_\mathrm{H} = \sqrt{\frac{3\sigma}{(D-2)\pi}} \stackrel{D=4}{\simeq} 0.691\sqrt{\sigma}. \tag{2.47}$$

Now, if we insert the Hagedorn temperature T_H the spectral density in D spacetime dimensions as a function of the mass m is

$$\hat{\rho}_D(m) = \frac{1}{T_\mathrm{H}} \left(\frac{\pi(D-2)}{3} \right)^{D-1} \left(\frac{T_\mathrm{H}}{m} \right)^D \exp\left(\frac{m}{T_\mathrm{H}} \right) \tag{2.48}$$

and for $D = 3 + 1$ it becomes

$$\hat{\rho}(m) = \frac{1}{m} \left(\frac{2\pi T_\mathrm{H}}{3m} \right)^3 \exp\left(\frac{m}{T_\mathrm{H}} \right). \tag{2.49}$$

This is the output of this string-inspired phenomenological model, as it describes, in the approximation of large masses, the exponential-like behaviour of the glueball spectrum provided that they can be effectively modelled as relativistic closed bosonic strings. The Nambu-Gotō action can be trusted completely as a reliable effective description of the glueball spectrum: in this case eq. (2.49) has *no free parameters*

and is fully predictive. However, one can simply take eq. (2.49) as a phenomenological input in which the Hagedorn temperature T_{H} can be fitted from numerical lattice results or it can be fixed in other ways. We will comment later and in section 2.3 on these options.

From a thermodynamic point of view, eq. (2.49) can be extensively used to account for the exponentially large number of heavy glueball states whose crucial contribution is missing when approaching the deconfinement transition from below. Thus, we can add a new term to the prediction given by eq. (2.34) using eq. (2.49). Namely we have that the trace of the energy-momentum tensor of a non-interacting glueball gas is

$$\frac{\Delta(T)}{T^4} = \sum_{m_i < m_{\mathrm{th}}} (2J_i + 1) \frac{\Delta(m_i, T)}{T^4} + n_C \int_{m_{\mathrm{th}}}^{\infty} \mathrm{d}m' \, \hat{\rho}(m') \frac{\Delta(m', T)}{T^4} \qquad (2.50)$$

where the first term on the right hand side accounts for the known glueball states whose masses have been computed on the lattice, while the second term considers the contribution of heavy glueball states of mass m' and degeneracy $\hat{\rho}(m')$. Similar formulas can be written for energy and entropy densities ϵ and s and for the pressure p.

Some important points concerning eq. (2.50) must be discussed before proceeding to a comparison with the numerical lattice results. Firstly, the mass threshold has been fixed to $m_{\mathrm{th}} = 2m_{0^{++}}$ as done previously in eq. (2.34): this value has a symbolic significance, since it is the energy threshold above which a massive glueball can decay into two 0^{++} states. More importantly, however, it represents a good practical estimate of the threshold below which glueball spectra computed via lattice simulations are reliable, in the sense that they are able to identify correctly all states with certain quantum numbers. Conversely, the spectral density $\hat{\rho}(m)$ clearly is not able to describe the masses of low-lying glueball states below such threshold, since its predictive power is limited to the limit of large m. For a reliable description of the light glueball spectrum one has to consider generalizations of the Isgur and Paton model [125] that have been mentioned in section 2.2.4. As a final remark we stress the fact that, since the exact value of m_{th} is somewhat arbitrary, any prediction of the glueball gas obtained with eq. (2.50) must be checked for small changes of m_{th} in order to keep systematic errors under control.

Another very important aspect of eq. (2.50) is the presence of the n_C factor: this term is necessary to take into account the fact that for $N \geq 3$ (where N is the number of colors of the SU(N) gauge theory under investigation) glueball states can have both charge conjugation number $C = +1$ and $C = -1$. This fact has a clear interpretation in terms of the closed string model: in the $N \geq 3$ case closed flux tubes can have two possible orientations and thus it is necessary to insert a double degeneracy in the spectral density by putting $n_C = 2$. We will see in section 2.2.6 how this further degeneracy will play a crucial role in the thermodynamics close to T_c. On the other hand, for the SU(2) case that was first considered in ref. [11], only glueballs with $C = +1$ are admitted, since all irreducible representation of the group are real or pseudoreal, and thus $n_C = 1$. Indeed, the low-lying glueball spectrum calculated in ref. [121] presents only $C = +1$ states (as can be seen in table 2.3), which is to be contrasted to the SU(3) one (see, for example, table 2.4).

The last comment is concerning the value of the Hagedorn temperature T_{H} to use in eq. (2.49): as already mentioned, in the most general approach this has to be considered as a free parameter of the model. However, the deconfinement transition for the SU(2) pure gauge theory is of the second order: this means that we can identify it with the Hagedorn transition itself and safely put $T_{\mathrm{H}} = T_c$, by using the value of eq. (2.29). This fixes all the parameters of the model, which is now fully predictive, since no fit to lattice data whatsoever is needed to compute each contribution of eq. (2.50).

Finally, we are in a position to describe the results for the equation of state of the SU(2) Yang-Mills theory in terms of a gas of non-interacting massive glueballs: as it can be seen in fig. 2.5 the solid curve manages to describe in a remarkable way the sudden increase that is observed in lattice data up to temperature very close to T_c. This result confirms how the exponential-like Hagedorn spectrum predicted by the string model successfully accounts for all the heavy glueball states which are extremely important in the vicinity of the transition.

A similar comparison can be done for the pressure: following the integral method [36] (for details see section 1.3.1) the results for the trace anomaly can be integrated using eq. (1.49). In practice, the results for the trace anomaly were first interpolated and then integrated numerically: the resulting data can be seen in fig. 2.6 along with the glueball gas prediction for the lightest glueball (dotted line), for all states under the two-particle threshold (dotted line) and for the whole glueball spectrum (solid line). We would like to comment on the fact that usually, in order to compute $p(T)/T^4$ with the integral method, the integration constant $p(T_0)/T_0^4$ is needed; in the case of ref. [11] this was set using the glueball gas itself, which is clearly an excellent approximation at relatively low temperatures. Very good agreement is present also in this case, thus confirming that the equation of state of the SU(2) Yang-Mills theory in the confining phase can be very well described in terms of a gas of non-interacting glueballs, provided that a Hagedorn spectrum is used to take the contribution of heavy states into account.

A word of caution is needed before moving to the next section: the Hagedorn temperature in this case was set to be equal to the deconfinement temperature; not surprisingly the value of T_c (2.29) is remarkably close to that predicted by the Nambu-Gotō action (2.47), but still the difference is significant. This is immediately clear if eq. (2.47) is used, as the glueball gas prediction would be completely spoiled by the presence of an unphysical divergence of the SU(2) partition function *before* the deconfining transition. This fact is evidence of the limits of the closed string model when looking at the thermodynamics very close to T_c: a more detailed discussion is postponed to the end of section 2.2.6.

2.2.6   A comparison with SU(3)

It is very insightful to repeat the glueball gas study of lattice results for the equation of state in the case of the SU(3) Yang-Mills theory. The importance of this further analysis does not lie simply in the fact that the theory with $N = 3$ colors is closer to QCD from a theoretical point of view and thus it is more "physical" than the SU(2) model. Indeed, SU(3) represents an even more stringent test for the closed string model, since we have to consider also the contribution of $C = -1$ glueball
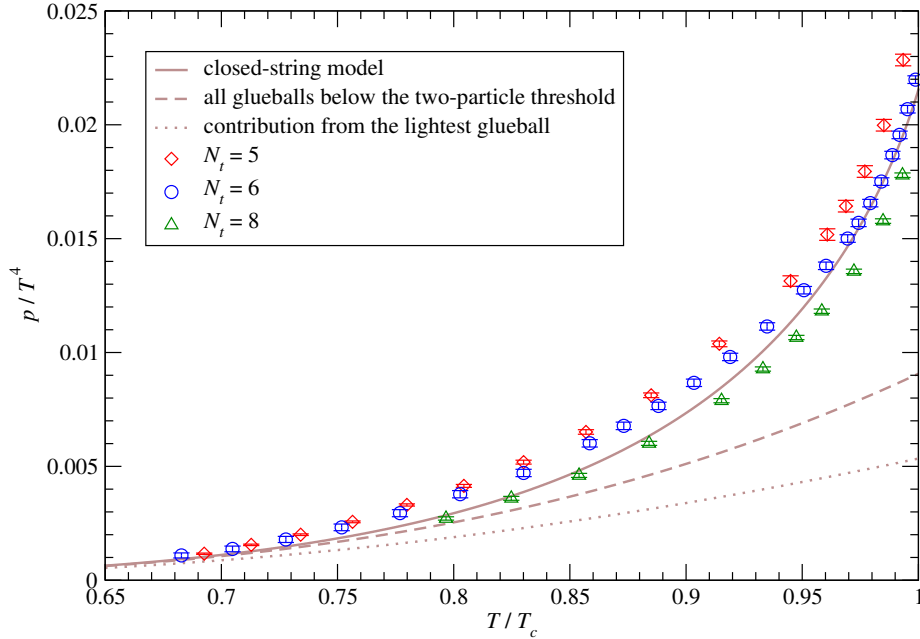
Figure 2.6: Same as in fig. 2.5, but for the pressure p in units of T^4.

states. Moreover the deconfinement transition is (weakly) first-order: this has been observed numerically on the lattice [4, 136]. The most important consequence of the first-order nature of the transition is that now $T_H \neq T_c$: this issue and the presence of $C = -1$ glueballs must be addressed by the string model.

First of all, in order to compute the prediction of the glueball gas in the same way it was done for SU(2), the value of the deconfinement temperature T_c and the masses of the low-lying glueball states are needed. The former is set to be the value computed in ref. [4], namely

$$\frac{T_c}{\sqrt{\sigma}} = 0.629(3); \tag{2.51}$$

we remark that actually this is not the only possible choice, with the value computed in ref. [115] being an alternative. However the recent, high-precision determination performed in ref. [137] agrees well with the older value of ref. [4], when the result is properly translated in units of the string tension. Even for what concerns the glueball spectrum a few different options are available, for example the one of ref. [138] or the one of ref. [122]. In ref. [11] the latter was chosen for the glueball gas prediction, following the original work on the Hagedorn spectrum of ref. [5]; we mention however that for example the analysis performed in ref. [6] used the first 12 glueballs of ref. [138].

We can now focus on the effective string model, and in particular on the aforementioned crucial differences with respect to the $N = 2$ case: to take $C = -1$ states into account, the charge conjugation degeneracy for the SU(3) prediction was set to $n_C = 2$ in ref. [11], while the Hagedorn temperature was fixed by the original Nambu-Gotō value of eq. (2.47) predicted by the effective string model. In practice we have that

$$T_{\mathrm{H}} = 1.098 T_c \qquad (2.52)$$

and thus the Hagedorn "transition" is located relatively far from the physical deconfinement temperature, which is to be contrasted with the SU(2) case ($T_{\mathrm{H}} = T_c$). On the whole the results were obtained again with no free parameters: as one can observe in fig. 2.7 there is a truly remarkable agreement with the lattice data already obtained in ref. [6] almost up to T_c.
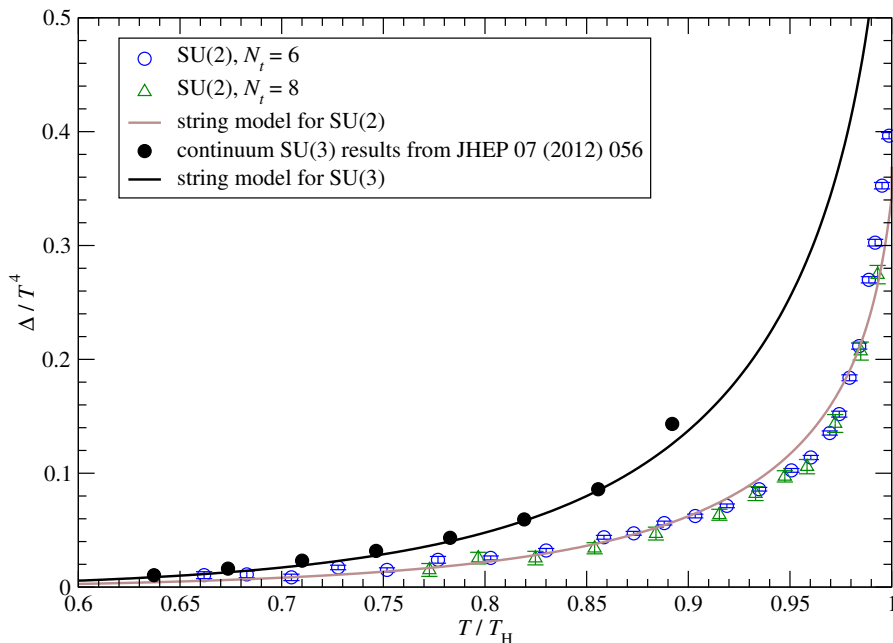
Figure 2.7: Comparison between the predictions of a free glueball gas, including the contribution from states modeled by a closed Nambu-Gotō string model, like in eq. (2.50), continuum-extrapolated data obtained in ref. [6] for SU(3) Yang-Mills theory and nonzero lattice spacing results for the SU(2) Yang-Mills theory (from simulations at finite lattice spacings corresponding to $N_t = 6$ and 8) obtained in ref. [11], as a function of T/T_{H}.

The results shown in fig. 2.7 are even more instructive when a comparison with SU(2) is performed: indeed, one can easily observe the doubling of the glueball spectrum at high temperatures both from the lattice data and the glueball gas prediction. This comparison is made much clearer by the fact that the data are

shown as a function of T/T_{H}: indeed, it is the value of the Hagedorn temperature that controls the exponential-like growth of the number of glueball states. Because of this, T_{H} represents the correct scale to use when representing lattice data and glueball gas predictions in the confining phase. However, when setting $n_C = 2$ in eq. (2.50) we are making a crude approximation, at best: this is because we are assuming that above the mass threshold m_{th} there is a perfect degeneracy between $C = +1$ and $C = -1$ states, which is clearly unlikely. A more sophisticate prediction for the glueball gas would take this into account by introducing for example another free parameter: such an approach was not taken into consideration in ref. [11] for the sake of simplicity and predictiveness of the string model.

We remark also that the glueball gas predictions both for $N = 2$ and $N = 3$ are robust under reasonable changes in the mass threshold m_{th}, which can be considered the only partially-free parameter in this model.

It is useful to review a few finer details to fully appreciate the difference between the two cases: first of all, the apparent "coexistence" of the Hagedorn and physical transitions makes a proper description of lattice data very close to T_c a little trickier. It is crucial to observe that the transition located at $T = T_c$ is in the same class of universality of the three-dimensional Ising model, as predicted by the Svetitsky-Yaffe conjecture [139]. This is in contrast with the closed string model, which at T_{H} predicts mean-field critical exponents; thus, technically it cannot be used up to T_c and even if the results present an interesting qualitative agreement to very high temperatures, a different mechanism must kick in in the proximity of the SU(2) deconfinement transition. Indeed, the work of ref. [11] is a semi-quantitative analysis, since no continuum extrapolation of lattice data was taken and no χ^2 tests were made to check quantitatively the reliability of the closed string model. More elaborate models can start from the observation of the existence of a string-like Hagedorn spectrum and, with the addition of phenomenologically motivated free parameters, they can try to explain with greater accuracy continuum-extrapolated numerical results from the lattice. One such attempt was made in ref. [12] and it will be reviewed in detail in section 2.3. On the other hand for SU(3) the Hagedorn temperature is placed deep in the deconfined phase, and it is not surprising that this case is somewhat easier to describe in terms of the string-model and that it does not apparently necessitates of further free parameters.

In conclusion we can affirm that these results are clear evidence of the presence of a Hagedorn spectrum for very massive glueballs, as it plays a crucial role in the glueball gas description of Yang-Mills thermodynamics in the confining phase. Indeed, in the proximity of the critical temperature a spectrum of the type of eq. (2.49) must be introduced in order to explain lattice results for the equation of state both in the $N = 2$ and $N = 3$ cases. Moreover, these studies also represent an indirect but very stringent test for the effective string theory in the description of the excitations of the chromoelectric flux tube: indeed a relativistic bosonic string model can predict with great accuracy the correct functional form of the density of glueball states: both the factors in front of the exponential in eq. (2.49) and the value of the T_{H} parameter.

2.3 An alternative approach: excluded-volume effects

In section 2.1 we reviewed the recent success of the hadron resonance gas model in describing several aspects of the thermodynamics of strongly-interacting matter in the confining phase. Indeed, in a rather simple way typical physical quantities such as the pressure p can be described in terms of a non-interacting gas of hadron resonances all of which contribute separately. If we generalize eq. (2.14) by including the nonzero chemical potential that appears in eq. (2.9), the pressure becomes

$$p^{\mathrm{HRG}} = \frac{T^2}{2\pi^2} \sum_i g_i m_i^2 \sum_{n=1}^{\infty} \frac{1}{n^2} \left[e^{n\mu_i/T} K_2\left(n\frac{m_i}{T}\right) - \frac{\eta_j + 1}{4} e^{2n\mu_i/T} K_2\left(2n\frac{m_i}{T}\right) \right]$$

(2.53)

where the factor η_i is -1 for bosons and $+1$ for fermions and the chemical potential for the i-th species μ_i is

$$\mu_i = \sum_a X_i^a \mu_{X^a} = b_i \mu_B + q_i \mu_Q + s_i \mu_S.$$

(2.54)

A possible improvement to the standard HRG approach is the inclusion of excluded-volume effects (see refs. [140–142]) that approximately model the repulsive interactions between resonances: a simple way to implement these is by a modification of the chemical potential μ_i itself which includes an additional term:

$$\tilde{\mu}_i = b_i \mu_B + q_i \mu_Q + s_i \mu_S - v_i p$$

(2.55)

where v_i denotes an "eigenvolume" parameter. This parameter takes the role of an effective volume which, assuming the resonances are hard, classical spheres (i.e. essentially neglecting quantum effects), can be written as

$$v_i = \frac{16\pi}{3} r_i^3$$

(2.56)

where the effective radius r_i appears. This approach can serve as a refinement of the HRG model predictions and has been applied successfully in the last few years [143–146]; in particular in comparison with lattice results the fits that included excluded volume effects generally yielded very good results.

In ref. [12], the investigation of hadronic excluded volume effects was extended to the particular case of pure gauge theories, which represent a somewhat clearer theoretical setup where high-precision lattice computations are easily available. Indeed the work of refs. [5, 9, 11, 105] described in section 2.2 showed how numerical lattice results for the Yang-Mills equation of state could give precious insight on the properties of the glueball spectrum: in a similar spirit the work of ref. [12] aims at providing an *alternative* description of the equation of state starting from the considerations of ref. [11], but assuming excluded volumes for glueball states. We want to stress the fact that this work is not meant as an improvement over previous papers (an honest, direct comparison cannot be made, as we will see below), but rather as a stringent test for the excluded volume approach which can lead to a better understanding of its use in the full theory. We remark that in purely gluonic theory the physical states have no baryonic number, electric charge or strangeness: thus,

the only contribution to the modified chemical potential comes from the excluded volume term, leading to a further simplification with respect to the QCD case.

The excluded volume analysis was performed both in the case of the SU(2) gauge theory and the more physical case with th SU(3) gauge symmetry group; for the description of the latter, the continuum-extrapolated data of ref. [6] were used. For the former instead, the lattice data of ref. [11] were used and combined with a new set of results: the lattice setup of all simulations is reported in table 2.2. The extrapolation of the results for the trace of the energy-momentum tensor, which is the primary observable of the simulations, was performed using for each temperature a quadratic fit in $1/N_t$. In practice, the results for each value of N_t were first fitted by cubic splines and then, for temperature comprised between $0.79T_c$ and T_c (with a step of $0.001T_c$), they were fitted with the form

$$\Delta(T, N_t) = \Delta^{(0)}(T) + \frac{\Delta^{(1)}(T)}{N_t^2} \tag{2.57}$$

where $\Delta^{(0)}(T)$ is the continuum-extrapolated value of the trace anomaly at temperature T. These results, along with those at finite lattice spacing with $N_t = 6, 7, 8, 10$, are reported in fig. 2.8: as expected, in proximity of the deconfinement transition the extrapolated results show non-negligible deviations from points obtained at finite lattice spacing.

Before numerical results can be analyzed, we need to define the parametrization of the effective radius r_i of eq. (2.56), in particular its behaviour with respect to the mass of the i-th species. Three possible options have been taken into account:

- a *fixed* effective radius, i.e.
$$r_i = r_{0^{++}} \quad \forall i;$$

- a volume *directly* proportional to the mass,
$$r_i = \sqrt[3]{\frac{m_i}{m_{0^{++}}}} r_{0^{++}}$$

- a volume *inversely* proportional to the mass,
$$r_i = \sqrt[3]{\frac{m_{0^{++}}}{m_i}} r_{0^{++}}$$

in which $m_{0^{++}}$ is the mass of the lightest glueball state and $r_{0^{++}}$ is its radius and the free parameter of the fits. These three choices represent some (but, of course, not all) of the possible ways which effectively encode the interaction between glueball states.

As showed in previous papers, a Hagedorn spectrum is strictly required in order to account correctly for all the heavy glueball states whose contribution is crucial in the proximity of the transition: thus, the same stringlike spectrum of ref. [11] (with a similar mass threshold m_{th}) has been used also in this work when performing the excluded-volume fit. Moreover, in the case of the SU(2) gauge theory, the spectrum for light glueballs (computed on the lattice), the value of the critical temperature T_c and the value of the Hagedorn temperature T_H are the same as those used in

SU(2), with $T_H = T_c$
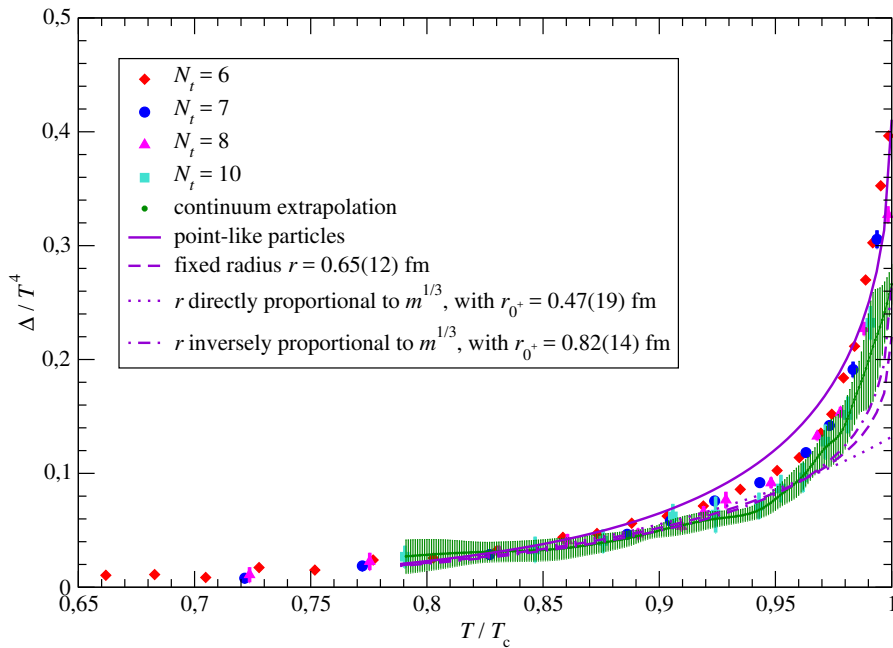
Figure 2.8: Lattice results for the trace of the energy-momentum tensor Δ (in units of T^4) in the confining phase of the SU(2) Yang-Mills theory, from lattice simulations at $N_t = 6$ (red diamonds), 7 (blue circles), 8 (magenta triangles) and 10 (cyan squares), and their extrapolation to the continuum limit (green curve) with the respective error band. The results are plotted against the temperature T in units of the critical deconfinement temperature T_c. The figure also shows the fits of the hadron-gas model with or without excluded-volume effects (violet curves). The solid line is obtained under the assumption that glueball states are point-like, the dashed line assumes that all states have the same radius, while the dotted line is based on the *Ansatz* that volumes of different glueballs are directly proportional to their mass, and finally the dash-dotted line is computed assuming that the volume of each particle is inversely proportional to the particle mass. Further details of these fits are summarized in table 2.5.

ref. [11] and reported in the previous section. The fitting procedure was performed minimizing the χ^2 with respect to continuum-extrapolated data; the results for the trace of the energy-momentum tensor are reported in table 2.5 and showed in fig. 2.8.

Integration of different fits for the trace anomaly provides the curves for the pressure, which are shown in fig. 2.9.

Somewhat surprisingly, the parametrization of the effective radius assigned to glueball states that best describes the SU(2) equation of state close to T_c is the one that predicts a volume that decreases when the mass increases. On the other hand the "point-like" description, that is exactly the one of ref. [11] with no free parameters, clearly is not compatible and thus yields a much higher χ^2_{red}.

The analysis was similarly performed again for the SU(3) gauge theory, using

Table 2.5: Results of the fits of our lattice data for the SU(2) interaction measure and of data from ref. [6] for SU(3), to the glueball gas model. The radius, with the corresponding error, of the lightest glueball state (the ground-state particle in the channel with quantum numbers $J^{\mathcal{P}} = 0^+$ or 0^{++}) and the χ^2_{red} value are shown for different scenarios.

$V(m)$ dependence	SU(2)			SU(3)		
	r_{0^+} (fm)	δr_{0^+} (fm)	χ^2_{red}	$r_{0^{++}}$ (fm)	$\delta r_{0^{++}}$ (fm)	χ^2_{red}
point-like	0	0	8.16	0	0	84.3
constant r	0.65	0.12	0.74	0.733	0.08	2.33
$V \propto m$	0.47	0.19	1.87	0.55	0.07	5.41
$V \propto m^{-1}$	0.82	0.14	0.39	0.91	0.10	0.82

SU(2)
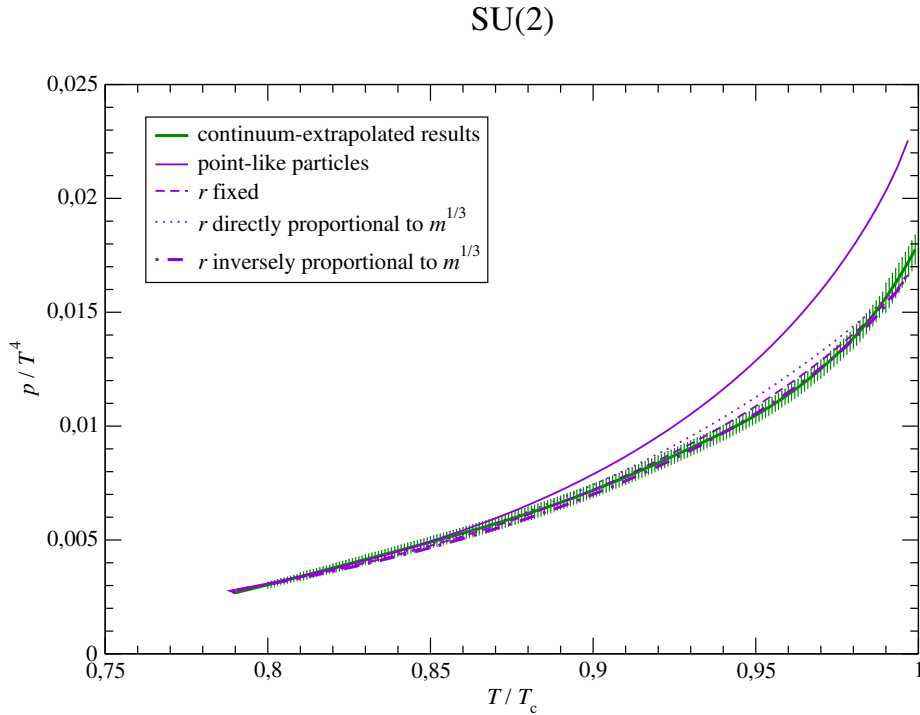
Figure 2.9: Pressure (in units of T^4) in SU(2) Yang–Mills theory: the figure shows a comparison of our continuum-extrapolated lattice results (green line) and the hadron-resonance-gas predictions obtained by integration of the different fits of Δ/T^4 in fig. 2.8, assuming point-like particles (violet solid line), particles of constant volume (violet dashed line), particles with eigenvolume directly proportional to their mass (violet dotted line), or particles with eigenvolume inversely proportional to their mass (violet dash-dotted line).

the same methodology of the $N = 2$ case. The low-lying glueball spectrum, the deconfinement temperature T_c as well as the mass threshold m_{th} for the Hagedorn spectrum are the same as those used in ref. [11]. An important difference concerns the value of the Hagedorn temperature: in this work the value computed numerically

in ref. [5], i.e. $T_{\mathrm{H}} = 1.024 T_c$ was assumed. The results of the fits with the excluded volume approach are reported in table 2.5 and the resulting curves for the trace of the energy-momentum tensor Δ/T^4 are shown in fig. 2.10. Results for the pressure obtained via integration of the trace anomaly are showed in fig. 2.11.

SU(3), assuming $T_{\mathrm{H}} = 1.024 T_c$
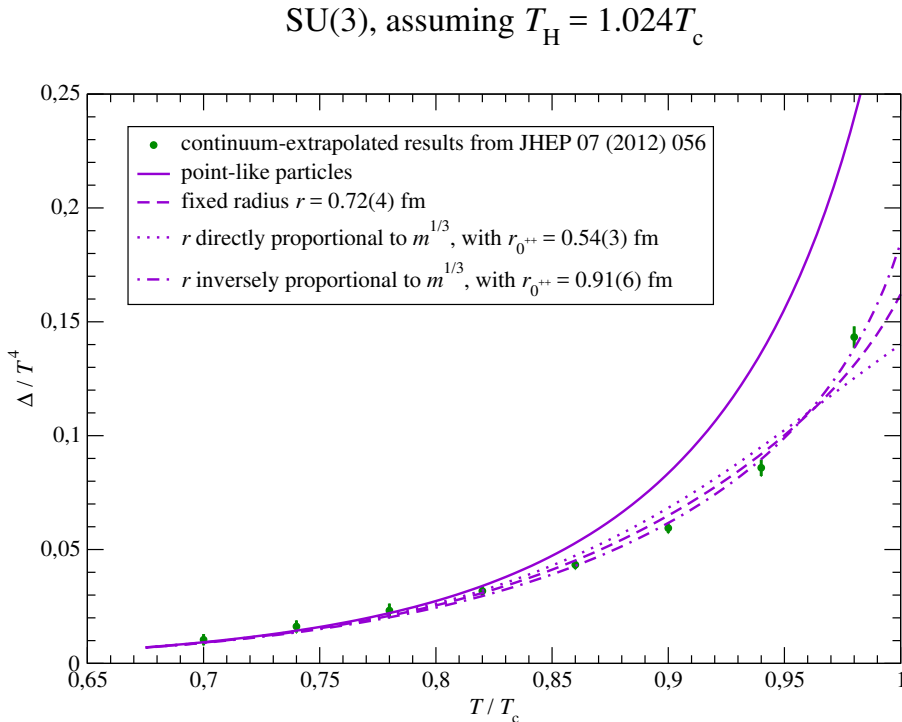
Figure 2.10: Same as in fig. 2.8, but for the continuum-extrapolated lattice results from ref. [6] for SU(3) Yang–Mills theory, assuming $T_{\mathrm{H}} = 1.024 T_c$ [5, 6]. These fits are summarized in table 2.5.

Interestingly, even if this pure gauge model presents a few radically different properties with respect to the SU(2) theory (as discussed in detail in section 2.2), the fits that take into account excluded-volume effects yield very similar results. Again, the most accurate description is that of glueballs whose effective volume is inversely proportional to the mass: also in this case the points close to the transition play a crucial role in the choice of the best phenomenological description.

Strikingly, when considering the result for the effective radius of the $J^{PC} = 0^{++}$ glueball state, i.e. the parameter used in the fits, there is substantial agreement between the values for the SU(2) and the SU(3) theory. Even if the error associated to such values is rather large, this fact serves as further confirmation that the description in terms of excluded volume effects leads to consistent results among various gauge models.

Before moving to further comments on these results, we have to point out that this work is not supposed to be an improvement of the analysis of ref. [11], but more as an independent and alternative approach for the description of the equation of

SU(3)
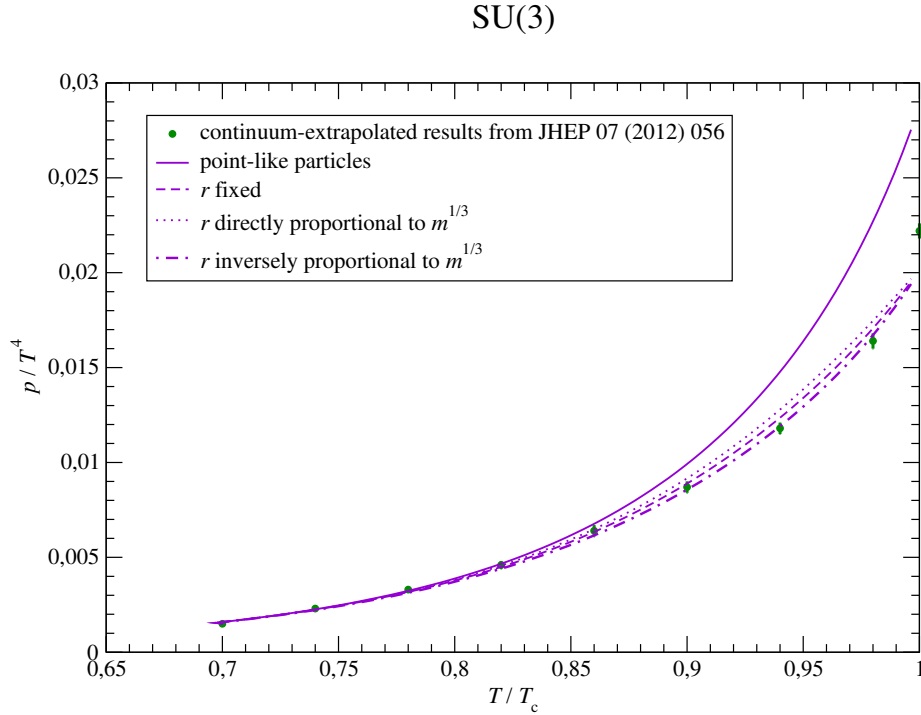
Figure 2.11:   Same as in fig. 2.9, but for SU(3) Yang–Mills theory: the plot shows a comparison of the lattice results from ref. [6] (green symbols) and the statistical-model predictions (violet lines) obtained by integration of the curves shown in fig. 2.10, assuming the integration constant $p/T^4 = 0.0015(1)$ for $T/T_c = 0.7$ [6].

state of Yang-Mills theories in the confining phase. Any attempt at studying the thermodynamics of pure gauge theories cannot disregard the need of a Hagedorn spectrum (possibly of string-like origin) for glueball states close to the transition: this is the main result of refs. [5, 9, 11], obtained with no truly free parameters, as described at length in section 2.2. On the other hand, a precision analysis of lattice data is possible only by introducing some physically-motivated parameters which allow for a sensible fit of numerical results. In this light the excluded volume approach provides a clean phenomenological framework that is able to include, albeit with some limits, an effective description of repulsive interactions between glueballs. The work reported in this section then aims at testing the efficacy of this methodology on models which are quite different from QCD: in this way we can show its consistency and provide novel insights which may be helpful also for full QCD.

An important difference with respect to the analysis of ref. [11] is the value of the Hagedorn temperature for the $N = 3$ case: in that work simply including the $C = -1$ glueball sector and using the Nambu-Gotō value for T_H provided an excellent qualitative description of thermodynamic observables. However, there is no reason to discard *a priori* the value of T_H computed in ref. [5], which was obtained by

determining the temperature at which the inverse correlation length of the temporal flux loop vanishes. In fact, this value provides an excellent quantitative agreement with lattice results when excluded-volume effects were taken into account, albeit with the use of a free parameter.

Looking again at the results reported in table 2.5, the finding of an eigenvolume inversely proportional to the glueball mass may seem surprising or even in contrast with phenomenological models: for example the Isgur-Paton model treated in section 2.2.4 clearly predicts larger and larger glueballs as their mass increases. However, we have to remark that such results are not necessarily at odds with the possibility of heavy and extended glueball states: indeed, the eigenvolume is not to be confused with the physical volume, but has to be intended as an effective volume which accounts for interaction among glueballs. Thus, such results then may indicate that heavy states interact more weakly than lighter ones with no clear indication on the actual physical size. More in general, the three parametrizations for the glueball radius described above must be intended simply as crude idealizations which do not account for nonperturbative dynamics underlying the existence of such states and are not able to determine the precise volumes of each particle; still, we can use them in order to keep the number of free parameters at a minimum and obtain precious physical intuition on the properties of the heavy glueball spectrum.

It should be noted that very similar results have been found in previous analyses in QCD [146]: again, the best description was that in terms of effective volumes decreasing with the mass of hadron resonances. We also add that effective sizes of glueball states are slightly larger than those found in the full theory for hadrons, giving some support for the idea that the repulsive interaction is stronger between glueballs.

Chapter 3

The ξ/ξ_{2nd} ratio in pure gauge theories

One method to circumvent the notorious "sign problem" that plagues Monte Carlo simulations in lattice QCD at finite baryonic density, which we already mentioned in section 1.2.2, is based on a family of models collectively denoted as effective Polyakov loop (EPL) models. This line of research, whose roots can be found in the Svetitsky-Yaffe conjecture [139], has enjoyed good success in the last decade, spawning many contributions in different directions [14–34]. In this approach, the original theory is mapped on a three-dimensional, center-symmetric spin model: the remaining dynamical degrees of freedom (the "spins") are the former Polyakov loops in the fundamental or higher representations. The main positive aspect of this set of models is that, in general, the sign-problem is milder or it can be even avoided entirely: of course, exact integration of timelike degrees of freedom is too difficult, so the first challenge is to build an effective spin model action that captures all the relevant properties of the original theory. The most important features that such an action should possess can be inferred from strong-coupling expansions:

- it should display nonlocality: as far-apart Polyakov loops are involved in the interaction as the order of the expansion increases;

- Polyakov loops in higher representations should be involved;

- multispin interactions should be included.

The latter of these properties is usually neglected for simplicity, and the dynamics of this family of models is described by a two-spin interaction with an action of the type

$$S_{\text{eff}} = \sum_p \sum_{|\mathbf{r}|\geq 1} \sum_{|\mathbf{x}-\mathbf{y}|=\mathbf{r}} \lambda_{p,\mathbf{r}} \, \chi_p(\mathbf{x}) \, \chi_p(\mathbf{y}) \tag{3.1}$$

where the sum on p runs on all the desired representations, $\chi_p(\mathbf{x})$ is the character in the p representation of the loop in the spatial site $\mathbf{x}$ and $\lambda_{p,\mathbf{r}}$ is the coupling between effective spins in the p representation at a given distance $\mathbf{r}$. Thus, the main challenge for each of these models is to devise a strategy to determine the huge number of spin couplings of the type $\lambda_{p,\mathbf{r}}$.

In ref. [35] a new quantitative way of evaluating possible EPL models was proposed, based on their ability of including relevant properties of the original four-dimensional gauge theory, namely the measurement of the ratio between the exponential correlation length ξ and the second moment correlation length ξ_{2nd}.

This study has been inspired by the observation that EPL models should be able to display the $1/R$ correction in the static quark-antiquark potential $V(R)$, i.e. the so-called "Lüscher term", that we already met in eq. (2.23). Such a term has been detected in the confining phase of $SU(N)$ pure gauge theories from the computation of Wilson loops and Polyakov loop correlators, and EPL models are expected to show the same behaviour. However, this is a highly nontrivial requirement, as the $1/R$ correction is deeply linked with the rich spectrum of excitations of the flux tube: indeed, the number of excitations shows an Hagedorn-like dependence on the energy, as discovered long ago [108]. Spin models usually do not reproduce such a rich spectrum easily, in particular if only short-distance interactions are included.

It is then crucial to find an observable which provides a quantitative way to keep track of the spectrum that EPL models are able to reproduce and that is also easy to compute. The ξ/ξ_{2nd} ratio is precisely the right quantity: in section 3.1 we will analyze how this ratio can give precious information on the composition of the flux tube excitations. On the other hand in section 3.2 we shall discuss the results of the ξ/ξ_{2nd} ratio for the SU(2) pure gauge theory from lattice simulations, in order to show the strikingly different behaviour of ξ_{2nd} with respect to ξ.

3.1   The relation between ξ and ξ_{2nd}

In a *d*-dimensional spin model the exponential correlation length ξ describes the long distance behavior of the connected correlator and is defined as

$$\frac{1}{\xi} = -\lim_{|\vec{n}|\to\infty} \frac{1}{|\vec{n}|} \log\langle s_{\vec{0}} s_{\vec{n}} \rangle_c \tag{3.2}$$

where $s_{\vec{n}}$ denotes the spin s in the position $\vec{n} = (n_1,...,n_d)$ and the connected correlator is defined as

$$\langle s_{\vec{m}} s_{\vec{n}} \rangle_c = \langle s_{\vec{m}} s_{\vec{n}} \rangle - \langle s_{\vec{m}} \rangle^2. \tag{3.3}$$

The square of the second moment correlation length ξ_{2nd} is defined as:

$$\xi_{2nd}^2 = \frac{\mu_2}{2d\mu_0} \, , \tag{3.4}$$

where

$$\mu_0 = \lim_{L\to\infty} \frac{1}{V} \sum_{\vec{m},\vec{n}} \langle s_{\vec{m}} s_{\vec{n}} \rangle_c \tag{3.5}$$

and

$$\mu_2 = \lim_{L\to\infty} \frac{1}{V} \sum_{\vec{m},\vec{n}} |\vec{m} - \vec{n}|^2 \langle s_{\vec{m}} \, s_{\vec{n}} \rangle_c \, , \tag{3.6}$$

$V = L^d$ being the lattice volume.

It is important to notice that ξ_{2nd} is not exactly equivalent to ξ: in fact the difference carries important information on the spectrum of the underlying theory. To better understand this, let us consider "wall" variables, which can be defined as

$$S_{n_1} = \frac{1}{L^2} \sum_{n_2,\ldots,n_d} s_{\vec{n}} \tag{3.7}$$

and the corresponding correlation function

$$G(\tau) = \sum_{n_1} \langle S_{n_1} S_{n_1+\tau} \rangle - \langle S_{n_1} \rangle^2 ; \tag{3.8}$$

the average on the $(n_2,\ldots,n_d)$ plane indicates a projection to zero spatial momentum. The exponential correlation length can be extracted from the large-τ behavior of $G(\tau)$

$$G(\tau) \sim \exp(-\tau/\xi) ; \tag{3.9}$$

on the other hand ξ_{2nd} can be rewritten by noticing that we can re-express μ_2 as follows:

$$
\begin{aligned}
\mu_2 &= \frac{1}{V} \sum_{\vec{m},\vec{n}} |\vec{n} - \vec{m}|^2 \ \langle s_{\vec{m}} s_{\vec{n}} \rangle_c \\
&= \frac{1}{V} \sum_{\vec{m},\vec{n}} \sum_{k=1}^{d} (n_k - m_k)^2 \ \langle s_{\vec{m}} s_{\vec{n}} \rangle_c \\
&= \frac{d}{V} \sum_{\vec{m},\vec{n}} (n_1 - m_1)^2 \ \langle s_{\vec{m}} s_{\vec{n}} \rangle_c \ .
\end{aligned}
\tag{3.10}
$$

where we made use of the fact that the lattice is symmetric in all d directions. We commute the spatial summation with the summation over configurations, getting

$$\mu_2 = dL^2 \sum_{\tau=-\infty}^{\infty} \tau^2 \ \langle S_0 \ S_\tau \rangle_c \tag{3.11}$$

and

$$\mu_0 = L^2 \sum_{\tau=-\infty}^{\infty} \langle S_0 \ S_\tau \rangle_c \tag{3.12}$$

so that if we now insert them in eq. (3.4), we obtain

$$\xi_{2nd}^2 = \frac{\sum_{\tau=-\infty}^{\infty} \tau^2 \ G(\tau)}{2 \sum_{\tau=-\infty}^{\infty} \ G(\tau)} \ . \tag{3.13}$$

Assuming a multiple exponential decay for $G(\tau)$,

$$\langle S_0 \ S_\tau \rangle_c \propto \sum_i c_i \ \exp(-|\tau|/\xi_i) \ , \tag{3.14}$$

where c_i represents the amplitude of the i-th state; replacing the summation by an integration over τ we get

$$\xi_{2nd}^2 = \frac{1}{2} \frac{\int_{\tau=0}^{\infty} \mathrm{d}\tau \ \tau^2 \sum_i c_i \exp(-\tau/\xi_i)}{\int_{\tau=0}^{\infty} \mathrm{d}\tau \ \sum_i c_i \exp(-\tau/\xi_i)} = \frac{\sum_i c_i \xi_i^3}{\sum_i c_i \xi_i} \ , \tag{3.15}$$

which is equal to the square of ξ if only one state contributes. Conversely, if the spectrum contains several massive states, then the ratio can be significantly larger than 1. It is clear that the ξ/ξ_{2nd} ratio is able to provide some insight on the spectrum of the theory and on the amplitude c_i of these states.

3.2   Numerical results for the SU(2) pure gauge theory

We performed a numerical study of the ξ/ξ_{2nd} ratio in the SU(2) non-Abelian pure gauge theory, regularized on a hypercubic lattice of spacing a and hypervolume $aN_t \times (aN_s)^3$. The Yang-Mills action is discretized with the standard Wilson action [3], eq. (1.19); the main observable of interest is the so-called Polyakov loop, eq. (1.24), that we slightly rewrite here as

$$P(x, y, z) = \frac{1}{2}\text{Tr} \prod_{0 \leq t/a < N_t} U_0(x, y, z, t) \ . \tag{3.16}$$

Following the definition used for the spin model, eq. (3.7), we can define the zero-momentum projection of the Polyakov loop by taking the average over the two spatial directions x and y

$$\bar{P}(z) = \frac{1}{N_x N_y} \sum_{x,y} P(x, y, z) \tag{3.17}$$

and we can write down the zero-momentum connected correlator $G(\tau)$

$$G(\tau) = \langle \bar{P}(0)\bar{P}(\tau) \rangle - |\langle P \rangle|^2 \tag{3.18}$$

which we can identify with the definition of eq. (3.8).

The temperature was varied using both N_t and the inverse bare coupling β: in order to do so the scale setting relation computed in ref. [11] was used to express the lattice spacing in units of $1/\sqrt{\sigma}$ (see section 2.2.1 for more details). Our results were reported in units of the critical temperature T_c using the value $T/T_c = 0.7091(36)$ computed in ref. [115]; the lattice setup of the Monte Carlo simulations used in this work is reported in table 3.1.

Table 3.1: Setup of the Monte Carlo lattice simulations performed for the SU(2) gauge theory in the confining phase. We report the Wilson parameter β in the first column and the spacetime volume of the lattice in units of a^4 in the second; the resulting temperature in units of T_c and the statistics for the measurements of zero-momentum Polyakov loop correlators $G(\tau)$ are presented in the third and fourth column.

β	$N_s^3 \times N_t$	T/T_c	n_{conf}
2.27	$32^3 \times 6$	0.59	4.5×10^5
2.33	$32^3 \times 6$	0.71	2.25×10^5
2.3	$32^3 \times 5$	0.78	5.5×10^5
2.357	$32^3 \times 6$	0.78	2.25×10^5
2.25	$64^3 \times 4$	0.84	3×10^4
2.4	$64^3 \times 6$	0.90	2×10^4

Results for the zero-momentum correlator $G(\tau)$ have been fitted with a functional form that takes into account also the "echo" due to periodic boundary conditions in the spatial directions, namely

$$G(\tau) \sim \exp\left(-\frac{\tau}{\xi}\right) + \exp\left(-\frac{L - \tau}{\xi}\right) \tag{3.19}$$

where ξ is the the exponential correlation length of the system, as defined in eq. (3.2), and L is the size of the three-dimensional space (in our case, $L = N_s$). Numerical results for ξ in units of a have been obtained for several temperatures $T < T_c$ and are reported in table 3.2. For each of the fits with eq. (3.19) the values $\tau = a$ and $\tau = 2a$ have been excluded, in order to avoid artifacts due to the lattice discretization. For the simulations close to the deconfinement transition (those reported in line 5 and line 6 of table 3.2) the spatial size N_s of the lattice was increased in order to accommodate larger correlation lengths and to reduce the effect of the echo due to the periodic boundary conditions.

Next, we computed ξ_{2nd} from μ_2 and μ_0: in order to do so, we followed a procedure similar to that used in ref. [147]. In particular, for μ_2 we employed an *Ansatz* that takes into account the contribution of the large-distance terms, which could be computed otherwise only on prohibitively large lattices. Namely, we used

$$\mu_2 = \sum_{\tau=1}^{\tau_{max}} \tau^2 \, G(\tau) + \sum_{\tau=\tau_{max}+1}^{\infty} \tau^2 \, G(\tau_{max}) \, e^{-(\tau-\tau_{max})/\xi} \qquad (3.20)$$

and similarly for the calculation of μ_0. The contribution of the tail, i.e. of the second term on the right-hand side of eq. (3.20), depends on the value assigned to the distance cutoff τ_{max}: during our analysis we kept $\tau_{max} \sim 3\xi$, which generally yielded stable results. Using eq. (3.4) (with $d = 3$) we computed ξ_{2nd} for different values of the temperature T: the results are reported in table 3.2.

Table 3.2: Results for the exponential correlation length ξ (third column) and the second moment correlation length ξ_{2nd} (fourth column) in units of the lattice spacing, along with their ratio $\frac{\xi}{\xi_{2nd}}$ (fifth column) in the confined phase.

T/T_c	N_s	ξ/a	ξ_{2nd}/a	ξ/ξ_{2nd}
0.59	32	1.31(2)	0.887(8)	1.48(3)
0.71	32	2.31(4)	1.842(15)	1.25(2)
0.78	32	2.56(2)	2.22(1)	1.153(11)
0.78	32	3.08(4)	2.67(2)	1.151(16)
0.84	64	3.05(6)	2.74(4)	1.11(3)
0.90	64	6.9(2)	6.6(3)	1.04(6)

In the *Ansatz* of eq. (3.20), the choice of τ_{max} is somewhat arbitrary and it introduces a systematic error in the computation of μ_0 and μ_2: in the former case, the contribution of the tail is negligible when compared to the first term on the right-hand side of eq. (3.20). Conversely, the computation of μ_2 has a substantial contribution coming from large values of τ, which becomes prominent for $T \sim T_c$; we made sure that such error is under control by comparing results obtained by changes in τ_{max} and checking that they were all compatible.

From fig. 3.1 it is clear that the ξ/ξ_{2nd} ratio depends nontrivially on T/T_c, showing in particular a dramatic increase of ξ over ξ_{2nd} as the temperature decreases. In order to test if the results are independent from the lattice volume and from the lattice spacing, we performed the simulations at $T/T_c = 0.78$ with two different combinations of β and N_t. The same value of ξ/ξ_{2nd} is found, even if the values of ξ and ξ_{2nd} in units of the lattice spacing were quite different in the two cases: thus,
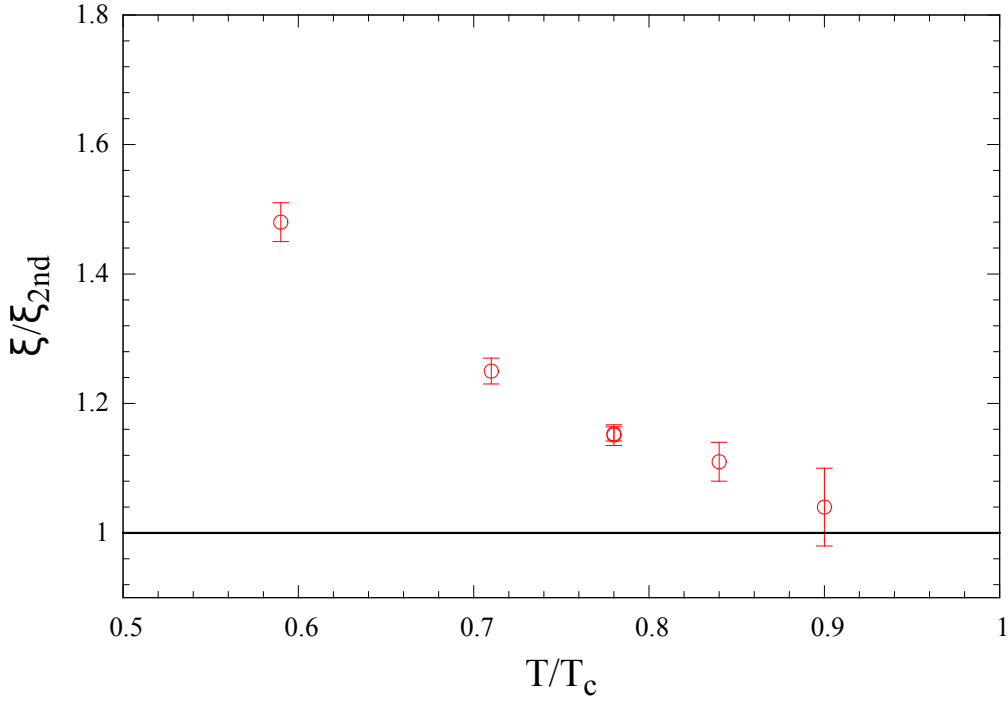
Figure 3.1: The ξ/ξ_{2nd} ratio for different values of the temperature T/T_c in the confining region.

we are confident that scaling corrections are under control and that our results are tracing a true physical behaviour of the SU(2) gauge theory.

In order to have a complete picture of what kind of physical mechanisms are underlying such behaviour, a description in terms of the effective string theory for the flux tube is in principle possible. Indeed, the effective string approach predicts in a natural and elegant way a rich spectrum of excitations for the color flux tube: it was realized recently [110, 148] that the Nambu-Gotō action [149, 150] is an excellent approximation of the true effective action, and it can be used explicitly. In this framework, the Polyakov loop correlator can be written in D spacetime dimensions [148, 151] as

$$\langle P(\mathbf{x})^* P(\mathbf{y}) \rangle = \sum_{n=0}^{\infty} w_n \frac{2r\sigma L_t}{E_n} \left(\frac{\pi}{\sigma}\right)^{\frac{D-2}{2}} \left(\frac{E_n}{2\pi r}\right)^{\frac{D-1}{2}} K_{\frac{D-3}{2}}(E_n r) \qquad (3.21)$$

where $r = |\mathbf{x} - \mathbf{y}|$, L_t is the extent of the compactified dimension, σ the string tension, while w_n and E_n are the multiplicity and the energy level of the n-th state, respectively. These can be computed, resulting in

$$w_n \sim \exp\left(\pi\sqrt{\frac{2(D-2)n}{3}}\right) \qquad (3.22)$$

and

$$E_n = \sigma N_t \left\{ 1 + \frac{8\pi}{\sigma N_t^2} \left[-\frac{1}{24}(D-2) + n \right] \right\}^{1/2}. \qquad (3.23)$$

(a) Multiplicity of states w_n

(b) Energy gap $(E_n - E_0)/E_0$
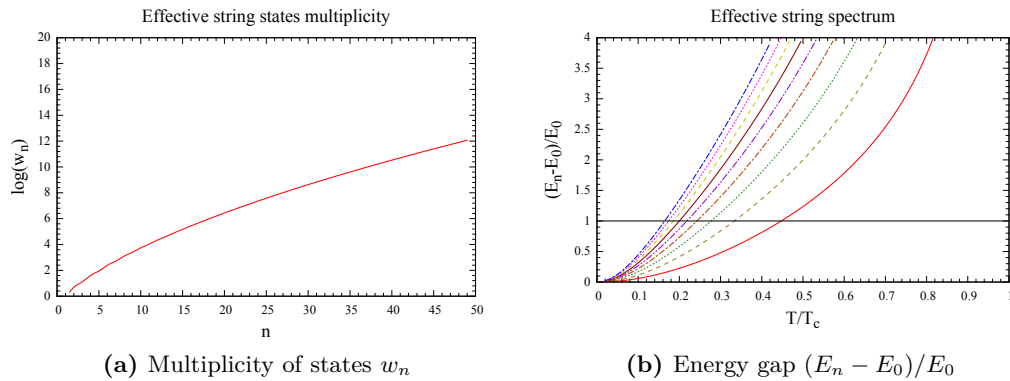
Figure 3.2: Left: the logarithm of the multiplicity w_n defined in eq. (3.22) as a function of the level n, for the first fifty levels. Right: the gap between the energy E_n of the n-th state and the energy of the lowest level E_0, as a function of T/T_c, for $1 < n < 9$, from $n = 1$ (red solid line) to $n = 9$ (blue dashed-dotted line); the black horizontal line represents the two particle threshold $E_n = 2E_0$.

This is exactly the kind of qualitative behavior that we expect: on one hand the spectrum is of the Hagedorn type, with an exponential increase of the states with E_n; on the other hand all the states tend to accumulate towards the lowest state with energy E_0 as the temperature decreases. To see this, we just have to recall that $T = 1/L_t$ and $T_c/\sqrt{\sigma} = \sqrt{3/(2\pi)}$ in $D = 3+1$ dimensions, so that eq. (3.23) becomes

$$E_n = \frac{2\pi T_c^2}{3T} \left\{ 1 + 12\frac{T^2}{T_c^2} \left[n - \frac{1}{12} \right] \right\}^{1/2}. \tag{3.24}$$

The increase in the number of states of the string-like flux tube and the energy gap $(E_n - E_0)/E_0$ as a function of the temperature are reported in fig. 3.2.

Qualitatively speaking, it is precisely the combination of these effects that drives the ξ/ξ_{2nd} ratio to larger values as the temperature decreases. However, the effective string approach is not able to provide reliable quantitative predictions for the ξ/ξ_{2nd} ratio: this is due to the fact that this framework can be used only in a context in which the relevant distances are larger than the Nambu-Gotō critical scale $1/\sqrt{2\sigma}$. Unfortunately a significant contribution to the ξ/ξ_{2nd} ratio comes from short-distance effects which cannot be described in terms of effective strings, setting a limit on its usefulness.

In the end, the work presented in ref. [35] showed how the ξ/ξ_{2nd} ratio is a crucial quantity when one studies the spectrum of the flux tube excitations; thus, EPL models should replicate this behaviour in case they are used to investigate regions of temperature below the deconfinement transition. Moreover, both ξ and ξ_{2nd} can be computed in an easy and computationally cheap way: thus, their ratio could represent a useful tool to perform a preliminary selection of the potentially very large set of parameters in the actions of the form of eq. (3.1).

Chapter 4

Jarzynski's equality

When dealing with systems which are far from equilibrium, the usual statistical mechanics relations are not valid anymore, leaving an large sector of phenomena which cannot be studied with near-equilibrium approximations. However there is a family of relations, called fluctuation theorems, that are applicable even out of equilibrium, and one of the most important ones goes by the name of Jarzynski's equality [38]. The discovery during the '90s of this set of relations in nonequilibrium statistical mechanics, has been developed in parallel with huge advancements on the experimental side in the study of microscopic systems at the molecular level. Such systems present peculiar properties which the scientific community could finally begin to study both from a theoretical and from an experimental point of view.

As we will see in this chapter, the theoretical framework on which Jarzynski's equality in particular is based can be extended and implemented in systems which are very far away from the ones in which they have been used originally. Namely, the application of Jarzynski's equality to Monte Carlo simulations opens up a large number of applications in high-energy physics and in particular in lattice field theory. This chapter is devoted first to a thorough analysis of the nonequilibrium work relation by Jarzynski and second, to an analysis of how it has been implemented successfully for the very first time in the study of strongly-interacting theories.

The first part of this chapter, section 4.1, is an introductory review to the nonequilibrium work relation, starting from classical thermodynamics and the behaviour of macroscopic systems, then examining in detail the equality by Jarzynski with some tools of statistical mechanics, and eventually reaching fluctuation theorems for microscopic systems. Section 4.2 is entirely devoted to the analysis of some derivations of Jarzynski's equality, both for deterministic and stochastic systems. In section 4.3 we will review some more recent theoretical advancements in the understanding of the nonequilibrium relation which are quite relevant for its practical use also in numerical experiments. The last part, section 4.4 will focus on the application of the nonequilibrium work relation for Monte Carlo simulations, along with a generalization of the equality for varying temperature; finally, the first true application of the nonequilibrium relation in the context of lattice gauge theories of ref. [44] will be reviewed at length.

4.1   The nonequilibrium work relation

In this section we will analyze the significance of the nonequilibrium work relation discovered by C. Jarzynski 20 years ago assuming from the reader no particular knowledge of nonequilibrium statistical mechanics. After a short review of classical thermodynamics (and in particular of the Second Law) the attention will be shifted to microscopic systems and thus to statistical mechanics; in section 4.1.2 the nonequilibrium equality will be stated and explained in detail and in section 4.1.3 its simple but deep relation to the Second Law itself will be highlighted. Its relation with recent advancements in nonequilibrium statistical mechanics and in particular with fluctuation theorems discovered in the '90s will be described in section 4.1.4. Finally, the experimental test of the nonequilibrium work relation presented in ref. [43] will be reported in section 4.1.5. We refer to the original paper [38], the pedagogical introductory review of ref. [152] and references therein for further details and insights. A clear and exhaustive introduction to the matter can be also found in ref. [153].

4.1.1   A few facts about macroscopic systems

This chapter will be mainly devoted to the behaviour of microscopic systems through the tools of statistical mechanics. However, it is certainly instructive to investigate a few basic facts about *macroscopic* systems by making a short review of classical thermodynamics.

We can start by examining a macroscopic system that depends only on two variables: the temperature T of the heat bath it is in thermal contact with, and a generic external parameter λ. A typical assumption of equilibrium thermodynamics is that for any set of values (T, λ), there exists only one "equilibrium state" that the system will eventually reach if (T, λ) are kept fixed. In thermodynamics we can introduce a set of *state functions* that take unique values for any equilibrium state, such as the internal energy $E(T, \lambda)$ and the entropy $S(T, \lambda)$.

Now, we can state the First Law of thermodynamics

$$\Delta E = Q + W \tag{4.1}$$

where ΔE indicates the difference in internal energy between a final state B and an initial state A, Q is the exchange of heat of our system with the external one and W is the work done on (if $W > 0$) or by (if $W < 0$) the system.

Then, we can proceed to the Second Law of thermodynamics, specifically in the form of the *Clausius inequality* [154, 155]:

$$\int_A^B \frac{\delta Q}{T} \leq \Delta S = S(B) - S(A); \tag{4.2}$$

here we are considering a thermodynamic transformation of our system from equilibrium state A to B performed through a series of heat reservoirs of varying temperature T. It is crucial to observe that the equality holds only for *reversible* transformations, that is transformations which at any moment are always at equilibrium with the heat reservoir. The infinitesimal heat exchange δQ is then integrated along this

particular transformation; if the transformation is *isothermal*, i.e. only one single heat reservoir (at fixed temperature T) is taken, then we have

$$\frac{Q}{T} \leq \Delta S. \tag{4.3}$$

Now it is a good moment to introduce a new state function, the Helmholtz *free energy F*

$$F = E - ST. \tag{4.4}$$

We can easily rewrite eq. (4.3) using the First Law (4.1) and the definition of free energy (4.4)

$$\frac{\Delta E - W}{T} \leq \Delta S = \frac{\Delta E - \Delta F}{T} \tag{4.5}$$

which leads to a compact version of the Second Law for isothermal transformations:

$$W \geq \Delta F = F(B) - F(A). \tag{4.6}$$

Let us take briefly a closer look at the work W: we can imagine a system equilibrated at a temperature T and some value λ_A of the external parameter, which undergoes an isothermal transformation and reaches a state (T, λ_B). If the transformation is reversible, then the work will be equal to the difference in free energy between the state (T, λ_B) and the state (T, λ_A); if it is irreversible, then only the inequality of eq. (4.6) will hold.

4.1.2 The nonequilibrium equality

From the general thermodynamical facts of section 4.1.1 we can now look at microscopic systems through the lens of statistical mechanics. Let $H(\Gamma, \lambda)$ be the Hamiltonian which describes the behaviour of the microscopic degrees of freedom that compose our system. Γ denotes a *microstate* of our system: for example, a system with N point-like particles will be characterized by microstates of the type

$$\Gamma(\mathbf{r}_1, ..., \mathbf{r}_N; \mathbf{p}_1, ..., \mathbf{p}_N)$$

where $\mathbf{r}_i$ and $\mathbf{p}_i$ are three dimensional vectors that indicate position and momentum of the $i-$th particle.

As usual we can define the *partition function $Z_\lambda(T)$* of this system

$$Z_\lambda(T) = \int \mathrm{d}\Gamma \, e^{-\beta H(\Gamma, \lambda)} \tag{4.7}$$

where $\beta = 1/(k_B T)$; the *ensemble average* of a generic quantity $\mathcal{A}$ is defined as the integral over the phase space

$$\overline{\mathcal{A}} = \frac{1}{Z_\lambda(T)} = \int \mathrm{d}\Gamma \, \mathcal{A}(\Gamma) \, e^{-\beta H(\Gamma, \lambda)}. \tag{4.8}$$

The free energy of the equilibrium state associated to the values (T, λ) is directly related to the partition function

$$F_\lambda(T) = -\beta^{-1} \log Z_\lambda(T) \tag{4.9}$$

which trivially leads to the thermodynamic definition of eq. (4.4) if energy and entropy are properly written in the canonical approach:

$$\overline{E_\lambda} = -\frac{\partial \log Z_\lambda}{\partial \beta} \quad \text{and} \quad S_\lambda = k_B(\log Z_\lambda + \beta E_\lambda). \tag{4.10}$$

Finally, we introduce the Boltzmann-Gibbs distribution [156]

$$f_\lambda^{\text{BG}}(\Gamma) = \frac{1}{Z_\lambda} e^{-\beta H_\lambda(\Gamma)} \tag{4.11}$$

which gives the probability of finding the system in the Γ microstate.

Following the approach of section 4.1.1 we consider transformations between an initial state with λ_A and a final one with λ_B: the Second Law (eq. (4.6)) now becomes

$$\langle W \rangle \geq \Delta F = F_{\lambda_B} - F_{\lambda_A} \tag{4.12}$$

where the $\langle ... \rangle$ indicate an average over an ensemble of transformations $A \to B$; we stress the fact that the average of eq. (4.12) is not the ensemble average of eq. (4.8), since the former is performed on values measured across different *transformations*.

For each transformation the system is first brought to the equilibrium state (T, λ_A), and then the work W is measured over different realizations of the transformation, in which the parameter λ is changed at a finite rate using the same prescription. In particular if the transformation is reversible, that is the λ parameter is changed infinitely slowly so that the system is always at equilibrium, then the equality $W = \Delta F$ holds. The same considerations hold if λ represents a *set* of parameters: any combination of them identifies a unique equilibrium state.

Now we are ready to state the nonequilibrium equality discovered by Jarzynski [38]

$$\langle e^{-\beta W} \rangle = e^{-\beta \Delta F} \tag{4.13}$$

which allows for the calculation of the difference in free energy $\Delta F = F_{\lambda_B} - F_{\lambda_A}$ between initial and final states A and B by taking the average of the exponential of the work W. In general this average is taken over an ensemble of *nonequilibrium* transformations of the set of parameters λ of the type $\lambda_A \to \lambda_B$. We can also rewrite eq. (4.13) equivalently as

$$\Delta F = -\beta^{-1} \log \langle e^{-\beta W} \rangle. \tag{4.14}$$

The result is independent of

- the path in the λ parameter space chosen to perform the ensemble of transformations $A \to B$

- the rate at which the switching process is done (or, equivalently, the prescription used to change the λ parameters) as long as it is kept fixed for any realization used to take the average.

The crucial quantity to measure is of course the work W, which we can define as

$$W = \int_0^{t_s} dt \, \dot{\lambda} \frac{\partial H_\lambda}{\partial \lambda}(\Gamma(t)) \tag{4.15}$$

where, without loss of generality, we are considering the switching of a single parameter $\lambda(t)$, that is varied from an initial state at $t = 0$ to a final one at $t = t_s$ following an unspecified switching prescription. $\Gamma(t)$ indicates the microstate of the system at a certain point of the transformation, i.e. the trajectory of the system in phase space which describes the time dependence of every variable in phase space. We remark that, in order to take the average of eq. (4.13), we need an *ensemble* of these transformations, that must be characterized by the same switching process $\lambda(t)$ and (in general) the same path in parameter space. When these conditions are fulfilled, then the average is in practice taken over the different trajectories $\Gamma(t)$ made by the system during the different realizations. In order to see how eq. (4.15) is not an arbitrary choice to define the *work* done on the system, we can simply observe how the total derivative of the Hamiltonian H_λ can be written as

$$\dot{H}_\lambda = \dot{\lambda}\frac{\partial H_\lambda}{\partial \lambda} + \dot{\Gamma}\frac{\partial H_\lambda}{\partial \Gamma} \tag{4.16}$$

which can be interpreted as the First Law of thermodynamics: the left hand side is the variation of internal energy, while in the right hand side we recognize in the first term the work performed on the system and in the second term the heat absorbed by the system.

Before moving to section 4.2 to analyse the possible derivations of eq. (4.13), we will analyse some insightful limiting cases where the nonequilibrium equality is already known to be valid. The first one is the case of an infinitely slow switching process ($t_s \to \infty$), in which the system is always in equilibrium at any intermediate state $(T, \lambda(t))$, or, more precisely, the system is in quasistatic equilibrium with the reservoir. In this limit, the nonequilibrium relation (4.14) reduces to

$$\Delta F = \int_{\lambda_A}^{\lambda_B} d\lambda \left\langle \frac{\partial H_\lambda}{\partial \lambda} \right\rangle_\lambda \tag{4.17}$$

where the $\langle ... \rangle_\lambda$ average refers to the canonical average taken at the generic intermediate (equilibrium) state λ; in other words, for a quasistatic transformation $\Delta F = W$.

The opposite case is the one of an instantaneous switching process, that is $t_s \to 0$. In this case the work is simply

$$W = H_{\lambda_B} - H_{\lambda_A} = \Delta H$$

and eq. (4.14) becomes

$$\Delta F = -\beta^{-1} \log \langle e^{-\beta \Delta H} \rangle_{\lambda_A} \tag{4.18}$$

where the average here is again a canonical average, taken at the (initial) equilibrium state λ_A.

The most important difference between eqs. (4.17)-(4.18) and the original nonequilibrium equality is that the former give the difference in free energy in terms of canonical averages, while the latter deals explicitly with trajectories $\Gamma(t)$ out of equilibrium.

Without loss of generality, we can write the nonequilibrium relation as

$$\int dW \rho(W) e^{-\beta W} = e^{-\beta \Delta F} \tag{4.19}$$

where $\rho(W)$ is the distribution of the values of the work on a ensemble of realizations of the transformation. In general, it will depend on the details of the system and on how the switching process is done. In practice what happens is that a finite number of realizations n_R is performed on the system and the work is measured for each of them. Eq. (4.19) becomes

$$\frac{1}{n_R} \sum_{i=1}^{n_R} e^{-\beta W_i} \simeq e^{-\beta \Delta F}. \tag{4.20}$$

Since the averaged quantity is highly nonlinear, a large number of realizations n_R might be needed in an experiment to get the correct ΔF. Further and more detailed considerations and comments on the statistics that is needed to get convergence to the right result will be made in section. 4.3.

4.1.3 Relation to the Second Law

We know that the Second Law of thermodynamics must be interpreted statistically: indeed, eq. (4.12) does not imply that the work W will be always be greater than the difference in free energy, since occasionally the opposite can be true, even if the probability of such an occurrence in a macroscopic system is extremely small. In fact, only the average over an ensemble of transformation has to be greater than ΔF: is this statement compatible with the nonequilibrium work relation?

The answer is yes, and it can be shown in a very simple way. We can consider Jensen's inequality [157]

$$\langle e^x \rangle \geq e^{\langle x \rangle} \tag{4.21}$$

which holds for an average on any value of a real variable x. If we combine it with eq. (4.13) we get

$$e^{-\beta \Delta F} = \langle e^{-\beta W} \rangle \geq e^{-\beta \langle W \rangle} \tag{4.22}$$

which trivially leads to the Second Law, eq. (4.12).

The nonequilibrium work relation gives also a hint to how small the probability that one realization of a nonequilibrium transformation violates the Second Law. Following eq. (4.19), $\rho(W)\mathrm{d}W$ is the fraction of realizations that correspond to trajectories with total work comprised between W and $W+\mathrm{d}W$. Then, the probability the Second Law is "violated" by a single transformation equals the probability that during one realization the work performed on the systems is $W = \Delta F - \epsilon$, with $\epsilon > 0$ being an energy, is

$$\int_{-\infty}^{\Delta F - \epsilon} \mathrm{d}W \rho(W).$$

A series of inequalities follow:

$$\int_{-\infty}^{\Delta F - \epsilon} \mathrm{d}W \rho(W) \leq \int_{-\infty}^{\Delta F - \epsilon} \mathrm{d}W \rho(W)\, e^{\beta(\Delta F - \epsilon - W)}$$

$$\leq e^{\beta(\Delta F - \epsilon)} \int_{-\infty}^{+\infty} \mathrm{d}W \rho(W)\, e^{-\beta W}$$

$$\leq e^{-\beta \epsilon} \,,$$

in the last step eq. (4.19) was used. This brief calculation implies that a violation of magnitude ϵ has a probability of happening that decreases exponentially with $\beta\epsilon$. For a macroscopic violation $\epsilon \gg k_B T$ the related probability is extremely small, thus confirming the validity of the Second Law for macroscopic systems (4.6).

4.1.4   Relation to fluctuation theorems

A few years before the discovery of the nonequilibrium work relation by Jarzynski, a series of new developments began to shed new light on the behaviour of small system out of equilibrium. These advancements were in the form of so-called *fluctuation theorems*, which are valid for systems perturbed far away from equilibrium by some time-dependent work process. Among the most important ones we mention the one by Evans and Searles [40] for driven thermostated deterministic systems and the one by Gallavotti and Cohen [41] for thermostated deterministic steady-state ensembles. They share the same general form

$$\frac{P(+\sigma)}{P(-\sigma)} \simeq e^{\tau\sigma} \tag{4.23}$$

where $P(+\sigma)$ is the probability of observing a entropy production rate σ over a nonequilibrium trajectory of time τ keeping the system in contact with an heatbath. The entropy production rate σ measures how much the system exchanges a certain amount of heat Q with the external heatbath at temperature T, i.e.

$$\sigma = \frac{Q}{T\tau}.$$

Theorems of the form of eq. (4.23) are able to explain quantitatively why macroscopic systems always tend to dissipate or, in other words, we never observe a breakdown of the Second Law. The heat Q is an extensive quantity, so for large systems σ grows with their size; eq. (4.23) tells us that the probability ratio of observing a dissipation (i.e. positive σ) over an equally large absorption (σ negative) grows *exponentially* with the size. Fluctuation theorems of this kind explain how macroscopic irreversibility arises from the time-reversible laws that govern microscopic systems: trajectories which would violate the Second Law become exceedingly rare when the system size increases.

A generalization of these results for stochastic and microscopically reversible systems was derived a few years later by Crooks [42]: it reads

$$\frac{P^{\mathrm{F}}(+\omega)}{P^{\mathrm{R}}(-\omega)} = e^{+\omega} \tag{4.24}$$

where ω is the entropy production of the system driven out of equilibrium over some time interval. $P^{\mathrm{F}}(\omega)$ is the probability distributions associated with ω, while $P^{\mathrm{R}}(\omega)$ is related to the same transformation performed in a time-reversed way. An important distinction with respect to fluctuation theorems of the type of eq. (4.23) is that here we do not consider the entropy production *rate*, and the nonequilibrium process is a time-dependent one, as for Jarzynski's equality. For a detailed derivation of eq. (4.24) we refer to Section II of ref. [42].

Interestingly, Crooks' fluctuation theorem can be seen as a generalization of the nonequilibrium work relation by Jarzynski: first we make use of the following relation

$$\langle e^{-\omega} \rangle = \int_{-\infty}^{+\infty} \mathrm{d}\omega P^{\mathrm{F}}(+\omega)e^{-\omega} = \int_{-\infty}^{+\infty} \mathrm{d}\omega P^{\mathrm{R}}(-\omega) = 1; \qquad (4.25)$$

then, Crooks theorem (eq. (4.24)) is valid for systems that start the process from an equilibrium state (as in the case of Jarzynski's equality) and that in such case

$$\omega = -\beta \Delta F + \beta W. \qquad (4.26)$$

Now, simply substituting eq. (4.26) in eq. (4.25) leads to the nonequilibrium equality, eq. (4.13). Equivalently, the theorem (eq. (4.24) can be expressed for a system that starts in equilibrium as

$$\frac{P^{\mathrm{F}}(+W)}{P^{\mathrm{R}}(-W)} = \exp\left[\beta(W - \Delta F)\right]. \qquad (4.27)$$

A direct consequence of this relation is that if we are able to draw the probability distribution of the forward process $P^{\mathrm{F}}(+W)$ and the specular one of the reverse process $P^{\mathrm{R}}(-W)$, the value of the work W for which they are equal, i.e. where they cross each other, is a good estimate of ΔF itself. For example, this method was compared to Jarzynski's equality and to usual thermodynamic integration in ref. [158] in the case of Monte Carlo simulations for the two-dimensional Ising model.

4.1.5 Experimental evidence

A few years after the introduction by Jarzynski of the nonequilibrium work relation, its validity was confirmed experimentally [43]. The system of interest has to be microscopic, since the standard deviation of the average of the work should not be greater than $k_B T$ so that the number of realizations of the transformation necessary to use in the equality is not too large. The value of the free-energy obtained with the nonequilibrium work relation is compared to that obtained using the value of the work performed in a *reversible* transformation (such that $\Delta F = \langle W \rangle$). The experimental setup is presented in fig. 4.1: during a transformation a molecule of RNA is stretched between two beads, thus letting it fold or unfold; the force acting on the molecule was measured by a light trap on the top bead.

The test was made possible by the fact that in this experimental setup the mechanical unfolding could be performed both reversibly (stretching the molecule very slowly) and irreversibly (when the RNA was stretched more rapidly). In this way the results of reversible transformations (for which $\langle W \rangle = \Delta F$) can be compared to those obtained from nonequilibrium transformations using Jarzynski's equality. The comparison between these two approaches is illustrated in fig. 4.2.

In a nutshell, after $n_R \sim 40$ realizations of the nonequilibrium transformation, i.e. of the unfolding of the molecule in an irreversible regime, the estimate of ΔF coming from Jarzynski's equality converges to the estimate obtained with slow, reversible unfolding within statistical error; further realizations would improve the convergence even more.
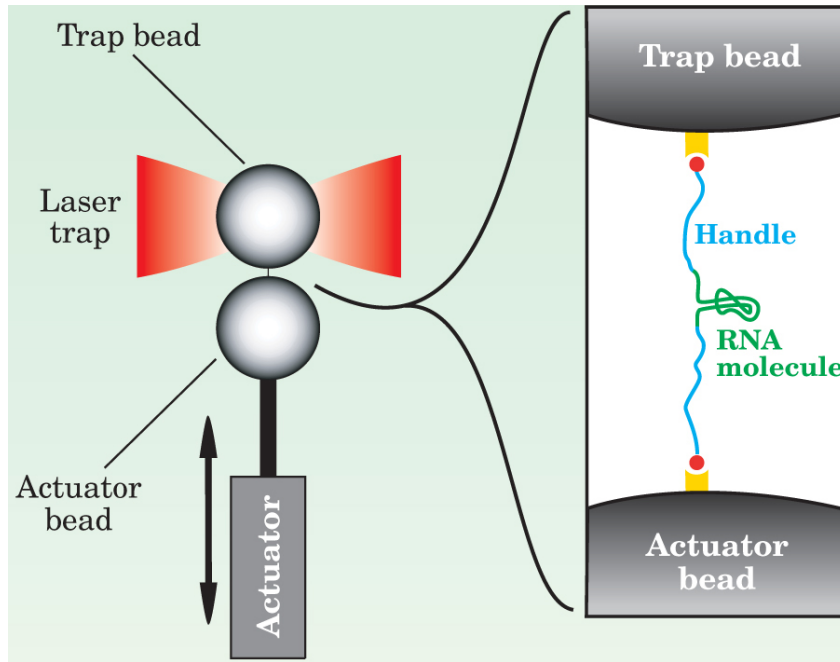
Figure 4.1: Experimental setup for the nonequilibrium work relation test in which a molecule of RNA is attached to two beads and folded and unfolded both in a reversible and irreversible way. The bottom bead is moved and stretches the RNA; its position is controlled by a piezoelectric actuator. A laser trap captures the top bead; the force exerted on the molecule connecting the beads is determined by the change in momentum of the light that exits the trap. Image taken from ref. [153].
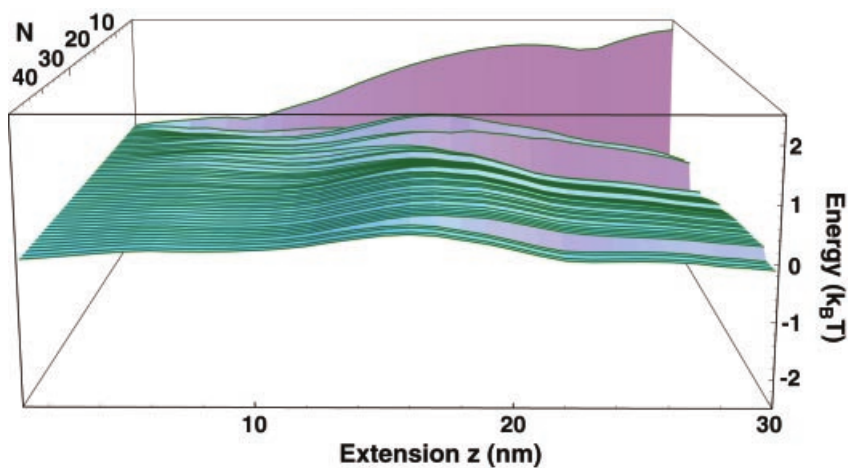
Figure 4.2: Convergence of results for the free energy difference ΔF obtained with Jarzynski's relation as a function of the number of realizations n_R of the transformation (in the image denoted as N), from 1 to 47, for various values of the extension z. On the vertical axis, the difference between the estimate of Jarzynski's equality and the estimate of reversible transformations. Image taken from ref. [43].

4.2   Derivations

In this section we will review some of the derivations of eq. (4.13) that have been proposed throughout the last two decades [38, 39, 42, 159–164]. In section 4.2.1 we will focus first on the case of a deterministic Hamiltonian evolution in order to understand the steps that bring to eq. (4.13) using only basic statistical mechanics. Then in section 4.2.2 we will review a more general derivation which extends the validity of the nonequilibrium relation to systems that evolve stochastically; this is by far the most interesting case if one has in mind an application to Markov chains and Monte Carlo simulations.

4.2.1   Hamiltonian evolution of an isolated system

A first, possible derivation of the nonequilibrium work relation (4.13) was presented in the original paper by Jarzynski [38] and it can be obtained in the rather simple case of no heat reservoir in thermal contact with the system.

The trajectory $\Gamma(t)$ describes the deterministic evolution of the system that evolves under H_λ when λ is changed throughout the transformation. At $t = 0$ (and $\lambda = \lambda_A$) the system is at equilibrium and is described by the Boltzmann-Gibbs distribution

$$f(\Gamma, t = 0) = f_{\lambda_A}^{\mathrm{BG}}(\Gamma) = \frac{1}{Z_{\lambda_A}} e^{-\beta H_{\lambda_A}(\Gamma)} \tag{4.28}$$

and it evolves under the Liouville equation

$$\frac{\partial f}{\partial t} + \{f, H_\lambda\} = 0. \tag{4.29}$$

Note that, in general, the system at $t > 0$ will not be described by the BG distribution (unless the variation of λ is performed very slowly), but by the potentially very complicated function $f(\Gamma, t)$.

A crucial point of this particular derivation is that, since the evolution is deterministic, a particular point at time t in phase space uniquely specifies the trajectory in phase space, which we denote $\Gamma_i(t)$ (where i is an index that runs on the total number of realizations of the nonequilibrium transformation). This allows us to define a work function $w(\Gamma_i, t)$ that represents the work performed on the particular trajectory Γ_i up to time t: the total work W of eq. (4.15) of a particular trajectory is simply $w(\Gamma_i, t_s)$. Now we can finally write down the ensemble average over all possible realizations (trajectories in phase space) of the exponential of the work of single trajectories as

$$\langle e^{-\beta W} \rangle = \int \mathrm{d}\Gamma\, f(\Gamma, t_s)\, e^{-\beta w(\Gamma, t_s)}. \tag{4.30}$$

Since the system is isolated, the work is the variation in internal energy, i.e.

$$w(\Gamma, t) = H_{\lambda(t)}(\Gamma(t)) - H_{\lambda_A}(\Gamma(0)) \,;$$

moreover the phase space density is conserved along any trajectory thanks to Liouville's theorem

$$f(\Gamma(t), t) = f(\Gamma(0), 0) = \frac{1}{Z_{\lambda_A}} e^{-\beta H_{\lambda_A}(\Gamma)}$$

and if we insert these last two relations inside eq. (4.30) we have

$$\langle e^{-\beta W} \rangle = \frac{1}{Z_{\lambda_A}} \int d\Gamma \, e^{-\beta H_{\lambda_B}(\Gamma(t_s))} = \frac{Z_{\lambda_B}}{Z_{\lambda_A}} \tag{4.31}$$

which is the central result of ref. [38].

For the case of a system in thermal contact with a heat reservoir, the derivation is similar: now the Hamiltonian of the overall system (system of interest + reservoir) is written as

$$H_\lambda \Gamma + \mathcal{H}(\Gamma') + H_{\text{int}}(\Gamma, \Gamma') \tag{4.32}$$

where H_{int} is the interaction term which depends on the microstates Γ and Γ' of the system and the reservoir respectively. The only additional hypothesis that is needed is that the coupling with the heat reservoir is weak and that H_{int} may be neglected.

Another way of understanding the derivation of the nonequilibrium work relation is by noting that we do not want to use the phase space density $f(\Gamma, t)$ to describe the evolution of our system, since it can be extremely complicated and most importantly non-universal. However, we can introduce an alternative statistical representation which is able to *weigh* any trajectory according to the work performed on the system up to a specific time. Let us consider a set of realizations of the transformation characterized by several distinct trajectories Γ_i, with $i = 1, ..., n_R$ and $n_R \gg 1$. We can write the usual phase space density for $t > 0$ as

$$f(\Gamma, t) \, d\Gamma \sim \frac{1}{n_R} \sum_{\Gamma_i \in \mathcal{V}} 1 \tag{4.33}$$

which essentially gives the number of realizations inside a volume $\mathcal{V}$ of size $d\Gamma$ centered around a point Γ in phase space. Such a density counts all realizations in the same way; but we can introduce another density $g(\Gamma, t)$ with a weight that depends on the *work*:

$$g(\Gamma, t) \, d\Gamma \sim \frac{1}{n_R} \sum_{\Gamma_i \in \mathcal{V}} e^{-\beta w(\Gamma, t)}. \tag{4.34}$$

We can write these distribution in a more formal way as

$$f(\Gamma, t) = \langle \delta(\Gamma - \Gamma(t)) \rangle \tag{4.35}$$

and

$$g(\Gamma, t) = \left\langle \delta(\Gamma - \Gamma(t)) e^{-\beta w(t)} \right\rangle \tag{4.36}$$

respectively; here the angular brackets represent the average on the ensemble of trajectories. At the beginning of the transformation $\lambda_A \to \lambda_B$ the two must be equal to the Boltzmann-Gibbs distribution:

$$g(\Gamma, 0) = f(\Gamma, 0) = \frac{1}{Z_{\lambda_A}} e^{-\beta H_{\lambda_A}}. \tag{4.37}$$

When $t > 0$ we have no hope of writing the general evolution of $f(\Gamma, t)$ (which follows the Liouville equation (4.29)), but we can do it for $g(\Gamma, t)$. First, we define a new

phase space density $h(\Gamma, w, t)$, that is an extended probability distribution of the trajectories which also takes into account the work associated to each trajectory:

$$h(\Gamma, t) = \langle \delta(\Gamma - \Gamma(t)) \, \delta(w - w(t)) \rangle \; ; \tag{4.38}$$

this distribution evolves in time following

$$\frac{\partial h}{\partial t} = \{H_\lambda, h\} - \dot{w}\frac{\partial h}{\partial w} = \{H_\lambda, h\} - \dot{\lambda}\frac{\partial H}{\partial \lambda}\frac{\partial h}{\partial w} \tag{4.39}$$

where in the last step we used the definition of $w(\Gamma, t) = \int \mathrm{d}t \, \dot{\lambda} \, \partial H_\lambda / \partial \lambda$. We can now rewrite $g(\Gamma, t)$ in a more useful form as

$$g(\Gamma, t) = \int \mathrm{d}w \, h(\Gamma, w, t) \, e^{-\beta w} \tag{4.40}$$

which agrees with the formal definition given in eq. (4.36). Now, the evolution of $g(\Gamma, t)$ is described by

$$\frac{\partial g}{\partial t} = \{H_\lambda, g\} - \beta\dot{\lambda}\frac{\partial H}{\partial \lambda}g \tag{4.41}$$

which follows from the evolution equation written for $h(\Gamma, t, w)$ (4.39) after integrating in $\mathrm{d}w$.

The evolution equation (4.41) has the solution

$$g(\Gamma, t) = \frac{1}{Z_{\lambda_A}}e^{-\beta H_{\lambda(t)}(\Gamma)} \tag{4.42}$$

assuming the initial condition (4.37) and using the chain rule for Poisson brackets

$$\{H_\lambda, e^{-\beta H_\lambda}\} = -\beta e^{-\beta H_\lambda}\{H_\lambda, H_\lambda\} = 0. \tag{4.43}$$

Then, if we formally integrate $g(\Gamma, t_s)$ in phase space we get

$$\int \mathrm{d}\Gamma \, g(\Gamma, t_s) = \frac{Z_{\lambda_B}}{Z_{\lambda_A}} \tag{4.44}$$

and recalling the definition of $g(\Gamma, t_s)$ (eq. (4.36)) we can rewrite the left-hand side as

$$\langle e^{-\beta W} \rangle = \frac{Z_{\lambda_B}}{Z_{\lambda_A}} \tag{4.45}$$

which is the central result of ref. [38].

4.2.2 Master equation approach

In this section we will derive the nonequilibrium relation in the framework of stochastic processes with the use of a master equation, following mostly the work of ref. [39]. We start by considering the case of a system whose time evolution is described by a stochastic phase space trajectory denoted as $\Gamma(t)$ like in the previous section. We will assume that the trajectory $\Gamma(t)$ is entirely characterized by a transition probability function

$$P(\Gamma, t + \Delta t | \Gamma', t) \tag{4.46}$$

that represents the probability of obtaining the system in a state Γ at time $t + \Delta t$ given that at time t it was in a certain state Γ'. Stochastic processes that satisfy this condition are called *Markov processes*: in practice, the new microstate Γ is determined only from the previous microstate Γ' and from any random numbers generated at time t. We define the transition function R by taking the derivative of P with respect to the time interval Δt

$$R(\Gamma' \to \Gamma, t) \equiv \left. \frac{\partial}{\partial(\Delta t)} P(\Gamma, t + \Delta t | \Gamma', t) \right|_{\Delta t \to 0} \tag{4.47}$$

which gives the instantaneous rate of transitioning to a state Γ coming from Γ' at time t and specifies the continuous-time Markov process. We assume that the dependence of $R(\Gamma' \to \Gamma, t)$ on t arises through the set of parameters λ of the system that are changed throughout the out-of-equilibrium trajectories, as it has been described in detail in the previous sections. Thus, we can write

$$R(\Gamma' \to \Gamma, t) = R_{\lambda(t)}(\Gamma' \to \Gamma) \tag{4.48}$$

that means that all the characteristics of the heat reservoir are constant and all the time dependence enters only via the λ parameter (from now on we will consider the case of only one parameter).

Now, since we are mostly interested in many different trajectories, we will consider the evolution of an ensemble of the Markovian processes which is described by a time-dependent phase space density $f(\Gamma, t)$, exactly as in the Hamiltonian evolution case. The evolution of such processes is described by the following equation:

$$\frac{\partial f}{\partial t}(\Gamma, t) = \int d\Gamma' \, f(\Gamma', t) \, R_{\lambda(t)}(\Gamma' \to \Gamma) \tag{4.49}$$

which is abbreviated as

$$\frac{\partial f}{\partial t}(\Gamma, t) = \hat{R}_{\lambda(t)} f \tag{4.50}$$

where $\hat{R}_{\lambda(t)}$ is a time-dependent operator which acts in the space of phase space densities $f(\Gamma, t)$. Eq. (4.50) is the master equation, which completely determines the evolution of the density f whenever the time-dependence of the parameter $\lambda(t)$ (that is the protocol of the switching process) is known and the initial distribution $f(\Gamma, t = 0)$ is specified. In the case of stochastic processes, the master equation takes the role that the Liouville equation for $f(\Gamma, t)$ has for the Hamiltonian evolution of section 4.2.1.

Another assumption on our stochastic process is required before moving to the derivation of the work relation. If we keep λ fixed, then we are dealing with a stationary Markov process in which the external forces acting on the system (by changing λ) are time-independent: we require the canonical distribution to be invariant under such evolution. In the formalism used in this section, this translates to

$$\hat{R}_{\lambda(t)} \exp{-\beta H_\lambda(\Gamma)} = 0 \tag{4.51}$$

that is, the $\hat{R}$ operator annihilates the Boltzmann-Gibbs distribution; Markovian processes that satisfy eq. (4.51) are called *thermal* Markov processes. There is a

stronger version of this assumption, that is usually referred to as detailed balance, which can be expressed as

$$\frac{R_\lambda(\Gamma' \to \Gamma)}{R_{\lambda(t)}(\Gamma \to \Gamma')} = \frac{\exp -\beta H_\lambda(\Gamma)}{\exp -\beta H_\lambda(\Gamma')}. \tag{4.52}$$

With proper multiplication and integration in Γ' of the terms of eq. (4.52) one can easily recover eq. (4.51).

Now we proceed as in the second half of section 4.2.1: we define the new phase space density $g(\Gamma, t)$ which incorporates a new density $Q(\Gamma, t)$:

$$g(\Gamma, t) = f(\Gamma, t)\, Q(\Gamma, t) \; ; \tag{4.53}$$

the function $Q(\Gamma, t)$ denotes the average value of $\exp -\beta w(t)$ over a set of trajectories. As before, we can readily express the ensemble average of the total work $W = w(t_s)$

$$\int \mathrm{d}\Gamma\, g(\Gamma, t_s) = \langle e^{-\beta W} \rangle. \tag{4.54}$$

Now $g(\Gamma, t)$ obeys an evolution equation very similar to the one obtained previously:

$$\frac{\partial g}{\partial t} = \left(\hat{R}_{\lambda(t)} - \beta \dot{\lambda} \frac{\partial H}{\partial \lambda} \right) g. \tag{4.55}$$

With the usual initial conditions of eq. (4.37) we write the solution

$$g(\Gamma, t) = \frac{1}{Z_{\lambda_A}} e^{-\beta H_{\lambda(t)}(\Gamma)} \tag{4.56}$$

from which the nonequilibrium relation is easily obtained, this time for arbitrary thermal Markov dynamics.

4.3   Rare events and dissipation

The peculiar nature of the exponential average of the nonequilibrium work relation, eqs. (4.13) and (4.14), has an unwanted consequence: the practical determination of the free energy difference is dominated by relatively few realizations of the nonequilibrium transformation among all those performed. The behaviour of the final result of the exponential average depends strongly on such "rare" realizations: because of this, convergence to the right result can be poor and the total number of realizations, that from now on we denote with n_R, can be rather large when the correct value is reached. In the last two decades, Jarzynski and collaborators developed a theoretical background to understand this issue and elaborate its best treatment in a series of works [165–167].

In order to understand this phenomenon we start by analysing the distributions showed in fig. 4.3: the first, $\rho(W)$, describes the distribution of the work W that is measured across several realizations of the transformation. We stress the fact that it does not have to be a Gaussian, as in general it will depend strongly on the properties of the system and how the transformation is performed.
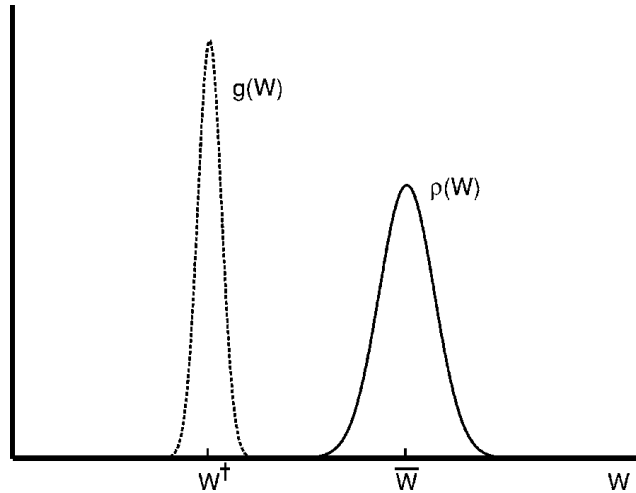
Figure 4.3: In this figure from ref. [165] the $\rho(W)$ distribution represents the distribution of the work among the realizations of a nonequilibrium transformation: the measured work will be found in the region around the peak of $\rho(W)$ with high probability. The distribution $g(W) = \rho(W)e^{-\beta W}$ represents the distribution of the values of the work that dominate the exponential average of Jarzynski's equality.

Of course $\rho(W)$ is the distribution we use to compute the average of the work:

$$\overline{W} = \int dW\, \rho(W)\, W. \tag{4.57}$$

Conversely, the other distribution that appears in fig. 4.3, defined as $g(W) = \rho(W)\, e^{-\beta W}$, is the one relevant for the nonequilibrium work relation. Indeed, the exponential average is nothing but

$$\langle e^{-\beta W} \rangle = \int dW\, \rho(W)\, e^{-\beta W} = \int dW\, g(W); \tag{4.58}$$

thus, the values of W distributed around the peak of $g(W)$, denoted with $W^\dagger$ (not to be confused with the notation for hermitian conjugation), are the ones that *dominate* the exponential average; because of this the realizations whose work happen to be close to $W^\dagger$ are also known as *dominant realizations*. To compute $W^\dagger$ we write

$$W^\dagger = c^{-1} \int dW\, g(W)\, W \tag{4.59}$$

with $c = \int dW\, g(W)$. In practice, the dominant realizations are those that are in the far left tail of $\rho(W)$ and, depending on its shape, can be quite rare if compared to the remaining ones centered around $\overline{W}$, which are usually denoted as *typical* realizations.

It is now clear that the tail of work distribution $\rho(W)$ has a special role in the nonequilibrium work relation; but how many realizations do we need in order to obtain convergence? In order to obtain an estimate of the minimum value of n_R, we have to take into consideration both the forward ("F") and the reverse ("R") processes: their respective work distributions, P^{F} and P^{R}, are showed in fig. 4.4 and, as predicted by Crooks' theorem, they cross each other exactly in $W = \Delta F$.
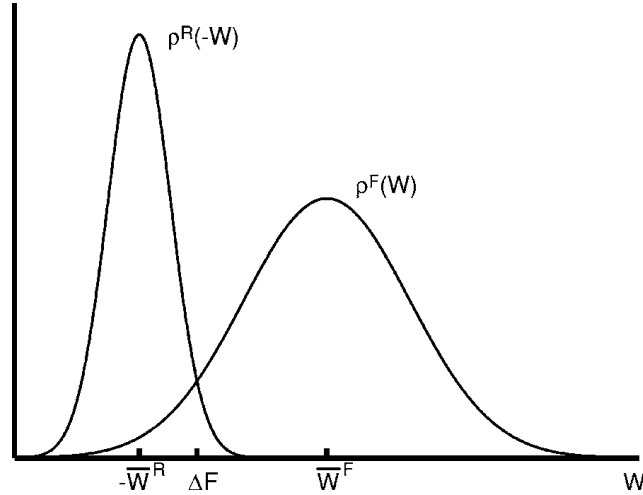
Figure 4.4: In this figure from ref. [165] the work distributions, P^{F} and P^{R}, of the same transformation performed in two opposite directions (forward and reverse, respectively) are presented. Note the minus sign for the reverse distribution to account for the specularity of the transformation; plus, the shape of the two distributions is different as in general they are not symmetric with respect to each other and depend strongly on the switching process and on the physical properties of the system.

In ref. [165] a crucial result for a solid estimate of n_R was presented: the idea is that dominant realizations of the forward process are *conjugate twins* of typical realizations of the backward process, and vice versa. Firstly, conjugate twins realizations are defined as phase space trajectories Γ (one forward, one reverse) which are related by time reversal: if $\Gamma^{\mathrm{F}}(t)$ is a possible trajectory of the forward process, then its conjugate pair will be

$$\Gamma^{\mathrm{R}}(t) = \Gamma^{\mathrm{F}*}(t_{fin} - t).$$

The asterisk refers the reversal of the momenta in phase space, that is $(\mathbf{q}, \mathbf{p})^* = (\mathbf{q}, -\mathbf{p})$; this means that the conjugate twin will describe the same events of $\Gamma^{\mathrm{F}}(t)$ but with time running backwards. A variant of Crooks' theorem can be written for twin trajectories

$$\frac{P^{\mathrm{F}}[\Gamma^{\mathrm{F}}]}{P^{\mathrm{R}}[\Gamma^{\mathrm{R}}]} = \exp(\beta W_d^{\mathrm{F}}[\Gamma^{\mathrm{F}}]) = \exp(-\beta W_d^{\mathrm{R}}[\Gamma^{\mathrm{R}}]). \qquad (4.60)$$

which represents a particular relationship between the two probability distributions.

In other words, dominant forward trajectories are typical reverse trajectories in which time seems to be running backwards: for a thorough physical description of this behaviour and a formal derivation of this result we refer to [165].

Making use of this duality between dominant and typical realizations, it is possible to make a good estimate of the probability that one forward trajectory falls into the dominant region. In particular, the number of realizations needed to reach convergence can be estimated using

$$n_R^{\mathrm{F}} \sim \exp(\beta \overline{W}_d^{\mathrm{R}}) \qquad \text{and} \qquad n_R^{\mathrm{R}} \sim \exp(\beta \overline{W}_d^{\mathrm{F}}) \qquad (4.61)$$

for forward and reverse processes respectively. Here $W_d = W - \Delta F$ is the *dissipated* work, which is the crucial quantity for the nonequilibrium relation as the number of needed realizations grows exponentially with it. In general, if the transformation is performed relatively slowly, then the dissipated work will be small and the two distributions will be rather close, leading to good convergence with few realizations, while if $\overline{W}_d$ turns out to be large the distributions will be distant and the results may not converge rapidly. Somewhat surprisingly, eq. (4.61) says that the number of necessary realizations of the forward process is determined by how much work is dissipated in the reverse process, and vice versa: counterintuitively the direction in which the process dissipates more is the one in which the exponential average converges more rapidly.

It is useful to mention that another way to examine this issue is by looking at how much the two work distributions P^{F} and P^{R} overlap. The amount of overlap can be quantitatively measured using the Kullback-Leibler divergence, or relative entropy, which for two generic distributions p_0 and p_1 is defined as

$$D[p_0||p_1] = \int p_0 \ln\left(\frac{p_0}{p_1}\right) \geq 0; \qquad (4.62)$$

if $D = 0$ the two distributions are perfectly overlapping. Computing the relative entropy for the forward and reverse distributions leads to

$$D[P^{\mathrm{F}}||P^{\mathrm{R}}] = \int \mathrm{d}\Gamma^{\mathrm{F}} P^{\mathrm{F}}[\Gamma^{\mathrm{F}}] \ln\left(\frac{P^{\mathrm{F}}[\Gamma^{\mathrm{F}}]}{P^{\mathrm{R}}[\Gamma^{\mathrm{R}}]}\right) \qquad (4.63)$$

where Γ^{F} and Γ^{R} are conjugate twins; using eq. (4.60) we get the simple result

$$D[P^{\mathrm{F}}||P^{\mathrm{R}}] = \beta\left(\overline{W}^{\mathrm{F}} - \Delta F\right) \equiv \beta\overline{W}_d^{\mathrm{F}} \geq 0 \qquad (4.64)$$

and similarly

$$D[P^{\mathrm{R}}||P^{\mathrm{F}}] = \beta\overline{W}_d^{\mathrm{R}} \geq 0. \qquad (4.65)$$

When the dissipated work is too large the overlap is small and thus there is no convergence; if the distance D is smaller (ideally close to 0), then the nonequilibrium work relation becomes reliable.

A more quantitative analysis of this issue, in particular a precise estimate of the bound on n_R, is reported in ref. [167].

4.4 From statistical mechanics to lattice gauge theory

In the context of lattice gauge theories the computation of differences in free energy via Monte Carlo numerical simulations is naturally related to a large number of physically interesting observables. The most typical case is the determination of the equation of state of QCD and QCD-like theories and more in general the exploration of the phase diagram of strongly-interacting theories by evaluating the pressure, i.e. *minus* the free energy density. Other notable examples include the free energy density associated with interfaces between center domains (see for example [168–170]) and the expectation values of operators such as 't Hooft loops [171], which are tightly related to the study of confinement and have been

closely analyzed on the lattice. In some models even other extended operators, like Wilson and Polyakov loops, can be expressed in terms of ratios of partition functions in a proper dual formulation of the theory.

For all the aforementioned observables, the computation either of the free energy difference or of the ratio of partition functions is usually rather complicated and cumbersome. Good examples are the "integral method" for the computation of the pressure (see section 1.3.1) or the "snake algorithm" (see for example its application for the computation of the v.e.v. of 't Hooft loops [172]): while these methods are rather reliable and widely used, they need several independent simulations and obtaining the final result is usually a non-trivial endeavour.

The constant need for new and efficient methods for the computation of free energy differences in Monte Carlo simulations is the motivation underlying the implementation of the nonequilibrium work relation. Indeed, Jarzynski's equality can be the foundation for new techniques in lattice gauge theory in which out-of-equilibrium numerical simulations are exploited to compute a large ensemble of observables both in an efficient and elegant manner. In this section we review the demonstration of the validity of the nonequilibrium relation in the context of Markov chains (even when the temperature is not constant) and then we present its first actual implementation in a simple lattice gauge model. A full-scale, high-precision numerical experiment will be later presented in chapter 5.

4.4.1   Jarzynski's equality for Markov chains

The derivation of the nonequilibrium relation in the case of a Markov chain follows the steps of the general derivation reviewed in section 4.2.2, with a few important distinctions. We introduce a slightly different notation with respect to the previous sections of this chapter, which reflects the fact that we have in mind an application to discrete statistical systems (such as spin models) that are simulated numerically. The collective values of the microscopic degrees of freedom of our system are denoted as ϕ, which is called a *configuration* of the system. The partition function is

$$Z_\lambda = \sum_\phi \exp\left(-\frac{H_\lambda[\phi]}{T}\right) \tag{4.66}$$

where H_λ is the Hamiltonian of the system which depends on the usual set of parameters λ. T is the temperature, having set $k_B = 1$. The Boltzmann-Gibbs distribution is

$$\pi_\lambda[\phi] = \frac{1}{Z_\lambda} \exp\left(-\frac{H_\lambda[\phi]}{T}\right) \tag{4.67}$$

and we recall that it is normalized to 1

$$\sum_\phi \pi_\lambda[\phi] = 1. \tag{4.68}$$

In a Markov chain, new configurations of the system are generated according to the transition probability function $P_\lambda[\phi \to \phi']$, which gives the probability of going from a configuration ϕ to ϕ'. It is normalized to 1 too:

$$\sum_{\phi'} P_\lambda[\phi \to \phi'] = 1. \tag{4.69}$$

Like in section 4.2.2, we assume that the system satisfies the detailed balance condition, which in this case reads

$$\pi_\lambda[\phi]\, P_\lambda[\phi \to \phi'] = \pi_\lambda[\phi']\, P_\lambda[\phi' \to \phi]. \tag{4.70}$$

The evolution of the system in a Monte Carlo simulation is of course not continuous, but goes through a discrete sequence of configurations $\phi_1, \phi_2, ...$; the jump from one configuration to the next will be denoted as an *update*. The out-of-equilibrium evolution driven by external forces that change the value of the parameters λ, which has been described in detail in section 4.1.2, now has to be discretized into a certain number of subintervals. Moreover, the continuous time t becomes a discrete Monte Carlo time t_n; thus the switching process of the $\lambda(t_n)$ parameters has to be discretized too. For clarity we will simply denote the intermediate values as $\lambda_n = \lambda(t_n)$, so that the entire transformation induced by an external force on the system will be

$$\lambda_0 \to \lambda_1 \to ... \to \lambda_N$$

where N is the number of subintervals. If we consider one particular trajectory of our system, we will also have a discrete set of N configurations

$$\phi(t_1) \to \phi(t_2) \to ... \to \phi(t_N)$$

which represent the microstates of the system during the nonequilibrium transformation.

The continuous-time definition of the work of eq. (4.15) has to be modified too, to accommodate the discrete-time dynamics of the Markov chain. In particular the work is nothing but the sum of the difference in the Hamiltonian at each step of the Markov process:

$$W = \sum_{n=0}^{N-1} \left(H_{\lambda_{n+1}}[\phi(t_n)] - H_{\lambda_n}[\phi(t_n)] \right). \tag{4.71}$$

It is of the utmost importance to state unambiguously how the entire nonequilibrium transformation is implemented in the language of a Markov chain. These are the steps that must be rigidly followed in order to obtain the correct results:

1. the nonequilibrium relation requires that the system at the beginning of the trajectory is in equilibrium. This means that the starting configuration $\phi(t_0)$ must obey the Boltzmann-Gibbs distribution $\pi_{\lambda_0}[\phi(t_0)]$ with respect to the initial value of the parameters λ_0;

2. then, the parameters switch from the initial value λ_0 to the first intermediate value λ_1, following the given protocol for the transformation

$$\lambda_0 \to \lambda_1;$$

3. afterwards, the work done on the system with this first "switch" of λ has to be computed simply by taking the difference of the Hamiltonian

$$H_{\lambda_1}[\phi(t_0)] - H_{\lambda_0}[\phi(t_0)];$$

note that the Hamiltonian is evaluated using the same configuration (microstate) but different λ;

4. now the system can go to the configuration $\phi(t_1)$ by updating the old configuration *using the new value* λ_1

$$\phi(t_0) \xrightarrow{\lambda_1} \phi(t_1);$$

5. steps 2, 3 and 4 now must be repeated until the end of the transformation. In general, the parameters are changed following the given prescription

$$\lambda_n \to \lambda_{n+1},$$

the work performed on the system to do so is calculated

$$H_{\lambda_{n+1}}[\phi(t_n)] - H_{\lambda_n}[\phi(t_n)],$$

and the system is updated using the new value of the parameters

$$\phi(t_n) \xrightarrow{\lambda_{n+1}} \phi(t_{n+1});$$

6. at the end of the trajectory, the total work (4.71) is computed.

7. a new equilibrium configuration $\phi(t_0)$ is generated by thermalizing the system with λ_0, and a new realization of the nonequilibrium transformation can begin.

The validity of the nonequilibrium relation implemented in Markov chains using the aforementioned procedure will be shown in section 4.4.2 with a derivation in a slightly generalized framework.

4.4.2   An extension for non-isothermal processes

In the first derivation that Jarzynski proposed in ref. [38] for the nonequilibrium relation he considered an isolated system whose dynamics are driven by Hamiltonian evolution. Crucially, the system is first brought to equilibrium with a heat reservoir at temperature T and then isolated from it so that no heat exchanges are possible: any variation of T has no effect at all on the transformation. The relation still holds when considering the system of interest in thermal contact with the heat bath, but only when interaction with it is weak enough to be negligible. However, when deriving the relation within the framework of Markovian dynamics like in ref. [39], the situation is somewhat different: now any interaction with the "heat reservoir" is encoded in the transition rates and thus heat exchanges are taken properly into account.

It is clear then that there is no motivation to leave the temperature of the heat bath unchanged during the transformation, and it is a simple exercise to re-derive the nonequilibrium equality treating the temperature T as a generic λ parameter. This was first done explicitly in ref. [173] in the case of a Markov chain; as we will see, the case of varying temperature leads to a new, generalized Jarzynski's equality which can be of great use especially in Monte Carlo simulations.

We review the derivation of ref. [173], which follows the one by Crooks at fixed T [159], properly adapted to the notation used in ref. [44] and in this thesis. The

temperature and the λ parameter(s) are changed using a given protocol along the N steps of the discretized transformation:

$$\lambda_0 \to \lambda_1 \to ... \to \lambda_N$$

$$T_0 \to T_1 \to ... \to T_N$$

where λ_0 and T_0 identify the state the starting configuration ϕ_0 is in equilibrium with. We start by generalizing the total work of eq. (4.71) to a new quantity that accounts for the variation in temperature of the "heat reservoir":

$$\sum_{n=0}^{N-1} \left(\frac{H_{\lambda_{n+1}}[\phi(t_n)]}{T_{n+1}} - \frac{H_{\lambda_n}[\phi(t_n)]}{T_n} \right). \tag{4.72}$$

Then, the quantity that is averaged over multiple realizations of the nonequilibrium transformation is the exponential of eq. (4.72), which can be rewritten using the Boltzmann-Gibbs distribution (4.67) as

$$\exp\left[-\sum_{n=0}^{N-1} \left(\frac{H_{\lambda_{n+1}}[\phi(t_n)]}{T_{n+1}} - \frac{H_{\lambda_n}[\phi(t_n)]}{T_n} \right) \right] = \prod_{n=0}^{N-1} \frac{Z_{\lambda_{n+1}} \, \pi_{\lambda_{n+1}}[\phi(t_n)]}{Z_{\lambda_n} \, \pi_{\lambda_n}[\phi(t_n)]}. \tag{4.73}$$

We know that this quantity must be averaged over an ensemble of trajectories $(\lambda_0, T_0) \to (\lambda_N, T_N)$: in order to do so we introduce an average over all possible "histories" of the system throughout the transformation as an average on all possible intermediate states. Formally, we write the sum on any trajectory $\{\phi(t)\}$ as a sum on every intermediate step

$$\sum_{\{\phi(t)\}} ... = \sum_{\phi(t_0)} \sum_{\phi(t_1)} ... \sum_{\phi(t_N)} ...$$

so that the average on any trajectory of the quantity of eq. (4.73) is

$$\sum_{\{\phi(t)\}} \pi_{\lambda_0}[\phi(t_0)] \prod_{n=0}^{N-1} \left[\frac{Z_{\lambda_{n+1}}}{Z_{\lambda_n}} \frac{\pi_{\lambda_{n+1}}[\phi(t_n)]}{\pi_{\lambda_n}[\phi(t_n)]} P_{\lambda_{n+1}}[\phi(t_n) \to \phi(t_{n+1})] \right] \tag{4.74}$$

where we used the fact that

- the system at t_0 is in equilibrium, and thus the configuration $\phi(t_0)$ obeys the Boltzmann-Gibbs distribution,

- every time the system is updated with a new parameter λ_{n+1}, it has to follow the transition probability $P_{\lambda_{n+1}}[\phi(t_n) \to \phi(t_{n+1})]$.

All the partition functions but two cancel in eq. (4.74); if we apply the detailed balance condition (4.70) for $\pi_{\lambda_{n+1}}$ and $P_{\lambda_{n+1}}$ we get

$$\frac{Z_{\lambda_N}}{Z_{\lambda_0}} \sum_{\{\phi(t)\}} \pi_{\lambda_0}[\phi(t_0)] \prod_{n=0}^{N-1} \left[\frac{\pi_{\lambda_{n+1}}[\phi(t_{n+1})]}{\pi_{\lambda_n}[\phi(t_n)]} P_{\lambda_{n+1}}[\phi(t_{n+1}) \to \phi(t_n)] \right].$$

Again, all the distributions cancel except for one, leaving

$$\frac{Z_{\lambda_N}}{Z_{\lambda_0}} \sum_{\{\phi(t)\}} \pi_{\lambda_N}[\phi(t_N)] \prod_{n=0}^{N-1} P_{\lambda_{n+1}}[\phi(t_{n+1}) \to \phi(t_n)]$$

which can be easily rewritten recalling the definition of $\sum_{\{\phi(t)\}}$, namely

$$\frac{Z_{\lambda_N}}{Z_{\lambda_0}} \sum_{\phi(t_0)} \sum_{\phi(t_1)} \cdots \sum_{\phi(t_N)} \pi_{\lambda_N}[\phi(t_N)] \prod_{n=0}^{N-1} P_{\lambda_{n+1}}[\phi(t_{n+1}) \to \phi(t_n)].$$

Here each of the terms of the type

$$\sum_{\phi(t_n)} P_{\lambda_{n+1}}[\phi(t_{n+1}) \to \phi(t_n)]$$

can be set to 1 using eq. (4.69), leaving

$$\frac{Z_{\lambda_N}}{Z_{\lambda_0}} \sum_{\phi(t_N)} \pi_{\lambda_N}[\phi(t_N)]$$

which, after using the normalization of the Boltzmann-Gibbs distribution (4.68), leads to the central result. Namely, we have that, for transformations in which also the temperature T is varied, the nonequilibrium relation

$$\left\langle \exp\left[\sum_{n=0}^{N-1} \left(\frac{H_{\lambda_{n+1}}[\phi(t_n)]}{T_{n+1}} - \frac{H_{\lambda_n}[\phi(t_n)]}{T_n}\right)\right]\right\rangle = \frac{Z_{\lambda_N}(T_N)}{Z_{\lambda_0}(T_0)} \qquad (4.75)$$

holds; if T is constant then we obtain the usual work relation

$$\left\langle \exp\left[-\frac{1}{T} \sum_{n=0}^{N-1} \left(H_{\lambda_{n+1}}[\phi(t_n)] - H_{\lambda_n}[\phi(t_n)]\right)\right]\right\rangle = \frac{Z_{\lambda_N}(T)}{Z_{\lambda_0}(T)} = \exp\left(-\frac{F_{\lambda_N} - F_{\lambda_0}}{T}\right).$$

4.4.3   A first application to lattice gauge theory

The interface free-energy in the two-dimensional Ising model has been already studied using Jarzynski's equality via out-of-equilibrium Monte Carlo numerical simulations in recent years [158, 174]; we mention also studies for the surface tension in three dimensions [173].

However, the nonequilibrium equality has been effectively implemented in the context of lattice gauge theories for the first time in ref. [44], in the study of the free energy associated to an interface in the $\mathbb{Z}_2$ gauge model. This model is a perfect benchmark for a large-scale test of the efficiency of Jarzynski's equality in a rather different context such as lattice gauge theories: indeed, it is the simplest lattice gauge theory in which a high-precision numerical study of interfaces is possible and it is a perfect bridge between statistical mechanics and lattice gauge theory. In the following we will review some of the theoretical aspects of this gauge model and will analyse in some detail how the calculation of the free energy was performed using the nonequilibrium work relation. Part of the motivation for this work was to

compare new accurate numerical results with the prediction of an effective string theory following a series of works by the Turin group over the last few years. This analysis will not be covered here; for more details about this and also for further physical insight on interfaces and their properties we refer to [44] and references therein.

The dynamics of the $\mathbb{Z}_2$ gauge theory in three Euclidean dimensions is described by the respective Wilson action

$$S_{\mathbb{Z}_2} = -\beta_{\mathrm{g}} \sum_{x \in \Lambda} \sum_{0 \leq \mu < \nu \leq 2} \sigma_\mu(x)\sigma_\nu(x + a\hat\mu)\sigma_\mu(x + a\hat\nu)\sigma_\nu(x) \tag{4.76}$$

which is structurally the same as the one defined in eq. (1.19): β_{g} is the usual inverse coupling, and the σ_μ are link variables that take value in the $\mathbb{Z}_2$ group, that is $\sigma_\mu(x) = \pm 1$. The partition function of the theory can be explicitly written as

$$Z_{\mathbb{Z}_2} = \sum_{\{\sigma_\mu(x)=\pm 1\}} \exp\left(-S_{\mathbb{Z}_2}\right) \tag{4.77}$$

where the sum runs over all possible configurations of the link variables. This gauge model possesses a confining phase for small values of β_{g} and a second order phase transition at $\beta_{\mathrm{g}} = 0.76141346(6)$ [175]. This theory is a perfect bridge between statistical mechanics and lattice gauge theory: indeed, using the Kramers-Wannier duality [176, 177] the partition function of eq. (4.77) can be exactly rewritten as the one of the three-dimensional Ising model, whose Hamiltonian reads

$$H = -\beta \sum_{x \in \tilde\Lambda} \sum_{0 \leq \mu \leq 2} J_{x,\mu} s_x s_{x+a\hat\mu}, \tag{4.78}$$

where the $s_x = \pm 1$ variables are defined on the sites of the *dual* lattice $\tilde\Lambda$ and the $J_{x,\mu}$ couplings are defined on the links of the lattice. The new parameter β is related to the gauge coupling β_{g} via the relation

$$\beta = -\frac{1}{2}\ln\tanh\beta_{\mathrm{g}}; \tag{4.79}$$

this notation will be used for simplicity only throughout this section: we stress that in all other chapters $\beta = 2N/g^2$. Note that the confining regime of the gauge model corresponds to the high-β, low-T ordered phase of the Ising model.

The couplings $J_{x,\mu}$ can be set to any value between 1 and -1, corresponding to ferromagnetic and anti-ferromagnetic couplings respectively. The first step in the analysis of the behaviour of an interface in this model is to consider one specific direction $\mu = 0$ and one slice of the lattice containing all the links from the sites x to sites $x + a\hat 0$: by setting $J_{x,0} = -1$ only for the sites belonging to that slice (while keeping all the remaining couplings set to 1) we can effectively impose *antiperiodic* boundary conditions. This has the effect of creating a frustration in the system, thus inducing the formation of an interface between two domains with opposite magnetization. On the other hand, *periodic* boundary conditions correspond to $J_{x,0} = +1$ for all links in the system, including those on the aforementioned slice of the lattice.

If we denote with Z_a and Z_p the partition function of the three-dimensional Ising model with antiperiodic and periodic boundary conditions respectively, we can give a first possible definition of the (adimensional) free energy associated to an interface:

$$F^{(1)} = -\ln\left(\frac{Z_a}{Z_p}\right) + \ln N_0. \tag{4.80}$$

N_0 represents the number the sites in the $\mu = 0$ direction, and the rightmost term accounts for the fact that the interface can be located anywhere in the 0 direction. Only one large interface should be created in the μ direction, and zero in the remaining two directions with periodic boundary conditions; however, in order to take into account the possibility of multiple interfaces forming in the system, an improved definition was proposed in ref. [178]

$$F^{(2)} = -\ln\operatorname{arctanh}\left(\frac{Z_a}{Z_p}\right) + \ln N_0 \tag{4.81}$$

which has been derived under the assumption that such interfaces are indistinguishable, dilute and non-interacting.

In ref. [44] a new methodology for the calculation of the free energy of an interface based on Jarzynski's equality was introduced. The main idea is to perform out-of-equilibrium Monte Carlo simulations in which the system switches from periodic to antiperiodic boundary conditions and vice versa: calculating the work performed when doing so allows one to compute the ratio Z_a/Z_p that defines the desired free energy via the nonequilibrium relation. The λ parameter defined in section 4.1.2, which is varied by external forces throughout the transformation, is identified in this situation with the couplings $J_{x,\mu}$ in the direction $\mu = 0$ and in a specific slice. In particular, the transformation is performed between two systems:

- one in which the couplings in the 0 direction and in the $N_0 - 1$ slice are set to -1, i.e. $J_{N_0-1,0} = -1$, while all the others are set to $J_{x,\mu} = 1$,

- and one in which all the coupling are set to $J_{x,\mu} = 1$.

The protocol that implements the switching process between these two systems is a linear one, namely

$$\lambda\left(t_0 + n\tau\right) = J_{(N_0-1,x_1,x_2),0}\left(t_0 + n\tau\right) = 1 - \frac{2n}{N}, \qquad \text{with } \tau = \frac{t_N - t_0}{N} \tag{4.82}$$

where t_n represent the "time" that keeps track of the steps performed during the nonequilibrium trajectory; we recall that the exact prescription that must be followed during the out-of-equilibrium Monte Carlo simulation is the one described in detail in section 4.4.1.

Several numerical simulations with different combinations of the number of steps N during a transformation and of the number n_R of realizations of such transformations have been performed. We report below in table 4.1 the results obtained for a lattice of sizes $N_0 = 96$, $N_1 = 24$ and $N_2 = 64$; in fig. 4.5 the same results, both from direct and reverse transformations, are presented and compared with those obtained independently in ref. [178].

Table 4.1: Results for the interface free energy of eq. (4.80) from "direct" and "reverse" realizations of the nonequilibrium transformation from periodic to antiperiodic boundary conditions in the $\mu = 0$ direction, on a lattice of size $N_0 \times N_1 \times N_2 = 96 \times 24 \times 64$, at $\beta = 0.223102$ (corresponding to $\beta_g = 0.758264$), and for a different number N of intermediate steps used to discretize the nonequilibrium evolution of λ. n_R is the number of realizations used in the average over nonequilibrium processes: the product $N \times n_R$ corresponds to the number n_{conf} of configurations generated. The reference value for the interface free energy determined in ref. [178] for these combination of parameters is $F_s^1 = 6.8887(20)$. The results listed in this table are also plotted in fig. 4.5.

N	n_R	n_{conf}	$F^{(1)}$, direct	n_R	n_{conf}	$F^{(1)}$, reverse
10^3	$64 \cdot 320$	2×10^7	$6.27(20)$	$64 \cdot 80$	5×10^6	$7.241(67)$
$5 \cdot 10^3$	$64 \cdot 320$	1×10^8	$6.794(20)$	$64 \cdot 80$	2.5×10^7	$6.996(24)$
10^4	$64 \cdot 320$	2×10^8	$6.845(12)$	$64 \cdot 80$	5×10^7	$6.941(17)$
$5 \cdot 10^4$	$64 \cdot 80$	2.5×10^8	$6.888(8)$	$64 \cdot 80$	2.5×10^8	$6.893(8)$
10^5	$64 \cdot 80$	5×10^8	$6.881(6)$	$64 \cdot 80$	5×10^8	$6.892(5)$
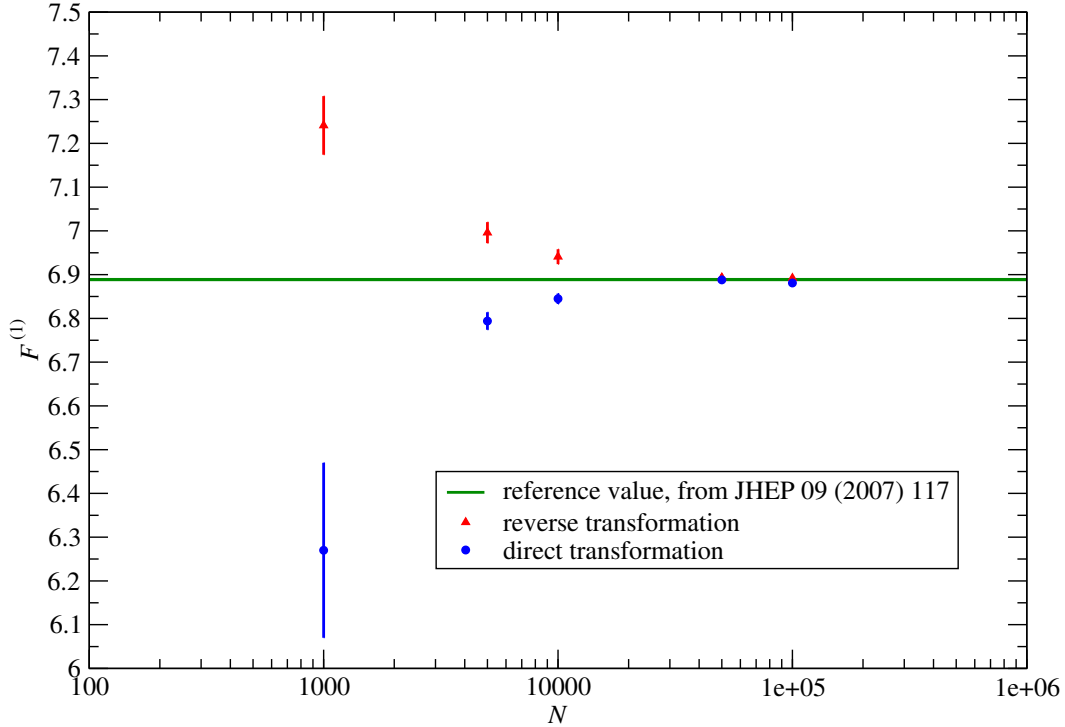
Figure 4.5: Convergence of our results for the interface free energy—defined according to eq. (4.80)—obtained in direct (blue bullets) and reverse (red triangles) transformations from Z_p to Z_a in Monte Carlo simulations at $\beta = 0.223102$ (corresponding to $\beta_g = 0.758264$) on a lattice of sizes $L_0 = 96a$, $L_1 = 24a$, $L_2 = 64a$. The green band denotes the value of the interface free energy determined in ref. [178] for these values of the parameters, and with a different method. N is the number of intervals used to discretize the temporal evolution of the parameter by which the boundary conditions of the system in direction $\mu = 0$ are switched from periodic to antiperiodic, according to eq. (4.82).

A clear pattern emerges when looking at the results for $F^{(1)}$: when the number N of steps is increased, the values obtained from direct and reverse transformations neatly converge to the reference value. This behaviour is exactly the one needed to have a reliable result, which is possible only if the number of realizations n_R is large enough to sample all possible transformation correctly. This is the first clue that a technique based on Jarzynski's equality is most effective in the context of a lattice gauge model when N is pushed to larger and larger values, i.e. when the transformation is performed as much close as possible to equilibrium.

There are, however, some caveats: the most important one is that a more correct comparison has to be made by keeping the number of configurations that are created during all the realizations fixed, that is for a given amount of computational resources. This is not the case of the data presented in table 4.1, except for the comparison between the results of line 3 and line 4: these are essentially obtained with the same number of configurations $N \times n_R$, but the difference in the final result is immediately evident, nevertheless.

A word of caution is in order also in the estimate of the correct error to be assigned to the result: the methodology chosen in the analysis performed in ref. [44] is to use the statistical error (computed with the jackknife technique among all different realizations) only if the *systematic* error is negligible. We remark that by *systematic error* here we mean the discrepancy between direct and reverse transformations: its origin is to be found in the insufficient sampling of the exponential average of the nonequilibrium relation. This is clearly not the case for the results of line 1 in table 4.1, in which the difference between the two results (direct and reverse) is much larger than the statistical error associated with the average. In such a case there are two ways to increase the statistics, that is the total number $N \times n_R$ of configurations: either by adding more realizations (i.e. increasing n_R) or by repeating the transformation from scratch with more intermediate steps N (i.e. more slowly). The analysis performed in ref. [44] states that the latter option is much more efficient than the former, in the sense that convergence to the right result is reached much faster.

A further comment is useful to explain why in fig. 4.5 the results of direct and reverse transformations are respectively below and above the reference value in a systematic way. We already know that, as explained above, any final result must be independent of the direction of the transformation and so it can be accepted only if the discrepancy is completely under control or, in other words, the exponential average is reliable. However, a satisfactory explanation is needed in order to fully appreciate what happens during the nonequilibrium simulations: as soon as the first step of the process is initiated the statistical distribution of the system starts to *lag behind* the equilibrium distribution, and this lag becomes larger as the transformation goes on. Since the direct and reverse transformations start from two rather (and sometimes completely) different distributions, they will reach the final step in different ways, leading to systematically different results. This phenomenon and the minimum amount of realizations of the transformation needed to obtain correct results have been discussed in ref. [166] and briefly reviewed in section 4.3.

Finally, we remark that in general, the use of Jarzynski equality is not supposed to be symmetric when switching the direction of the transformation, in the sense that one of them will be more efficient and will converge more rapidly than the

opposite one. This is clear when analysing the results for the interface free energy: if we consider again the results of line 1 of table 4.1 it is clear from fig. 4.5 that the result of the reverse transformation is both closer to the reference value and with a smaller statistical error. Thus, we conclude that for this particular physical system, using transformations in which the interface is *destroyed* is more efficient and reliable than using transformations in which it is created. We also have to add that in this setup this distinction is in practice not relevant, since the only regime in which our results are truly reliable is the one in which the number of steps N is very large. In such conditions the system is much closer to equilibrium throughout the transformation and the asymmetries between the two possible directions become smaller as N grows larger: because of this, the results for the largest value of N are essentially equally precise and accurate.

Chapter 5

The equation of state from Jarzynski's equality

In the last section of chapter 4 we studied how Jarzynski's equality can be readily implemented in the context of lattice gauge theories, albeit in a rather simple case such as the $\mathbb{Z}_2$ gauge model. However, the problem of computing differences in free energy is rather common, as they are related to a vast set of physically relevant observables. Indeed, a most natural candidate would be the pressure, which, in the thermodynamic limit, is simply minus the free energy density, see eq. (1.39). This chapter, thus, will be entirely devoted to an in-depth analysis of the ongoing effort [44, 179] to use, in the context of non-Abelian gauge theories, Jarzynski's equality for high-precision computations of the equation of state. Namely, we envision nonequilibrium transformations during a Monte Carlo simulation, in which the temperature of the system is varied, thus allowing the determination of differences in the pressure.

In section 5.1, following the work of ref. [44], we will analyse in great detail several aspects of this novel technique; namely, the efficiency of the method, in particular with respect to older techniques, the dependence on the volume and other features will be thoroughly discussed. In the second part of this chapter, contained in section 5.2, we will discuss recent results for the equation of state of the SU(3) pure gauge theory, with a particular focus on the setup of the out-of-equilibrium numerical simulations and on the comparison with existing high-precision determinations. A preliminary version of these results has been presented in ref. [179].

5.1 The pressure via Jarzynski's equality

Recalling eq. (1.44), we know that the pressure in units of the temperature to the fourth power is directly related to the logarithm of the partition function $Z(T)$ of our lattice model in the thermodynamic limit. Moreover, we are usually interested in differences of the kind $p(T)/T^4 - p(T_0)/T_0^4$ which can be immediately written as follows:

$$\frac{p(T)}{T^4} - \frac{p(T_0)}{T_0^4} = \frac{N_t^3}{N_s^3} \left[\ln Z(T) - \ln Z(T_0) \right] = \frac{N_t^3}{N_s^3} \ln \left(\frac{Z(T)}{Z(T_0)} \right) ; \qquad (5.1)$$

the final value of $p(T)/T^4$ is usually obtained either by choosing T_0 small enough so that $p(T_0)/T_0^4 \simeq 0$, or fixing $p(T_0)/T_0^4$ with some other theoretical input.

Now, the idea is that the ratio of partition functions on the right-hand side of eq. (5.1) can be evaluated using the nonequilibrium relation by Jarzynski. Since the partition functions correspond to two different temperatures, the nonequilibrium trajectories will vary the parameters that define the temperature in the system under investigation, switching from T_0 to T (and vice versa). We know from chapter 1 that in Euclidean field theories the temperature T is identified with the inverse of the extent L_t of the compactified dimension, namely

$$T = \frac{1}{L_t} = \frac{1}{a(\beta)N_t}.$$

In principle, both N_t and a can be varied during a nonequilibrium transformation in order to change the temperature; however, the former option has not been taken into consideration in this work, as it presents a few more technical difficulties in the practical implementation during a simulation. It would be interesting in the future to explore this direction too, taking as a reference the fixed scale method briefly reviewed at the end of section 1.3.1.

The best and most flexible way to implement nonequilibrium trajectories in which the temperature is switched between two values, is certainly by varying the lattice spacing a: in practice, this is done by changing the inverse coupling β (which is not to be confused with the inverse temperature) between the corresponding values of T. We denote these values respectively β_0 and β_N (such notation will be clear in a moment), so that

$$T_0 = \frac{1}{a(\beta_0)N_t} \quad \longleftrightarrow \quad T = \frac{1}{a(\beta_N)N_t}$$

and the nonequilibrium trajectory can be discretized into N intermediate steps, as thoroughly discussed in the context of Markov chains and Monte Carlo simulations earlier in section 4.4.1. The switching protocol for the Wilson parameter β can be implemented, similarly as in the $\mathbb{Z}_2$ gauge model in eq. (4.82), as a linear increase, namely

$$\beta_n = \beta_0 + n\frac{\beta_N - \beta_0}{N} \equiv \beta_0 + n\,\Delta\beta \tag{5.2}$$

with $n = 0, ..., N - 1$ indicating the intermediate steps and $\Delta\beta$ the increase in the Wilson parameter at each step in the transformation. Other protocols (e.g. non-linear ones) are perfectly valid, but have not been taken into account in this series of works: however, we remark that different switching processes may increase the efficiency of the method and more work is needed in this direction.

The exact steps one has to follow during such a nonequilibrium transformation in a Monte Carlo simulation is described in detail in section 4.4.1: we still have to specify what in this case is the total "work" (see for example eq. (4.71)), that is, what we have to actually measure during a trajectory. What we need is the quantity defined in eq. (4.72), which has to be translated from the language of statistical mechanics to the language of lattice field theory. In a natural way, the differences in the ratio H/T appearing in eq. (4.72), that must be computed each time the

temperature T is varied, are interpreted as differences in the Euclidean action of the lattice theory when the β parameter is varied.

In fact, this is a somewhat delicate point, since the temperature appearing in eq. (4.72) must not be confused with the temperature defined in the lattice model. The temperature T is varied indirectly by changing the bare coupling g^2 (which is absorbed into the definition of the action S) and this lets us compute the ratio of partition functions of systems characterized by physical temperatures T and T_0 respectively.

Before moving on, we observe that from now on, we will focus on the specific case of pure gauge theories, with no dynamical fermion fields included. The action S will be the Wilson action, eq. (1.19), or in principle also the Symanzik-improved version, eq. (1.21) (used, for example, in refs. [6, 106]).

Finally, starting from eq. (4.75), we can write the slightly modified nonequilibrium relation that can be used to compute the pressure p/T^4 in the lattice theory:

$$\frac{p(T)}{T^4} - \frac{p(T_0)}{T_0^4} = \frac{N_t^3}{N_s^3} \ln \left\langle \exp \left[\sum_{n=0}^{N-1} \left(S[\beta_{n+1}, U(t_n)] - S[\beta_n, U(t_n)] \right) \right] \right\rangle \qquad (5.3)$$

and in the following we will denote the total difference in the Euclidean action with

$$\Delta S[\beta_0, \beta_N] = \sum_{n=0}^{N-1} \left(S[\beta_{n+1}, U(t_n)] - S[\beta_n, U(t_n)] \right); \qquad (5.4)$$

in this notation, $U(t_n)$ represents the configuration of the link variables U at the Monte Carlo time t_n, where t_0 indicates the first configuration (at equilibrium) and t_{N-1} the last configuration of the trajectory. We stress again the fact that each term of the sum of eq. (5.4) must be computed using the same configuration U_n; for more details on how to compute these terms correctly we refer to section 4.4.1. In practice, if we take for example the Wilson action —see eq. (1.19)— the total difference in the action for a linear switching process such as that of eq. (5.2), can be written

$$\Delta S[\beta_0, \beta_N] = 6 N_s^3 N_t \Delta\beta \sum_{n=0}^{N-1} U_{\mathrm{p}}(t_n) \qquad (5.5)$$

where $U_p(t_n)$ is the action density, i.e. the average plaquette at the n-th configuration during the nonequilibrium trajectory. Moreover, we remind the fact that the $\langle \dots \rangle$ notation indicates precisely the average over an ensemble of n_R realizations of the transformation $\beta_0 \to \beta_N$, as discussed at length in chapter 4.

As usual, before being able to compute the physical value of the pressure p, we have to get rid of the quartic divergence in the lattice spacing: a simple and intuitive way to do so is to follow what is routinely done for example in the integral method [36]. As explained in section 1.3.1, each plaquette expectation value (i.e. action density) is computed also at $T = 0$ and its value is subtracted from the $T \neq 0$ value. In the same way, the exponential average on several trajectories of the quantity defined in eq. (5.4) must be computed also at zero temperature; the resulting value must be then "subtracted" in order to obtain the correct result for the pressure. This leads to the following final formula for the determination of the

physical value of p/T^4:

$$\frac{p(T)}{T^4} = \frac{p(T_0)}{T_0^4} + \left(\frac{N_t}{N_s}\right)^3 \ln \frac{\left\langle \exp\left[-\Delta S_{N_t \times N_s^3}\right]\right\rangle}{\left\langle \exp\left[-\Delta S_{\widetilde{N}^4}\right]\right\rangle^\gamma}. \tag{5.6}$$

On the right-hand side of eq. (5.6), $\Delta S_{N_t \times N_s^3}$ is the total variation in the Euclidean lattice action calculated on a lattice of sizes $N_t \times N_s^3$ during a non-equilibrium trajectory starting from a configuration of the initial, equilibrium ensemble with Wilson parameter β_0, to a final configuration, obtained driving the system out of equilibrium until the inverse coupling reaches its value β_N. Similarly, $\Delta S_{\widetilde{N}^4}$ denotes an analogous total variation in the gauge action, but evaluated on a symmetric lattice of sizes $\widetilde{N}^4$; the exponent $\gamma = \left(N_s^3 \times N_t\right)/\widetilde{N}^4$ is the ratio between the sizes of the two lattices and it is necessary since the lattice spacetime volumes at $T = 0$ and $T \neq 0$ are in general different.

We note that, for a linear switching process such as that of eq. (5.2) and using the standard Wilson action, we can rewrite eq. (5.6) as

$$\frac{p(T)}{T^4} = \frac{p(T_0)}{T_0^4} + \left(\frac{N_t}{N_s}\right)^3 \ln \frac{\left\langle \exp\left[-6N_s^3 N_t \Delta\beta \sum_{n=0}^{N-1} U_{\mathrm{p}}^{T \neq 0}(t_n)\right]\right\rangle}{\left\langle \exp\left[-6\widetilde{N}^4 \Delta\beta \sum_{n=0}^{N-1} U_{\mathrm{p}}^{T=0}(t_n)\right]\right\rangle^\gamma}; \tag{5.7}$$

this formula will be useful for the comparison with the integral method in section 5.1.2; moreover, it is clear from this equation that the only quantity that is actually measured during the nonequilibrium transformation is the value of the plaquette averaged over the spacetime volume at each intermediate step of the transformation.

In the work reported in section IV of ref. [44], a first benchmark study on the applicability of the nonequilibrium relation for the equation of state of the SU(2) pure gauge theory was performed. The pressure in units of T^4 was calculated with eq. (5.6) using the Wilson action S_W –see eq. (1.19)– on lattices of size $N_t \times N_s^3 = 6 \times 72^3$; data obtained both with direct transformations, i.e. when the temperature is increased, and reverse transformations (in which T is decreased) are presented in table 5.1.

The results obtained with this novel technique have been compared with the values of the pressure obtained with the integral method in ref. [11] in the very same conditions, that is using identical lattices and update algorithms; these results were previously discussed in section 2.2.5 and shown in fig. 2.6. The temperature range that corresponds to the values of β reported in table 5.1 is approximately between $0.9T_c$ and T_c: indeed, the simulations were performed in a rather delicate region, in the very proximity of the deconfinement transition, where thermodynamic quantities such as p and Δ grow rapidly. As it can be inferred from fig. 5.1, there is a remarkable agreement with older results and among the results of direct and reverse trajectories. A detailed comparison of the results and of the technique with the integral method will be discussed later in section 5.1.2.

In principle, the out-of-equilibrium transformations can be performed in several ways: indeed, in addition to the choice of how many steps N and how many realizations n_R, there is a relative freedom in choosing other characteristics of the transformation. First of all, we must choose how to perform the "update" of the

Table 5.1: Results for p/T^4 at different values of β (first column), from simulations on lattices with $N_t = 6$ and spatial sizes $N_s^3 = 72^3$ (while the simulations at $T = 0$ were run on lattices of sizes $\widetilde{N}^4 = 40^4$) using Jarzynski's relation eq. (5.6) with a direct (second column) or a reverse implementation (third column) of the parameter switch, in comparison with those obtained with the integral method [36] in ref. [11] (fourth column). The temperature range probed by these values of the inverse coupling β for $N_t = 6$ is $\sim [0.9T_c, T_c]$. The data in the last line provide a comparison of results from the method based on Jarzynski's relation and the integral method, for the same number (3×10^4) of gauge configurations.

β	p/T^4, direct	p/T^4, reverse	p/T^4, integral method
2.4058	–	–	0.00980(22)
2.4108	0.01122(9)	0.01130(11)	0.01114(22)
2.4157	–	–	0.01274(22)
2.4158	0.01276(15)	0.01304(14)	–
2.4186	–	–	0.01381(22)
2.4208	0.01492(20)	0.01505(16)	–
2.4214	–	–	0.01501(22)
2.4228	–	–	0.01569(22)
2.4243	–	–	0.01656(22)
2.4257	–	–	0.01751(22)
2.4258	0.01780(35)	0.01774(24)	–
2.4271	–	–	0.01867(22)
2.428	–	–	0.01956(22)
2.429	–	–	0.02068(22)
2.43	–	–	0.02198(22)
2.4308	0.02354(37)	0.02402(27)	–
2.431	–	–	0.02341(22)
2.4108	0.01122(9)	0.01130(11)	0.01116(51)

system after the change of the parameter, as described in section 4.4.1. Since we are dealing with a pure gauge theory on the lattice, the choice naturally comes down to the heatbath and the overrelaxation algorithms, which are routinely used in Monte Carlo simulations. A good question is, how many times do we have to use these update routines before proceeding to the next step in the switching protocol? Or, equivalently, how do we perform step 4 of the procedure described in section 4.4.1? Our choice was a rather conservative one, opting for one heatbath step plus 5–10 overrelaxation steps before changing again β and evaluating the value of the action: this is quite customary in this kind of simulations, when computing plaquette expectation values. We remark however that this is not compulsory, since the nonequilibrium relation by Jarzynski is valid independently of the specifics of the update: what may vary is the efficiency of the relation in computing p/T^4. By adding updates we are of course increasing the computational cost of each trajectory, but on the other hand the system is going closer to equilibrium after each step, possibly improving the accurateness of the transformation. Each step would also be less correlated with the previous one, but the implications of this are not entirely clear yet. In conclusion, more work is needed to understand the dependence of the efficiency of this method on how the update is practically implemented.
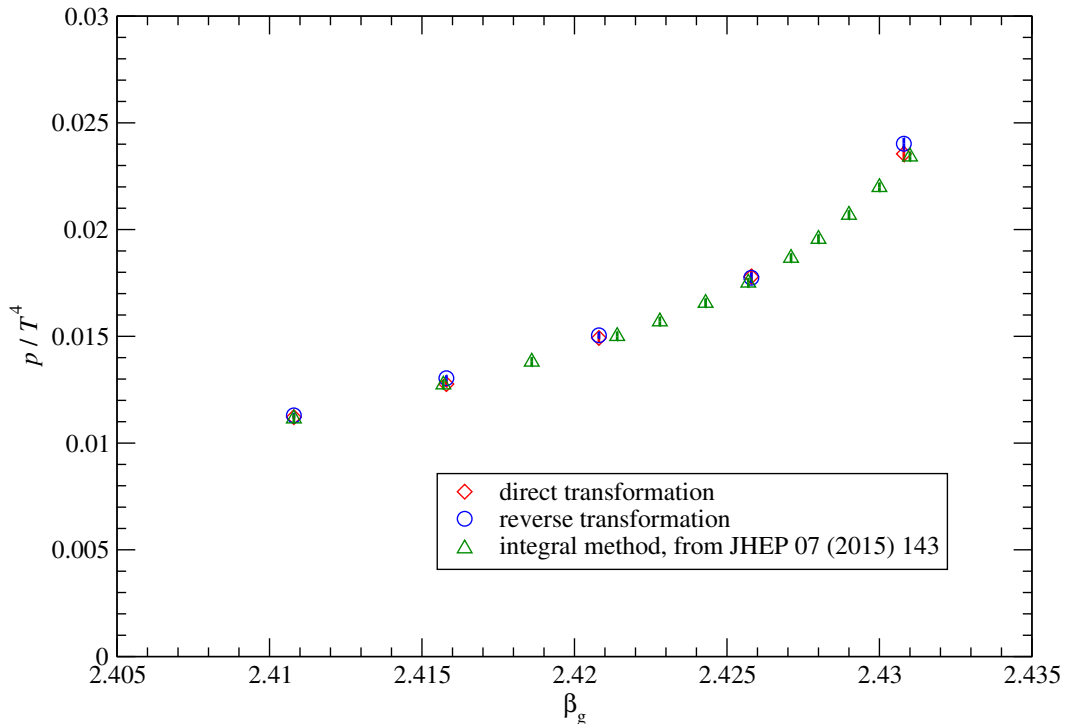
Figure 5.1:   Results for the pressure p (in units of T^4) in the confining phase of SU(2) Yang–Mills theory, as a function of the inverse coupling β (which controls the lattice spacing a, and, thus, the temperature $T = 1/(aN_t)$), from simulations on lattices with $N_t = 6$ and spatial sizes $N_s^3 = 72^3$ (while the corresponding simulations at $T = 0$ were performed on lattices of sizes $\widetilde{N}^4 = 40^4$). The results obtained using Jarzynski's relation eq. (5.6) with a direct (red squares) and a reverse (blue circles) implementation of the parameter transformation converge to those obtained in ref. [11] using the integral method [36] (green triangles).

Before discussing the combined choice of N and n_R, it is worth noting that in order to get the final value of p/T^4, eq. (5.6) can be used in several ways: one can either build a unique, very long transformation from T_0 to T, or combine several independent transformations $T_0 \to T_1$, $T_1 \to T_2$... until reaching the final value T. In the latter case, the final value of the pressure is obtained by progressively summing terms obtained with independent calculations, i.e.

$$\frac{p(T)}{T^4} - \frac{p(T_0)}{T_0^4} = \left(\frac{p(T_1)}{T_1^4} - \frac{p(T_0)}{T_0^4}\right) + \left(\frac{p(T_2)}{T_2^4} - \frac{p(T_1)}{T_1^4}\right) + \dots ;$$

this is the technique that we chose in order to compute the data in table 5.1: the results presented in the second column are indeed obtained summing the corresponding terms in the parentheses on the right-hand side of the previous formula. Thus, in practice the transformations performed in ref. [44] were rather "short", in contrast for example with the possibility of a single transformation from $\beta = 2.4058$ to $\beta = 2.4308$. We will see in detail in section 5.2 that in addition to N and n_R, this implementation of Jarzynski's equality is quite sensitive to *how long* the trajectory is, and thus the temperature range that one intends to probe must be divided accordingly.

As mentioned in the previous paragraph, the results from Jarzynski's relation presented in table 5.1 were obtained with 5 independent transformations: each of these was discretized using $N = 2000$ steps and repeated in $n_R = 15$ independent realizations. A total of 3×10^4 configurations were generated for each transformation (not including thermalization), but we recall that the average of eq. (5.6) was taken *only* on the results for ΔS of the $n_R = 15$ realizations. Such transformations were thus performed very close to equilibrium, as for each step the change in the Wilson parameter is only of $\Delta\beta = 0.0000025$. We would like to remark that this approach is something slightly different from the spirit of Jarzynski's equality, which is applicable when the system during the transformation is truly far from equilibrium.

It is interesting then to ask what happens when other combinations of N and n_R are chosen, possibly keeping the number of generated configurations fixed: in order to do so, we performed more realizations of the transformation $\beta = 2.4158 \to 2.4208$, discretizing it with $N = 100, 250, 500$ and 1000 intermediate steps. The results, repeated with enough realizations so as to keep $N \times n_R$ constant, are presented in fig. 5.2. Here the histograms of the values of ΔS_W obtained in direct and reverse transformations are shown; the logarithm of the exponential average of eq. (5.3), that we symbolically denote as ΔA:

$$\Delta A = \ln\langle\exp\left[-\Delta S_{N_t \times N_s^3}\right]\rangle$$

is shown in fig. 5.2 as a vertical line with the relative error.

Several insightful aspects of Jarzynski's relation can be analysed by looking at these histograms: first of all, in the bottom figure ($N = 1000$ steps) the system during the transformation is closest to the equilibrium distribution, while it is farthest from it in the upper one ($N = 100$ steps). The shape of the distributions of ΔS_W is clearly modified, as they become broader and less centered on ΔA the farther they are from equilibrium. In the top figure we can distinguish the *dominant* realizations that we described in section 4.3: the tails of both the direct and reverse transformations which dominate the exponential average are clearly visible. On the other hand, when getting closer to equilibrium, the overlap of the two distributions massively increases, until they are almost coincident and centered on ΔA. This is clearly what we expect, since we know from the Second Law (see section 4.1.3) that for quasistatic transformations the relation $\langle W \rangle = \Delta F$ holds: in our case it translates to $\langle \Delta S_W \rangle = \Delta A$. Moreover, all values of ΔA are approximately in agreement with each other, indicating good convergence for any combination of N and n_R.

If we look at the efficiency in computing the average instead, we know that both the statistical and the systematic error must be taken into account: for both of them a pattern emerges, as the lower figure presents the smallest discrepancy between direct and reverse transformations and also the smallest error bars. We also would like to add that, since each realization must be independent, the initial configuration at temperature T_0, which must be at equilibrium, has to be uncorrelated from the initial configuration used for the other trajectories. This means that the number of configurations that must be generated grows with n_R: thus, if n_R is very large, using Jarzynski's relation is not convenient anymore in terms of computational cost, since many initial independent configurations must be produced. For this reason, in the analysis presented in fig. 5.2 we did not consider transformations with $N < 100$.
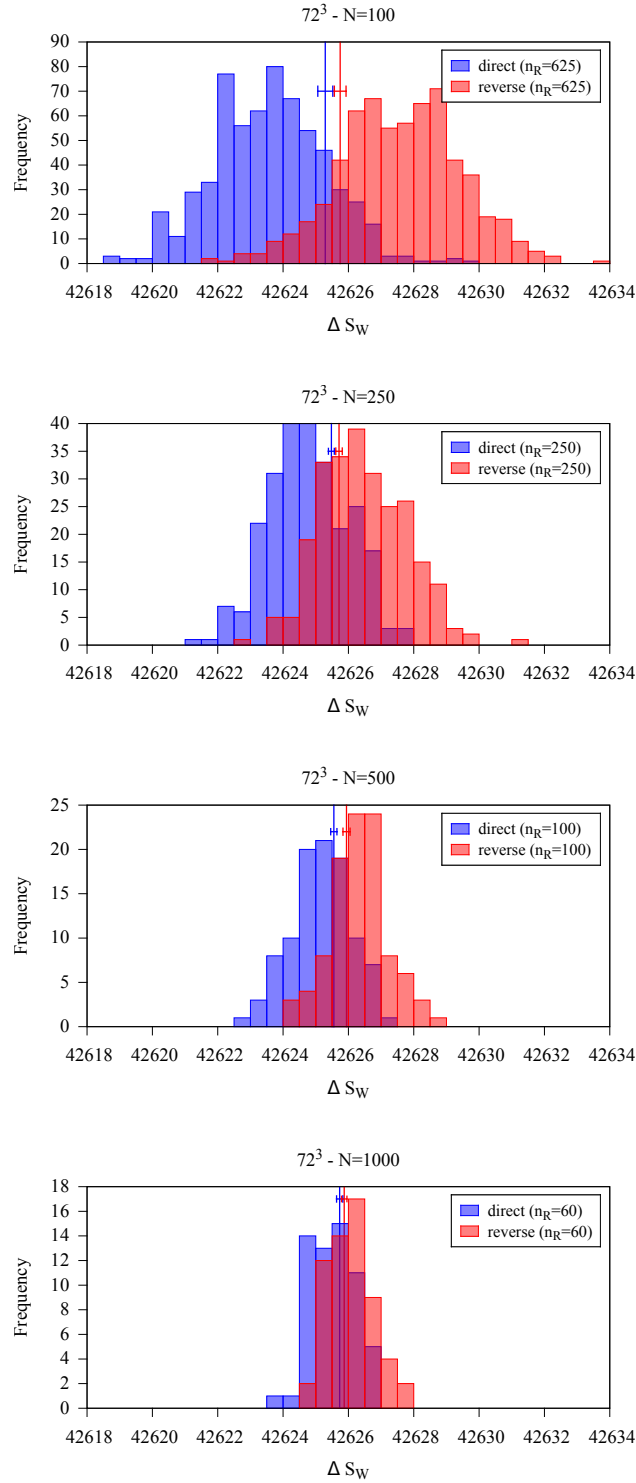
Figure 5.2: Histograms for the total difference in the Euclidean action ΔS_W of forward and reverse distributions of nonequilibrium transformations in the SU(2) gauge theory on a lattice of spatial size $V = N_s^3 = 72^3$ and temporal extent $N_t = 6$. ΔS_W has been computed for the transformation between $\beta = 2.4158$ and $\beta = 2.4208$. Vertical lines represent the value of the free energy difference $\Delta F = \ln\langle\exp\left[-\Delta S_{N_t \times N_s^3}\right]\rangle$ (with the relative error) calculated with the corresponding distribution. The $T = 0$ contribution (see eq. (5.6)) has not been subtracted yet.

In the end, this test provides qualitative support for the idea that choosing transformations which are "slow", i.e. closer to a quasistatic transformation, is the most efficient way of using the nonequilibrium equality for systems with many degrees of freedom such as a lattice gauge theory. This is to be contrasted with the other "specular" option, i.e. constantly increasing n_R while keeping the same discretization of the transformation, which in some cases may be more practical, since one has simply to increase the statistics of the trajectories instead of generating new ones. However, in section 5.2, where we will deal with "long" transformations on larger ranges of temperatures, we will observe that by simply increasing n_R the convergence to the correct result is much slower.

5.1.1   Volume dependence

It is extremely interesting to examine the behaviour of this computational method when the volume of the system increases: in this section we will attempt to perform a qualitative test of how the distributions of the total change in the action ΔS are modified when V changes. First of all, in fig. 5.3 and in fig. 5.4 we can observe the same ΔS_W distribution of fig. 5.2, i.e. with identical lattice spacing, but for spatial volumes $V = 96^3$ and $V = 112^3$, respectively.

From the $N_s = 96$ simulations we cannot easily discern any qualitative difference in the patterns that already emerged in the smaller volume case. Instead, in fig. 5.4, for $N_s = 112$, the two distributions are visibly farther apart from each other with respect to the $N_s = 72$ results; in other words, for a given number of steps N the overlap of the two distributions is smaller. We can easily provide an explanation of this behaviour: on one hand, the distribution of ΔS_W becomes narrower whenever the volume is increased since, quantitatively, the width of the distributions has to go as $\sim 1/\sqrt{V}$. This happens because the statistics increases with the volume, since at each step the plaquette is averaged over a larger set of variables.

In order to fully appreciate the qualitative dependence on the volume of the ΔS_W distributions, the histograms of the direct distributions for $N_s = 72, 96, 112$ are showed in fig. 5.5 for a given N.

From these graphs, which are plotted on the total difference in the action normalized with the volume, the narrowing of the distributions is clearly visible. In principle this is a potential problem of this technique, since increasing the volume means that the tails of the distributions are less populated: thus, it would be more complicated to sample the dominant realizations that control the exponential average. A possible way to address this problem would be again to choose slower transformations, i.e. to increase the number of intermediate steps: in this way the distributions would be essentially centered around ΔA and the relevant trajectories would be sampled without effort. However, in fig. 5.4 both statistical and systematic errors are visibly smaller when compared with $N_s = 72$ and 96, and the results appear to be highly accurate for any value of N: this peculiar behaviour is still under investigation and provides a strong motivation for further analyses of this issue.
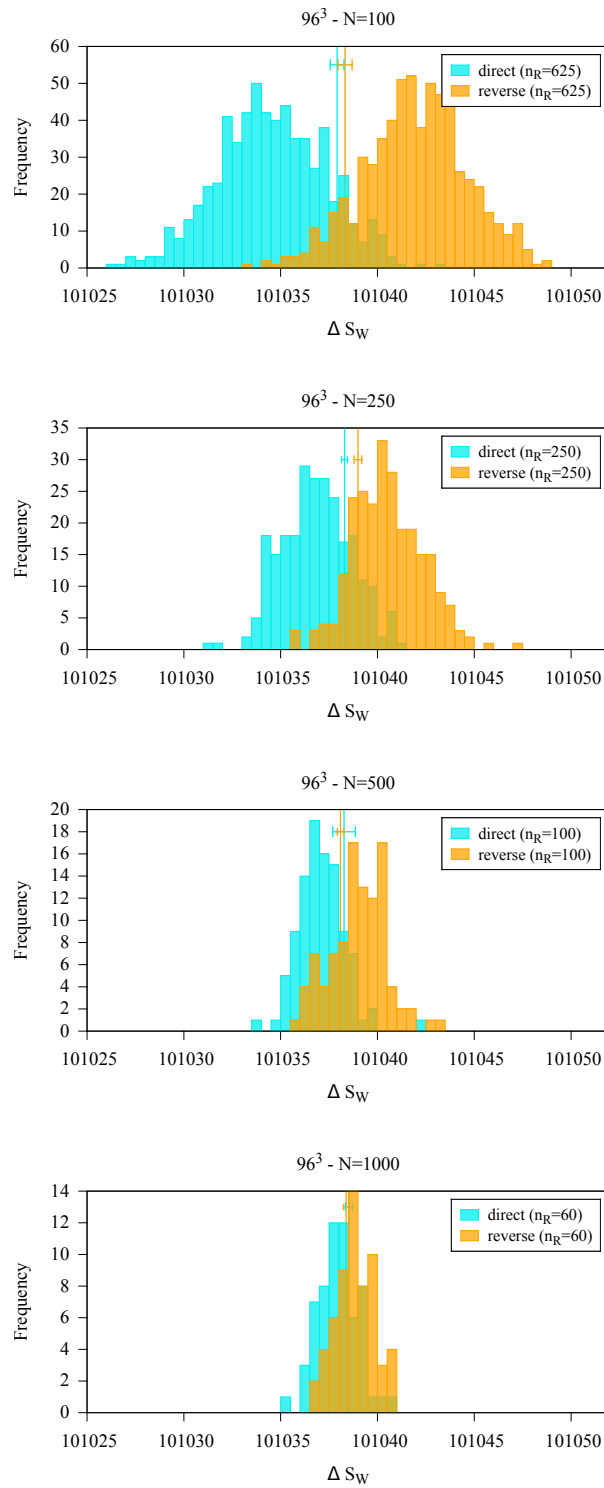
Figure 5.3: Same as fig. 5.2, but for spatial volume $V = 96^3$.
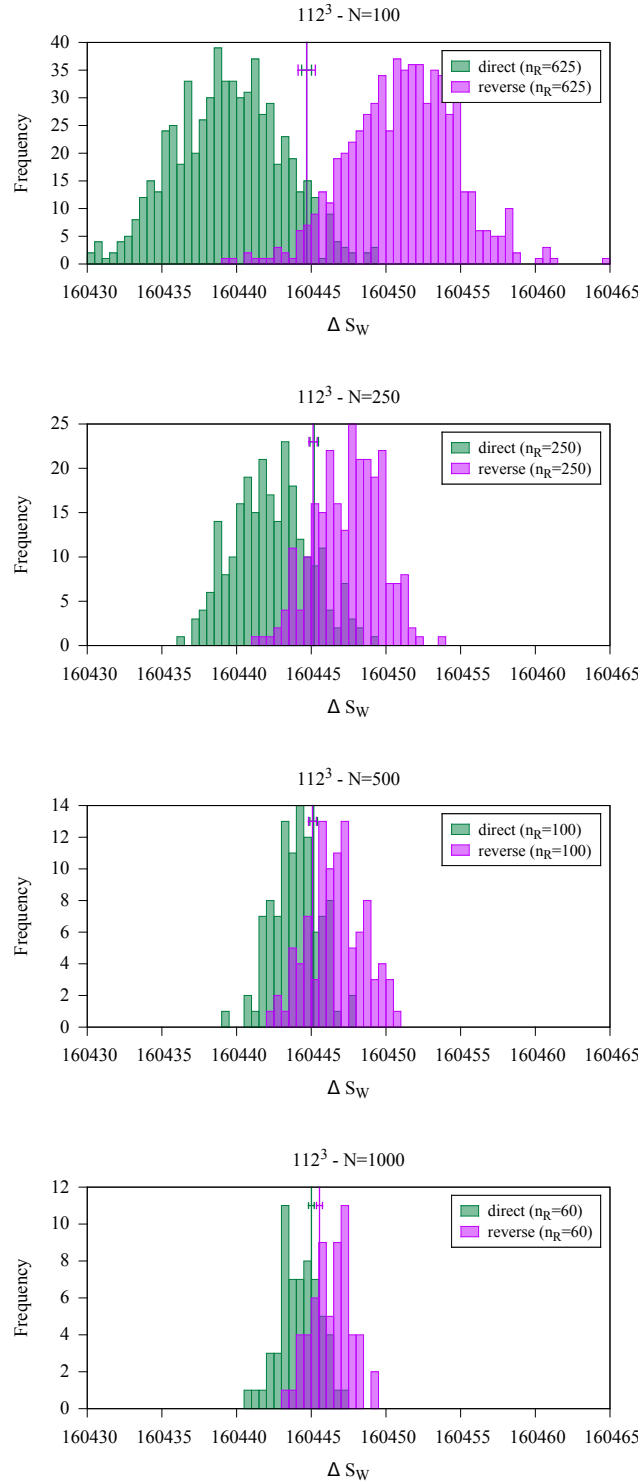
Figure 5.4: Same as fig. 5.2, but for spatial volume $V = 112^3$.
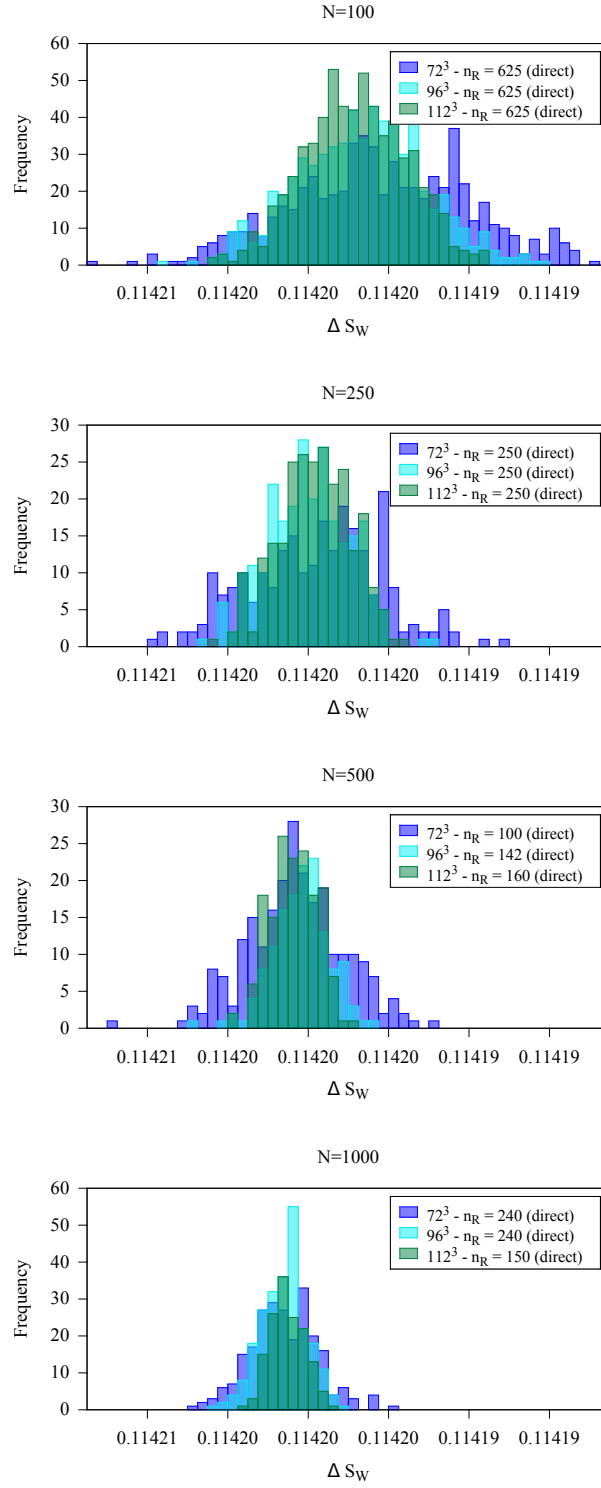
Figure 5.5: Histograms for the total difference in the Euclidean action ΔS_W of direct nonequilibrium transformations in the SU(2) gauge theory on lattices with increasing spatial sizes $N_s = 72, 96, 112$ and temporal extent $N_s = 6$.

5.1.2 A comparison with the integral method

In section 4.1.2, we showed how two different limiting cases of Jarzynski's equality actually correspond to two methods widely used for numerical simulations in statistical mechanics. One of these is the so-called thermodynamic integration, which is reached in the limit of an extremely slow (quasistatic) transformation, so that every intermediate configuration of the system is in (quasi-)equilibrium. In this special limit, the $\Delta\beta$ defined previously is very small and the average over different realizations of the transformation in eq. (5.7) disappears, as its place is taken by the expectation value of the plaquette of the system in equilibrium at a certain β. Most importantly, the sum over all the steps of the transformation becomes an integral on the infinitely many intermediate steps and the discrete increase $\Delta\beta$ becomes an infinitesimal $\mathrm{d}\beta$: in the end, what we obtain is nothing but the main formula of the integral method, eq. (1.47).

Indeed, whenever one is interested in computing ratios of partition functions, there is a deep relation between this approach and the integral method, in the sense that the nonequilibrium relation can be seen as a generalization of the methodology introduced in [36]: since many details, such as the subtraction of the zero temperature contribution, are the same, a quantitative comparison can be set up rather straightforwardly.

However, before entering the details of such comparison, a word of caution is in order: in practice, the integrand of eq. (1.47) is often evaluated only for a limited number of values of β which are subsequently fitted with some reasonable functional form. For example, in ref. [11] the pressure was determined by integrating a fit with spline curves, as reported in section 2.2. This methodology is widely used, but in principle it can introduce some systematic errors that, in practice, are kept smaller than the statistical ones and thus under control. It cannot be ignored, though, the fact that the choice of how many values of β for which U_{p} is computed in eq. (1.47) is somewhat arbitrary and any related effect on the integration is somewhat difficult to directly control. This fact makes the comparison with the nonequilibrium relation more complicated and less rigorous, as the effect on the final result of p/T^4 with respect to the number of values of β which are effectively simulated is difficult to discern. Even if we do not deem this observation to be of the utmost importance, we stress that using Jarzynski's relation we can check *directly* the effect of changing N and n_R on the final result, simply by comparing direct and reverse transformations.

In ref. [44] a comparison between the procedure based on Jarzynski's relation and the integral method for the determination of the pressure in the SU(2) pure gauge theory was attempted. The results are reported in table 5.1 and correspond to a range of temperatures in the confining phase rather close to the deconfinement transition; the same starting value of $p(T_0)/T_0^4$ is used, while statistical errors are propagated using the jackknife technique in both methods. With the exception of the last line, the relative data are not obtained with the same statistics: we recall that for the integral method we considered the sum of the configurations used to compute all values of U_{p}, while for the nonequilibrium relation the full statistics is given by $N \times n_R$.

From the data reported in table 5.1 we observe that:

- in our method the error steadily increases with β, as expected, while for the

integral method it is extremely stable instead: the statistics in the latter case is higher, since many values of β were simulated, but the spline interpolation may have also a role in this unusual behaviour;

- in the last line the two methods are compared with the same statistics for the computation of a single value with high precision: the nonequilibrium relation seems to be more precise, but on the other hand, it is just a single point and thus it represents a small sample of the temperature range of interest;

- more in general, the quantitative comparison is somewhat inconclusive: even if the two methods are closely related to each other, a direct, fair comparison is complicated by the fact that the pressure is a primary observable in our technique, but it is not in the integral method.

We would like to conclude this section by noting that, even if directly comparing the efficiency of these methods for a given amount of computer time is subject to a degree of arbitrariness, the technique based on Jarzynski's equality is a clean and reliable method to compute the pressure in lattice gauge theories.

5.2 $\mathrm{SU}(3)$ **thermodynamics with Jarzynski's equality**

The determination of the equation of state of the SU(3) pure-glue theory has been a perfect testing ground for any novel technique that has been proposed in recent years to compute equilibrium thermodynamics: this is the case of the gradient flow-based method (see section 1.3.4 and refs. [45, 73]) and for the equation of state with shifted boundary conditions (see section 1.3.3 and refs. [7, 66]). Indeed, the pure gauge sector is immune from many of the systematic errors and technical issues that plague computations with fermion fields, thus presenting in principle a cleaner framework in which it is possible to analyze the efficiency of any new tool and method. Moreover, many features of the Yang-Mills theory are very similar to full QCD, at least on the qualitative and semi-quantitative level, so that high-precision tests, especially at temperatures not accessible with simulations that include quark fields, are physically interesting nonetheless.

In this section we present results for SU(3) equilibrium thermodynamics in the $[0.7T_c, 2.5T_c]$ temperature range, obtained using eq. (5.6) via nonequilibrium transformations in Monte Carlo simulations. A preliminary version of this study was reported in ref. [179]. In the following, we will describe with great detail the setup of these transformations, how systematic errors related to Jarzynski's equality have been handled and how these results compare with respect to existing ones.

5.2.1   Lattice setup

As for the benchmark test for the SU(2) case (see section 5.1), the standard Wilson action, eq. (1.19), was used in all computations. The simulations were performed on lattices with temporal extents $N_t = 6, 7, 8$ and 10, in order to provide a reliable continuum extrapolation. The aspect ratio was always kept quite large, namely at least $N_s/N_t \geq 12$ and in most cases around 16, so that we are in a position to safely neglect finite volume effects.

The scale of lattice simulations was set using the Sommer scale r_0: in particular, we used the scale setting relation determined in [112], which is suitable for temperatures up to $2.5T_c$ for any of the values of N_t that we used. In order to express the temperature associated to our results in units of the deconfinement temperature T_c, we used the value $T_c r_0 = 0.7457(45)$ computed in [137]. This is not the only option, though: for example in ref. [7] the authors used $T_c r_0 = 0.750(4)$ from [4] (properly converted in units of r_0^{-1} from $\sqrt{\sigma}$); since the difference is very small in principle there should not be issues from this slight discrepancy.

As already mentioned previously in this chapter, the temperature range of interest was not probed by a single nonequilibrium transformation, but it was divided in a number of independent transformations that we will denote with n_{transf}. A single transformation is not practically feasible, first of all because of the existence of the deconfinement phase transition, which puts strong constraints on how Jarzynski's equality can be used in the proximity of T_c. We will discuss in section 5.2.2 the technical problems that the (weakly) first-order transition poses when computing p/T^4. Anyway, even in regions far away from T_c, very long transformations have not been used for two different reasons: first, they are not very practical, since the number of configurations required to have convergence and good precision is usually very large and, thus, very long simulations would be necessary. Most importantly, however, they are not efficient: in order not to lag too much behind the equilibrium distribution during a transformation, the value of intermediate steps N has to be relatively high; otherwise, i.e. simply increasing the number of realizations n_R, convergence is reached very slowly.

A review of the details of all simulations performed in this work, including the number of nonequilibrium transformations n_{transf} and the total number of generated configurations n_{conf} used during them, are included in table 5.2.

Table 5.2: Setup of lattice simulations for the SU(3) equation of state using Jarzynski's equality in the confined and deconfined phase, from $0.7T_c$ up to $2.5T_c$. Nonzero temperature transformations are performed on lattices of sizes $N_t \times N_s^3$ (first two columns), while those at $T = 0$ are always performed on lattices of sizes $\widetilde{N}^4 = 48^4$. The range of interest of the inverse coupling β and the corresponding temperature range are indicated in the third and fourth columns respectively. The number of transformations n_{transf} used to cover the relative temperature range is reported in the fifth column. The approximate total number of configurations generated during the nonequilibrium transformations is indicated in the sixth column.

N_t	N_s	β range	T range	n_{transf}	n_{conf}
6	96	$[5.72785, 5.89985]$	$[0.7T_c, T_c]$	3	1.7×10^5
6	96	$[5.89985, 6.50667]$	$[T_c, 2.5T_c]$	6	3.7×10^5
7	112	$[5.79884, 5.98401]$	$[0.7T_c, T_c]$	3	2.4×10^5
7	112	$[5.98401, 6.6279]$	$[T_c, 2.5T_c]$	4	3.3×10^5
8	120	$[5.86415, 6.06265]$	$[0.7T_c, T_c]$	3	2.6×10^5
8	120	$[6.06265, 6.72223]$	$[T_c, 2.5T_c]$	9	1.2×10^5
10	120	$[5.98408, 6.2068]$	$[0.7T_c, T_c]$	5	3.1×10^5
10	160	$[6.2068, 6.9033]$	$[T_c, 2.5T_c]$	8	1.3×10^5

Different ways of dividing the temperature range have been analysed and experimented with: for instance, only 4 transformations were needed to probe the deconfined phase on $N_t = 7$ lattices, while 9 were used for $N_t = 8$. What emerged from the analysis performed in this work, is that the length of each transformation plays a major role in determining the most efficient setup to simulate the desired temperature range. On one hand, longer transformations require slower switching protocols and, thus, larger N and more statistics: this is needed in order to avoid large discrepancies with the result of reverse realizations. On the other hand, a larger number of transformations n_{transf} can provide in principle more reliable results, but, at the same time, requires more thermalized configurations at the start of each transformation. Indeed, equilibration time has a role in choosing the right setup: in this work we always used 5000 configurations for $T = 0$ transformations and 15000 for finite-T transformations.

The general strategy we devised consisted in evaluating first the reliability of the method with a given combination of N and n_R by comparing direct and reverse transformations; then, if the results were not satisfying, we increased N while keeping n_R fixed until all discrepancies were under control. The other way around, i.e. simply increasing n_R and adding more realizations, was not as fast in reaching convergence and was mostly deprecated.

We would like to remark that the use of Jarzynski's relation for the computation of the pressure, eq. (5.6), provides a very fine analysis of the equation of state with a handful of configurations. Indeed, for each trajectory we can compute the change in the Euclidean action not necessarily on the whole transformation, but at any intermediate step N', i.e.

$$\sum_{n=0}^{N'} \left(S[\beta_{n+1}, U(t_n)] - S[\beta_n, U(t_n)] \right) \; ; \tag{5.8}$$

this in principle allows us to compute the pressure difference at any intermediate step, i.e. for a very large set of temperatures. However, in this work, we opted to compute differences in p/T^4 every few hundred steps: thus, we produced very fine results that are also uncorrelated between each other.

5.2.2   Numerical results and discussion

The complete set of results for the pressure in units of T^4 computed on the lattice at nonzero lattice spacing is reported in fig. 5.6; data obtained in the confining phase is also showed separately in fig. 5.7.

The setup we chose to probe the temperature range of interest is the following: each of the n_{transf} transformations was realized with a number N of intermediate steps comprised between 10^3 and 10^4, corresponding approximately to a change in the inverse coupling for each step of

$$\beta_{n+1} - \beta_n \sim 10^{-4} \text{ or } 10^{-5}.$$

For what concerns the number of trajectories n_R of each transformation, we always kept it fixed between 10 and 20.

Computations in the confining phase were particularly challenging, especially for the largest value of N_t, for which the signal is rather small because of the $T = 0$
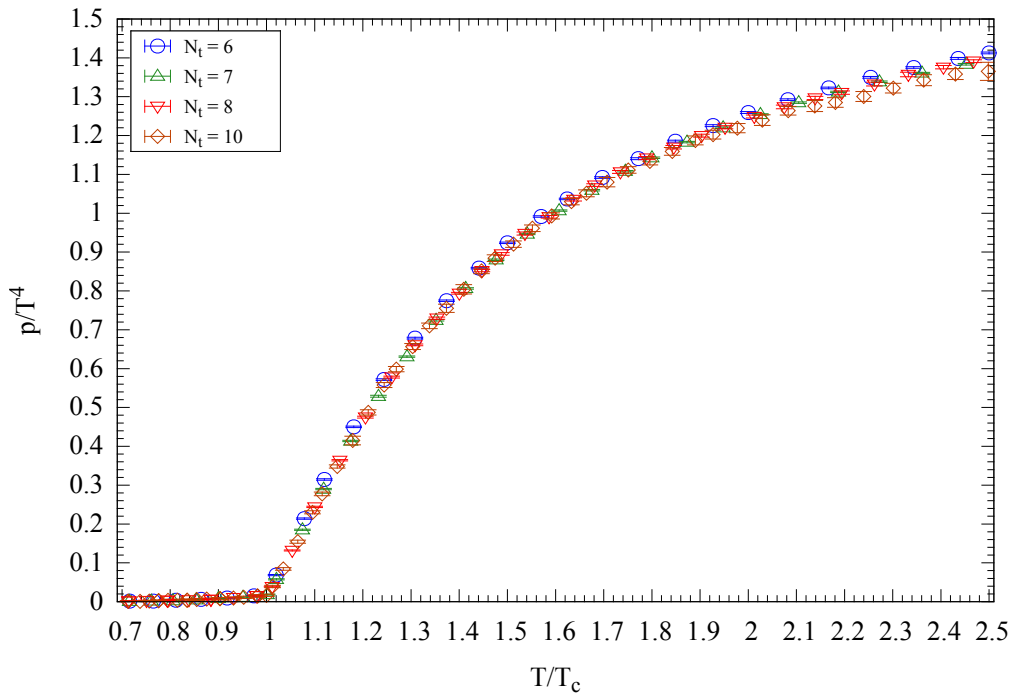
Figure 5.6: Overall results at finite lattice spacing for the pressure in units of the temperature to the fourth power in the $[0.7T_c, 2.5T_c]$ temperature range obtained with Jarzynski's relation. Data include values obtained on lattices with $N_t = 6$ (blue circles), $N_t = 7$ (green triangles), $N_t = 8$ (red triangles) and $N_t = 10$ (orange squares).

subtraction in eq. (5.6). In this region, the number of steps N reached its largest value across the whole set of transformations: we note that in the end this strategy proved very effective, radically decreasing statistical and systematic errors even with modest increases in N.

We recall that, as explained in section 1.3.1 for the integral method, a value for the initial value of $p(T_0)/T_0^4$ deep in the confining phase has to be set. Either T_0 is low enough so that the pressure is negligible and $p(T_0)/T_0^4$ can be set to zero, or it can be evaluated with the prediction of a glueball gas, as explained in chapter 2. As in ref. [11] we chose the second option, computing the pressure of a gas of glueball states at $T_0 = 0.7T_c$ using the masses reported in table 2.4 and using it as the starting value. In particular we have that the glueball gas predicts

$$p_g(T_0)/T_0^4 = 0.00086$$

for $T_0 = 0.7T_c$. We recall that all differences in p/T^4 computed with Jarzynski's equality are added progressively to that value.

In the previous sections of this chapter we stressed the importance of reverse transformations as an independent check on the result from the usual direction of the trajectories: indeed, this check has been done for every transformation performed in this study. An interesting fact emerged from this analysis: in several instances, even if results from direct and reverse transformations at nonzero T had a relevant
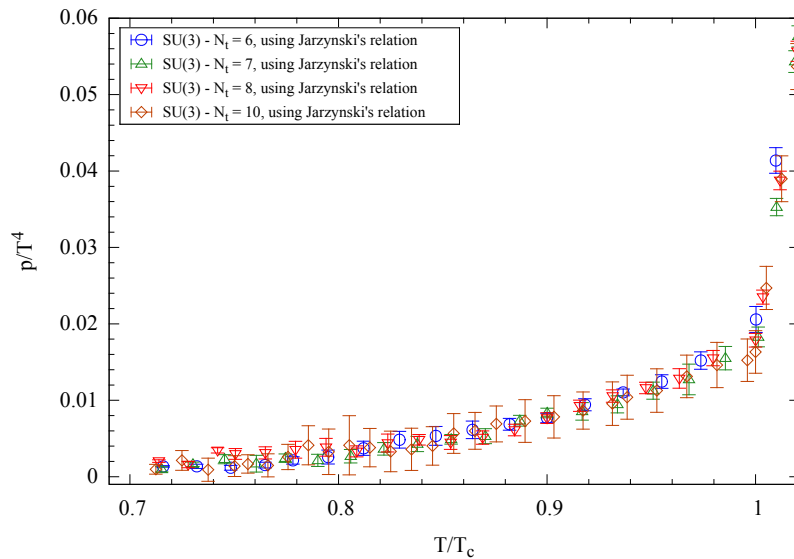
Figure 5.7: Lattice results for the pressure in units of T^4 in the confining phase ($T < T_c$) at finite lattice spacing as in fig. 5.6.

discrepancy, the final, *physical* result (i.e., the one in which the $T = 0$ contribution has been subtracted) was in perfect agreement. This phenomenon is imputable to the fact that for each difference in p/T^4, two nonequilibrium transformations are involved, as stated in eq. (5.6): simulations at finite T can present discrepancies which are attributable to an insufficient sampling of the ensemble of realizations, as explained at length in section 4.3. At the same time however, such discrepancies are the same as those observed from simulations on symmetric lattices: what happens, then, is that these systematic errors mostly cancel each other, resulting in a generally very good agreement on the renormalized, physical value of p/T^4. A word of caution is in order though: whenever a discrepancy in the final result is observed, one has to investigate if and why this cancellation is not present; one way to do so is by examining the distributions of $T \neq 0$ and $T = 0$ transformations separately, as in the analysis performed on the "work" distributions in section 5.1.

An important consideration that we want to stress is that the transformations used in this method cannot cross the deconfinement transition: strong disagreement is observed between results of trajectories going from the confined to the deconfined phase, and trajectories which perform the same transformation in the reverse direction. However, this is not a insurmountable issue, as all trajectories can be tuned so that they never cross the transition: transformations in the confining phase terminate at $T = T_c$, exactly where those in the deconfined phase begin.

Even more intriguing options are in principle available to avoid the transition completely: one possibility would be to slowly add a coupling to Polyakov loops in the action during a transformation that crosses the transition and then, when $T > T_c$, slowly removing it. In this way one could elegantly bypass the transition by moving in a sort of transverse phase space, and, at the same time, obtaining the true physical result. Such inventive approaches to the study of the equation of

state can be implemented straightforwardly in this kind of technique, albeit their practical effectiveness is a matter of further study.

To take the continuum limit, the results for each value of N_t have been interpolated using cubic spline curves and then the continuum extrapolation has been performed at fixed temperature with a linear fit in $1/N_t^2$ of finite lattice spacing results, i.e. with a functional form of the type

$$p(T, N_t) = p^{(0)}(T) + \frac{p^{(1)}(T)}{N_t^2} \tag{5.9}$$

where $p^{(0)}(T)$ and are $p^{(1)}(T)$ the fit parameters, the former of which corresponds to the value of the pressure in the continuum limit. The complete set of continuum-extrapolated results for the pressure in units of T^4 are reported in table 5.3 and also in fig. 5.8, along with determinations by the Wuppertal-Budapest collaboration [6] and by L. Giusti and M. Pepe [7].
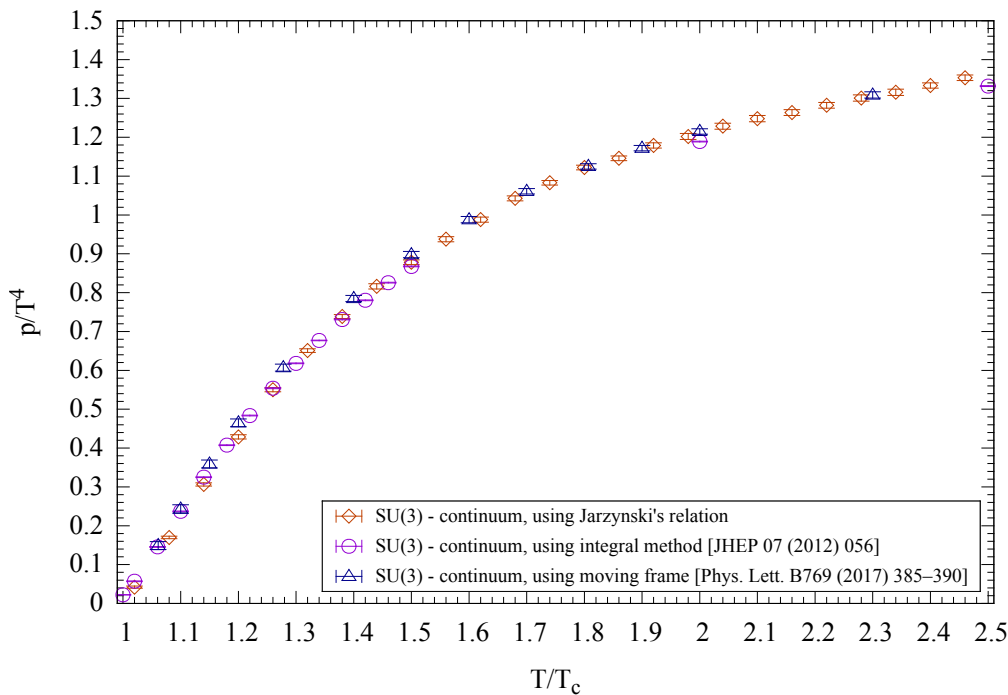
Figure 5.8: Results for the pressure in units of T^4 in the continuum limit obtained with an implementation of the nonequilibrium relation by Jarzynski. Data obtained in this work (orange squares) are presented along with recent results by the Wuppertal-Budapest collaboration [6] (violet circles) and by L. Giusti and M. Pepe [7] (blue triangles).

With the help of fig. 5.8 we can attempt a comparison between results obtained with radically different methods in the region above the deconfinement transition: we can safely affirm that good qualitative agreement is found between our novel method based on Jarzynski's equality and previous determinations. However, it is rather evident from this set of data that such agreement is not perfect: indeed, a significant

discrepancy between the results of the Wuppertal-Budapest collaboration [6] and the ones obtained by L. Giusti and M. Pepe [7] appears for $T > T_c$.

This issue was discussed at length in ref. [7]: this discrepancy is clearly visible for temperatures comprised between T_c and $1.5T_c$, and it slowly decreases when the temperature increases, eventually disappearing for $T > 3T_c$. We already mentioned this tension in the data in section 1.4 and it is well illustrated in fig. 1.4, where results for the trace anomaly are shown in a narrow temperature range. In the same work, it was observed that results obtained with the integral method in [6] at very fine lattice spacings agreed well with those extrapolated in the continuum limit obtained with shifted boundary conditions.

The accuracy reached in computing the pressure p using Jarzynski's equality and nonequilibrium transformations is such that a precise comparison with other computations is possible. Our results apparently tend to favor those of ref. [7] for temperatures above $1.6T_c$, displaying a similar discrepancy with those of ref. [6]. On the other hand, in the region just above the transition, our results are in disagreement with both previous determinations, as the data for p/T^4 show a slightly different shape. More in general, our statistical errors are comparable with those associated to the results of shifted boundary conditions, while those of ref. [6] are reportedly much smaller, almost by an order of magnitude.

In order to investigate this issues more in detail, we also computed other equilibrium observables, such as the trace of the energy-momentum tensor Δ, the energy density ϵ and the entropy density s. We recall that, in order to obtain these quantities, it is necessary to numerically derive the pressure p with respect to T. For example, the trace anomaly is obtained via eq. (1.42), that we report here

$$\Delta(T) = T^5 \frac{\partial}{\partial T} \left(\frac{p(T)}{T^4} \right).$$

This is to be contrasted with the integral method [36] and computations in a moving frame, in which a secondary observable such as the pressure requires numerical *integration* of the quantity that is directly computed on the lattice, i.e. the trace anomaly Δ or the entropy density $s = (\epsilon + p)/T$.

In order to perform the numerical derivation of the pressure, we opted for a reliable fit of the data that could also be easily derived. In particular, following ref. [7], we performed first a Padé interpolation of the continuum-extrapolated results for the pressure, namely using in the region $T \in [T_c, 2.5T_c]$ the functional form

$$\frac{p}{T^4} = \frac{p_1 + p_2 w + p_3 w^2}{1 + p_4 w + p_5 w^2} \tag{5.10}$$

where $w = \ln(T/T_c)$ and the p_i are the coefficients of the fit; the fit yielded $\chi^2_{\text{red}} = 0.33$. By deriving the functional form of eq. (5.10) we obtain the results for the trace of the energy-momentum tensor, which are reported in table 5.3 and shown in fig. 5.9.

Values for the energy density and for the entropy density can be recovered simply using a linear combination of p and Δ:

$$\epsilon = \Delta + 3p \quad \text{and} \quad s = \frac{\Delta + 4p}{T}.$$
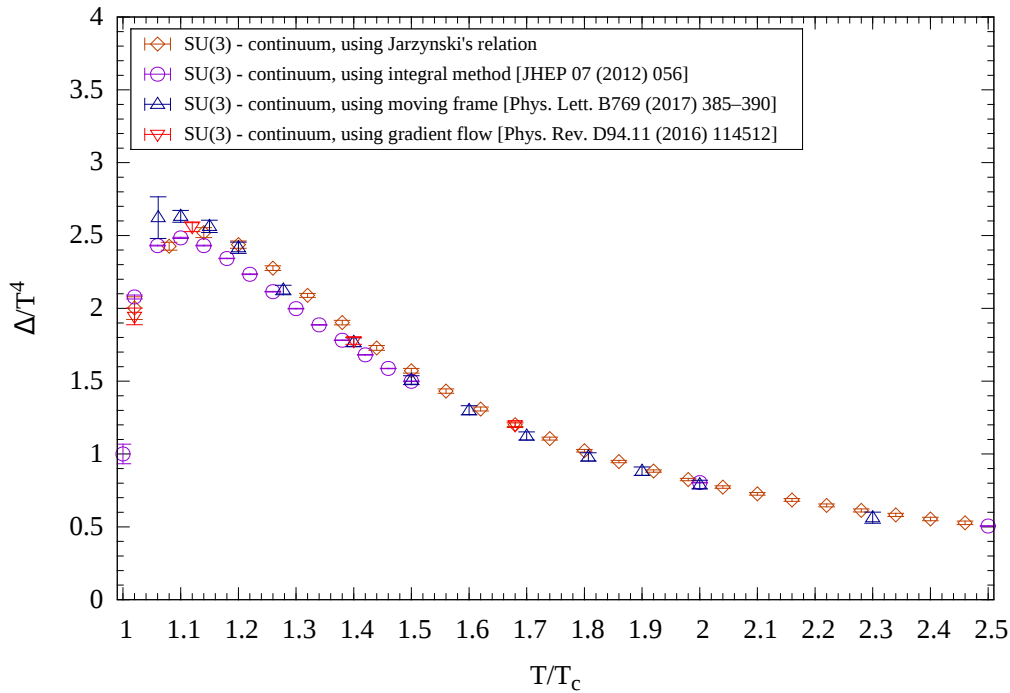
Figure 5.9: Same as in fig. 5.8, but for the trace of the energy-momentum tensor $\Delta = \epsilon - 3p$ in units of T^4. Also results by Kitazawa et al. [45] (red triangles) are shown.

Results for ϵ/T^4 and s/T^3 are reported in table 5.3 and shown in fig. 5.10 and fig. 5.11, respectively.

Looking at fig. 5.9 we can conclude that, again, the determination of the equation of state performed with nonequilibrium transformations is in remarkable quantitative agreement with the results of [7] for temperatures above $1.6T_c$, while in the proximity of T_c the situation is markedly different, as the peak of Δ/T^4 does not seem to correspond with that of previous computations. The agreement with [7] is substantially better in figs. 5.10 and 5.11, where no discrepancies are observed above $1.2T_c$. Again, significant discrepancies with [6] are still present throughout the region of interest, with the exception of the highest temperatures simulated in this work (where all determinations tend to agree) and also briefly very close to T_c. The fact that the disagreement with [6] is more significant for secondary observables, is certainly due to the fact that, from the perspective of our method, the values of Δ, ϵ and s are (at least partially) obtained from *derivation* of the pressure. Thus, they are more sensitive to slight changes in the behaviour of p: indeed, apparently small discrepancies in fig. 5.8 are now more evident.

In figs. 5.9 and 5.11 we also added recent results obtained with the method based on the gradient flow (see section 1.3.4 for more details). In the case of the trace anomaly Δ, only a few points are available and they are in good quantitative agreement with our data; the same cannot be said for the entropy density s, though. A severe discrepancy with our results appears in the region around $1.4T_c$ and is present also at higher temperatures.
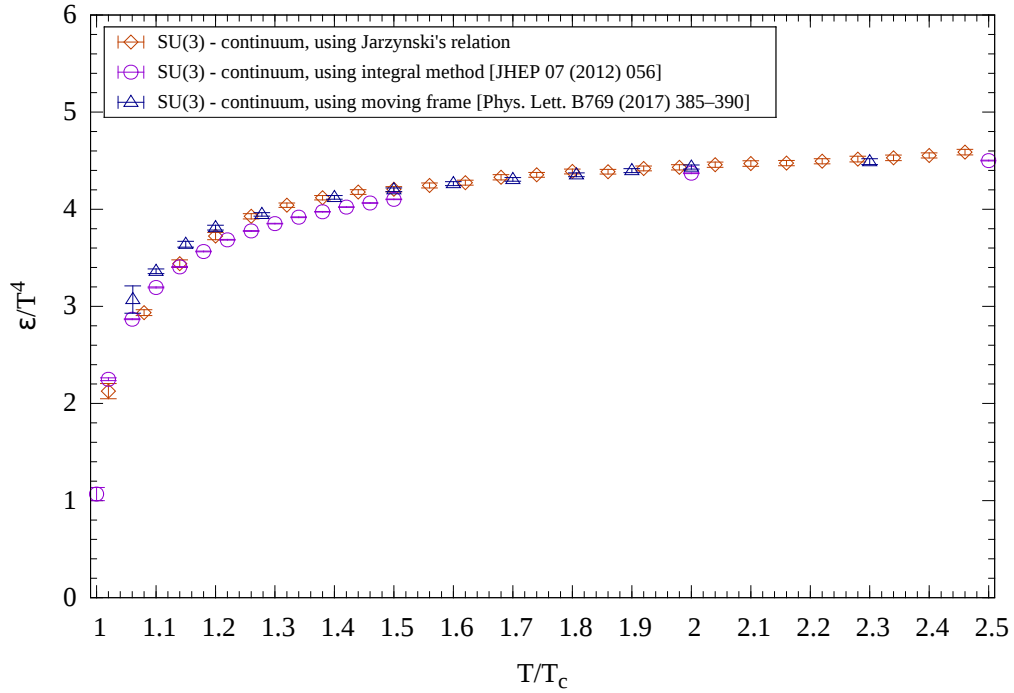
Figure 5.10: Same as in fig. 5.8, but for the energy density ϵ in units of T^4.

For what concerns the equation of state in the confining phase, the results for the pressure are illustrated in fig. 5.8; good agreement is found with results obtained with all previous determinations

For the computation of the trace anomaly we picked, for the fit of the pressure, a different functional form with respect to that of eq. (5.10): following what done in ref. [6], we used a fit inspired by the closed bosonic string model described in section 2.2.5, namely

$$\frac{p}{T^4} = a\frac{T}{T_c} + b\log\left(\frac{T_H}{T_c} - \frac{T}{T_c}\right) \tag{5.11}$$

in which the T_{H}/T_c ratio was set to be 1.098, following [11]; the fit yielded $a = -0.0133$ and $b = -0.0122$. From the derivation of eq. (5.11), the trace is readily obtained, as well as energy and entropy density: all these observables show good agreement with previous results within statistical errors.

Before moving to the conclusions, we would like to add a few more comments regarding the comparison between our results and other determinations.

- In the secondary observables for $T > T_c$, the agreement between our results and [7] is not as good as it is for the pressure: this is particularly evident for the trace anomaly Δ, which presents non-negligible discrepancies. One possible explanation could lie in the Padé interpolation used to numerically derive the pressure p, which might add a systematic effect not completely under control.

- More in general, when comparing our results with previous determinations, the discrepancies are quantitatively different depending on the observable:
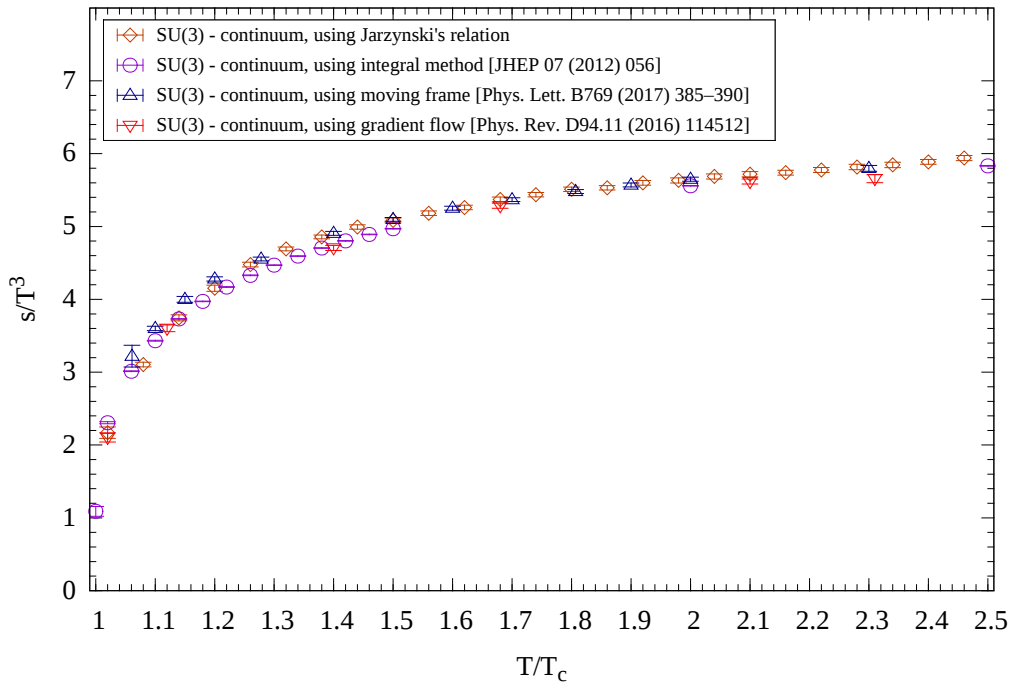
Figure 5.11: Same as in fig. 5.8, but for the entropy density $s = (\epsilon + p)/T$ in units of T^3. Also results by Kitazawa et al. [45] (red triangles) are shown.

this might be a clue that the numerical derivation/integration performed to compute secondary quantities in each technique might not provide the correct statistical error.

- Finally, if one picks the value of $r_0 T_c$ used in [7] (instead of that computed in [137] and used in this work), the disagreement with the data obtained in a moving frame is more modest, even if these two values of the critical temperature are compatible with each other; thus, we would like to remark that uncertainties in T_c may play a role in understanding such discrepancies.

The method based on Jarzynski's equality has proved to be highly reliable in computing the pressure and, thus, the observables related to the equation of state of the SU(3) pure gauge theory. We have to remark that the use of nonequilibrium transformations to compute differences in p/T^4 requires a careful planning: indeed, it is highly recommended to perform a preliminary study on the efficiency and on the reliability of such transformations. Three main factors must be taken into account when establishing the setup of the simulations: the number n_{transf} of transformations to use to cover the entire temperature range, the number n_R of realizations used to repeat each transformation and the number N of intermediate steps used to discretize each nonequilibrium trajectory in the Markov chain. The interplay between these factors is crucial in minimizing the computational cost, while keeping at the same time any systematic discrepancy under control.

We cannot stress enough the importance that reverse transformations have when
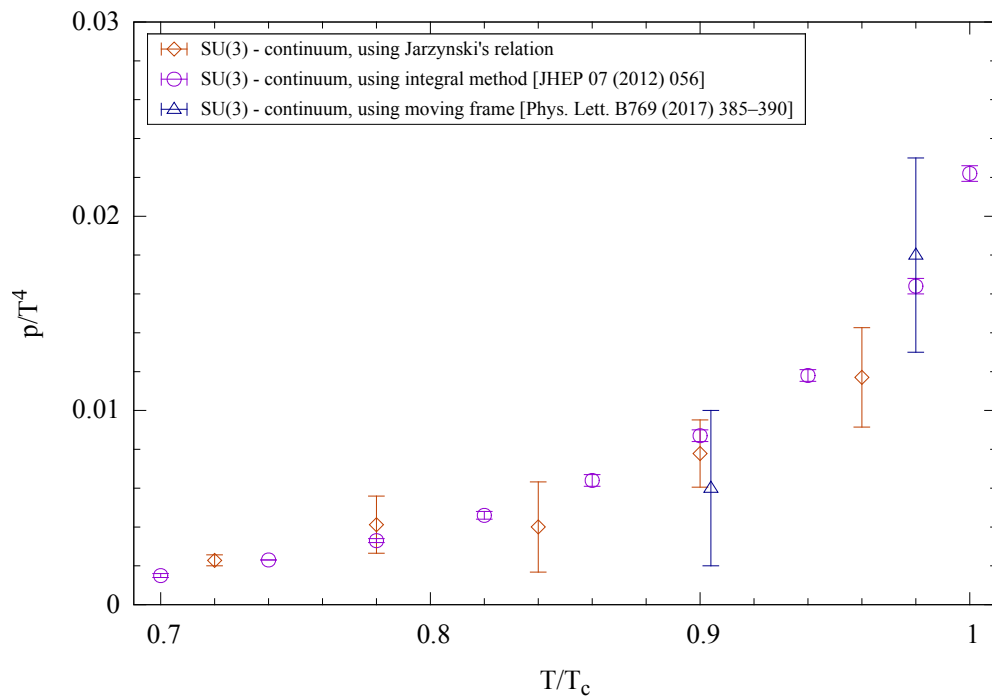
Figure 5.12:   Same as fig. 5.8, but in the confining phase, for temperature comprised between $0.7T_c$ and T_c.

using Jarzynski's equality: they represent a crucial tool for checking in an independent way the reliability of each transformation. The comparison between the results of direct and reverse trajectories is able to tell if the sample of realizations is good enough, and in principle even which of the two directions is to be preferred. They are truly independent, since the initial configuration of the reverse transformation is thermalized with a distribution which is quite different with respect to the direct one.

Another interesting implication of the possibility of performing transformations either increasing or decreasing the temperature can be found in the proximity of the transition, where it is more difficult to correctly thermalize the system and in general any simulation is more expensive. In this situation, we can easily perform transformations that go towards the critical temperature, from above or from below, since the initial configuration has been thermalized far from T_c: indeed, we observed that the results are far more reliable than those from transformations that begin close to T_c.

We also remark that this method can be extremely efficient: instead of producing large amounts of configurations (approximately) at equilibrium like in other methods, during a nonequilibrium transformation we can exploit the autocorrelation between configurations. This is true since, in the end, the average is not done on the measurements of each configuration, but on different (and uncorrelated) realizations of the same transformation. Moreover, this technique is also very effective in producing several points at different temperatures within the same transformation:

in eq. (5.8) we observed how at any intermediate step the difference in p/T^4 can be calculated. If a transformation is discretized in a few thousand steps, ten or even more values of p/T^4 can be extracted, making the most of each configuration that we generate.

Table 5.3: Complete set of results in the continuum limit for the equation of state of the SU(3) pure-glue theory as a function of the temperature, namely the pressure (second column), the trace of the energy-momentum tensor (third column), the energy density (fourth column) and the entropy density (fifth column).

T/T_c	p/T^4	Δ/T^4	ϵ/T^4	s/T^3
0.72	0.0023(3)	0.0137(38)	0.021(17)	0.023(17)
0.78	0.0041(15)	0.0200(57)	0.032(20)	0.036(21)
0.84	0.0040(23)	0.0286(87)	0.041(23)	0.045(25)
0.90	0.0078(17)	0.044(14)	0.067(24)	0.075(26)
0.96	0.0117(26)	0.072(23)	0.107(32)	0.119(35)
1.02	0.0418(28)	2.001(78)	2.127(78)	2.169(79)
1.08	0.1698(32)	2.426(27)	2.936(30)	3.106(32)
1.14	0.3064(42)	2.520(34)	3.439(39)	3.746(41)
1.20	0.429(6)	2.438(25)	3.724(38)	4.153(43)
1.26	0.550(5)	2.276(16)	3.927(27)	4.477(32)
1.32	0.651(5)	2.089(14)	4.041(23)	4.693(27)
1.38	0.739(5)	1.902(15)	4.118(22)	4.856(26)
1.44	0.816(7)	1.728(16)	4.177(24)	4.993(30)
1.50	0.878(6)	1.571(16)	4.206(27)	5.084(32)
1.56	0.938(7)	1.432(15)	4.245(26)	5.182(31)
1.62	0.988(7)	1.309(14)	4.273(26)	5.261(31)
1.68	1.043(7)	1.201(12)	4.329(27)	5.372(34)
1.74	1.083(6)	1.106(10)	4.355(25)	5.437(30)
1.80	1.122(6)	1.022(9)	4.389(25)	5.511(31)
1.86	1.146(6)	0.949(8)	4.386(24)	5.532(30)
1.92	1.179(7)	0.883(8)	4.420(25)	5.599(32)
1.98	1.202(8)	0.825(8)	4.431(27)	5.633(35)
2.04	1.229(8)	0.773(8)	4.459(28)	5.687(35)
2.10	1.248(8)	0.727(9)	4.471(29)	5.719(37)
2.16	1.264(8)	0.685(9)	4.476(27)	5.739(34)
2.22	1.282(7)	0.647(10)	4.494(27)	5.776(34)
2.28	1.301(8)	0.613(11)	4.516(30)	5.817(37)
2.34	1.316(8)	0.582(11)	4.530(29)	5.846(37)
2.40	1.333(7)	0.554(12)	4.554(26)	5.887(33)
2.46	1.353(7)	0.528(12)	4.588(28)	5.941(35)

Concluding remarks

In this thesis, many aspects regarding the thermodynamics of pure gauge theories have been investigated, with a particular focus on the determination of the equation of state. The calculation of quantities such as the pressure and the trace of the energy-momentum tensor of strongly-interacting theories encloses precious physical information on the mechanisms at work both in the confining and deconfining phases, which can be revealed through the predictions of effective theories and phenomenological models.

For what concerns the confining phase, the study discussed at length in chapter 2 [11] is a clear example of how it is possible to use precise thermodynamical results from lattice simulations to extract new insights on the physical degrees of freedom of the theory, and in particular to investigate the spectrum of high-lying glueball states. Indeed, the equation of state of SU(2) and SU(3) pure-glue theories is a perfect test not only for the hypothesis that a weakly-interacting glueball gas is able to describe the behaviour of these models for $T < T_c$, but also to *quantitatively* determine whether the glueball spectrum is indeed Hagedorn-like, and what kind of density of states it might possess. In this work, which is a natural prosecution of older studies [5, 9], the theoretical input of an effective string model for the flux tube of SU(N) theories has been crucial, providing an accurate prediction for the exponential-like spectrum with *no free parameters*. The fact that this approach provides remarkable agreement between lattice results and the contribution of a gas of glueballs *both* in the $N = 2$ and $N = 3$ cases highlights its predictiveness: even if they are qualitatively similar, their quantitative differences (the order of the transition and the presence of $C = -1$ states) are elegantly taken into account by the effective closed string model. Moreover, this study also serves as a new and intriguing way to analyze the predictions of effective string theory: namely, we find quantitative support to the idea that low-energy dynamics of SU(N) non-Abelian gauge theories can be well described with a bosonic string model, whose details coincide with those predicted by the Nambu-Gotō action.

This line of research can be developed also with an alternative, more phenomenological approach [12], which has also been discussed at the end of chapter 2. For the first time in pure-glue theories, repulsive interactions among glueball states have been taken into account by including effective-volume effects, as previously done in QCD with the HRG model [143–146]. As in the non-interacting case, pure gauge theories provide a relatively simple framework from a conceptual and computational point of view, in which new approaches can be accurately tested. Starting from the inclusion of an Hagedorn-like glueball spectrum, as in [11], this study modeled the contribution to thermodynamics of a repulsive interaction with a new free parameter,

namely the "effective radius" for the lightest glueball. An accurate quantitative description of lattice data is indeed possible: the best results have been obtained by assuming that the eigenvolume assigned to a glueball state is inversely proportional to its mass. Remarkably, the value of the 0^{++} effective radius obtained from these fits was consistent between SU(2) and SU(3) pure gauge theories, confirming *a posteriori* the robustness of the analysis.

Even if not directly related to the equation of state, in chapter 3 we introduced the use of a new quantity in gauge theories (i.e., the ξ/ξ_{2nd} ratio) which could be instrumental, albeit in an indirect way, in the study of the QCD phase diagram. Indeed, the ratio between the exponential correlation length and the second moment correlation length provides extremely precious information on the spectrum of the excitations of the flux tube, with modest computational effort. In practice, this quantity can be computed in the context of effective Polyakov loop models, to see if they are able to capture the rich spectrum of the original theory and, in principle, which kind of terms have to be added to the Polyakov loop action that characterizes them. In a recent work [35], the ξ/ξ_{2nd} ratio has been calculated in the confining region of the SU(2) pure gauge theory. The results provided clear evidence of what kind of behaviour one has to expect from the original theory: namely, that this ratio is very close to 1 in the very proximity of the transition, and that it gets larger and larger as the temperature decreases. Moreover, as shown at the end of the chapter, effective string theory provides a qualitative description of the mechanisms underlying the sudden increase of ξ/ξ_{2nd}; however, intrinsic limitations of the effective string approach prevent a quantitative study of the phenomenon. We also mention that, very recently, the ξ/ξ_{2nd} ratio has been computed in ref. [180] for an effective Polyakov loop model built with the relative weights method on a SU(3) gauge theory with dynamical staggered fermions of mass 695 MeV. In this work, large-distance couplings between Polyakov loops were included; in this setup the value $\xi/\xi_{2nd} = 1.27(3)$ was found, clearly compatible with a rich spectrum of excitations.

The last part of this manuscript is devoted to the introduction of a novel method for the calculation of the equation of state in pure gauge theories, based on Jarzynski's equality. In chapter 4 we discussed how this well-known relation of nonequilibrium statistical mechanics has been recently [44] generalized and implemented for the first time in numerical simulations of lattice field theories, namely in the computation of the free energy associated to an interface in the $\mathbb{Z}_2$ gauge model. The possible applications of this result in lattice gauge theory cover a vast range of observables, as, in principle, any quantity related to differences in free energy (or, equivalently, to ratios of partition functions) can be computed using Jarzynski's equality. We remark however that the practical implementation of this relation is limited to cases in which the expectation value of the observable can be sampled efficiently in a Monte Carlo simulation: a perfect example is the measurement of the pressure of non-Abelian gauge theories at nonzero temperature. As noted multiple times throughout this thesis, new methods [66, 72] have been recently proposed as an alternative to the integral method [36], i.e. the standard (but computationally challenging) way to calculate p and other quantities. In chapter 5 we showed how Jarzynski's equality provides a simple and efficient technique to compute *directly* the equation of state of SU(N) Yang-Mills theories, through the use of nonequilibrium transformations

during Monte Carlo simulations. Results obtained with this technique proved to be very competitive when compared to recent determinations [6, 7, 45]: moreover, a few discrepancies with results of other methods emerged, more or less significant depending on the observable under investigation. It would be interesting then, to generalize this method to simulations with dynamical fermion fields, in order to pursue this kind of comparisons also for results of the equation of state of full QCD, either with Wilson or staggered fermions.

Bibliography

[1] D. J. Gross and F. Wilczek. "Ultraviolet Behavior of Non-Abelian Gauge Theories". *Phys. Rev. Lett.* 30 (26 June 1973), pp. 1343–1346.

[2] H. D. Politzer. "Reliable Perturbative Results for Strong Interactions?" *Phys. Rev. Lett.* 30 (26 June 1973), pp. 1346–1349.

[3] K. G. Wilson. "Confinement of Quarks". *Phys. Rev.* D10 (1974), pp. 2445–2459.

[4] G. Boyd et al. "Thermodynamics of SU(3) lattice gauge theory". *Nucl. Phys.* B469 (1996), pp. 419–444. arXiv: `hep-lat/9602007 [hep-lat]`.

[5] H. B. Meyer. "High-Precision Thermodynamics and Hagedorn Density of States". *Phys. Rev.* D80 (2009), p. 051502. arXiv: `0905.4229 [hep-lat]`.

[6] S. Borsányi et al. "Precision SU(3) lattice thermodynamics for a large temperature range". *JHEP* 07 (2012), p. 056. arXiv: `1204.6184 [hep-lat]`.

[7] L. Giusti and M. Pepe. "Equation of state of the SU(3) Yang–Mills theory: A precise determination from a moving frame". *Phys. Lett.* B769 (2017), pp. 385–390. arXiv: `1612.00265 [hep-lat]`.

[8] M. Panero. "Thermodynamics of the QCD plasma and the large-N limit". *Phys. Rev. Lett.* 103 (2009), p. 232001. arXiv: `0907.3719 [hep-lat]`.

[9] M. Caselle et al. "Thermodynamics of SU(N) Yang-Mills theories in 2+1 dimensions I - The confining phase". *JHEP* 06 (2011), p. 142. arXiv: `1105.0359 [hep-lat]`.

[10] M. Caselle et al. "Thermodynamics of SU(N) Yang-Mills theories in 2+1 dimensions II. The Deconfined phase". *JHEP* 05 (2012), p. 135. arXiv: `1111.0580 [hep-th]`.

[11] M. Caselle, A. Nada, and M. Panero. "Hagedorn spectrum and thermodynamics of SU(2) and SU(3) Yang-Mills theories". *JHEP* 07 (2015), p. 143. arXiv: `1505.01106 [hep-lat]`.

[12] P. Alba et al. "Excluded-volume effects for a hadron gas in Yang-Mills theory". *Phys. Rev.* D95.9 (2017), p. 094511. arXiv: `1611.05872 [hep-lat]`.

[13] R. Hagedorn. "Statistical thermodynamics of strong interactions at high-energies". *Nuovo Cim. Suppl.* 3 (1965), pp. 147–186.

[14] C. Gattringer. "Flux representation of an effective Polyakov loop model for QCD thermodynamics". *Nucl. Phys.* B850 (2011), pp. 242–252. arXiv: `1104.2503 [hep-lat]`.

[15]   Y. Delgado Mercado and C. Gattringer. "Monte Carlo simulation of the SU(3) spin model with chemical potential in a flux representation". *Nucl. Phys.* B862 (2012), pp. 737–750. arXiv: `1204.6074 [hep-lat]`.

[16]   J. Greensite and K. Splittorff. "Mean field theory of effective spin models as a baryon fugacity expansion". *Phys. Rev.* D86 (2012), p. 074501. arXiv: `1206.1159 [hep-lat]`.

[17]   J. Greensite. "The potential of the effective Polyakov line action from the underlying lattice gauge theory". *Phys. Rev.* D86 (2012), p. 114507. arXiv: `1209.5697 [hep-lat]`.

[18]   J. Greensite and K. Langfeld. "Effective Polyakov line action from the relative weights method". *Phys. Rev.* D87 (2013), p. 094501. arXiv: `1301.4977 [hep-lat]`.

[19]   J. Greensite and K. Langfeld. "Effective Polyakov line action from strong lattice couplings to the deconfinement transition". *Phys. Rev.* D88 (2013), p. 074503. arXiv: `1305.0048 [hep-lat]`.

[20]   J. Greensite and K. Langfeld. "Finding the effective Polyakov line action for SU(3) gauge theories at finite chemical potential". *Phys. Rev.* D90.1 (2014), p. 014507. arXiv: `1403.5844 [hep-lat]`.

[21]   J. Greensite and R. Höllwieser. "Relative weights approach to SU(3) gauge theories with dynamical fermions at finite density". *Phys. Rev.* D94.1 (2016), p. 014504. arXiv: `1603.09654 [hep-lat]`.

[22]   R. Höllwieser and J. Greensite. "Polyakov line actions from SU(3) lattice gauge theory with dynamical fermions via relative weights". *EPJ Web Conf.* 137 (2017), p. 03007. arXiv: `1611.03973 [hep-lat]`.

[23]   J. Langelage, S. Lottini, and O. Philipsen. "Centre symmetric 3d effective actions for thermal SU(N) Yang-Mills from strong coupling series". *JHEP* 02 (2011). [Erratum: JHEP07,014(2011)], p. 057. arXiv: `1010.0951 [hep-lat]`.

[24]   M. Fromm et al. "The QCD deconfinement transition for heavy quarks and all baryon chemical potentials". *JHEP* 01 (2012), p. 042. arXiv: `1111.4953 [hep-lat]`.

[25]   G. Bergner, J. Langelage, and O. Philipsen. "Effective lattice Polyakov loop theory vs. full SU(3) Yang-Mills at finite temperature". *JHEP* 03 (2014), p. 039. arXiv: `1312.7823 [hep-lat]`.

[26]   G. Bergner, J. Langelage, and O. Philipsen. "Numerical corrections to the strong coupling effective Polyakov-line action for finite T Yang-Mills theory". *JHEP* 11 (2015), p. 010. arXiv: `1505.01021 [hep-lat]`.

[27]   L. Dittmann, T. Heinzl, and A. Wipf. "An Effective lattice theory for Polyakov loops". *JHEP* 06 (2004), p. 005. arXiv: `hep-lat/0306032 [hep-lat]`.

[28]   T. Heinzl, T. Kaestner, and A. Wipf. "Effective actions for the SU(2) confinement-deconfinement phase transition". *Phys. Rev.* D72 (2005), p. 065005. arXiv: `hep-lat/0502013 [hep-lat]`.

[29]   C. Wozar et al. "Phase structure of Z(3)-Polyakov-loop models". *Phys. Rev.* D74 (2006), p. 114501. arXiv: `hep-lat/0605012 [hep-lat]`.

[30] C. Wozar et al. "Inverse Monte-Carlo determination of effective lattice models for SU(3) Yang-Mills theory at finite temperature". *Phys. Rev.* D76 (2007), p. 085004. arXiv: `0704.2570` [`hep-lat`].

[31] M. Billó et al. "Toward an analytic determination of the deconfinement temperature in SU(2) LGT". *Nucl. Phys.* B472 (1996), pp. 163–193. arXiv: `hep-lat/9601020` [`hep-lat`].

[32] G. Aarts and F. A. James. "Complex Langevin dynamics in the SU(3) spin model at nonzero chemical potential revisited". *JHEP* 01 (2012), p. 118. arXiv: `1112.4655` [`hep-lat`].

[33] P. Scior et al. "Effective SU(2) Polyakov Loop Theories with Heavy Quarks on the Lattice". *PoS* LATTICE2014 (2015), p. 173. arXiv: `1412.7089` [`hep-lat`].

[34] B. Bahrampour, B. Wellegehausen, and L. von Smekal. "Non-Local effective SU(2) Polyakov-loop models from inverse Monte-Carlo methods". *PoS* LATTICE2016 (2016), p. 070. arXiv: `1612.00285` [`hep-lat`].

[35] M. Caselle and A. Nada. "The ξ/ξ_{2nd} ratio as a tool to refine Effective Polyakov Loop models" (2017). arXiv: `1707.02164` [`hep-lat`].

[36] J. Engels et al. "Nonperturbative thermodynamics of SU(N) gauge theories". *Phys. Lett.* B252 (1990), pp. 625–630.

[37] Y. Taniguchi et al. "Exploring $N_f = 2+1$ QCD thermodynamics from the gradient flow". *Phys. Rev.* D96.1 (2017), p. 014509. arXiv: `1609.01417` [`hep-lat`].

[38] C. Jarzynski. "Nonequilibrium Equality for Free Energy Differences". *Phys. Rev. Lett.* 78 (14 1997), pp. 2690–2693. arXiv: `cond-mat/9610209` [`cond-mat`].

[39] C. Jarzynski. "Equilibrium free-energy differences from nonequilibrium measurements: A master-equation approach". *Phys. Rev.* E56 (5 1997), pp. 5018–5035. arXiv: `cond-mat/9707325` [`cond-mat`].

[40] D. J. Evans and D. J. Searles. "Equilibrium microstates which generate second law violating steady states". *Phys. Rev. E* 50 (2 Aug. 1994), pp. 1645–1648.

[41] G. Gallavotti and E. G. D. Cohen. "Dynamical Ensembles in Nonequilibrium Statistical Mechanics". *Phys. Rev. Lett.* 74 (14 Apr. 1995), pp. 2694–2697.

[42] G. E. Crooks. "Entropy production fluctuation theorem and the nonequilibrium work relation for free energy differences". *Phys. Rev. E* 60 (3 Sept. 1999), pp. 2721–2726.

[43] J. Liphardt et al. "Equilibrium Information from Nonequilibrium Measurements in an Experimental Test of Jarzynski's Equality". *Science* 296.5574 (2002), pp. 1832–1835. ISSN: 0036-8075.

[44] M. Caselle et al. "Jarzynski's theorem for lattice gauge theory". *Phys. Rev.* D94.3 (2016), p. 034503. arXiv: `1604.05544` [`hep-lat`].

[45] M. Kitazawa et al. "Equation of State for SU(3) Gauge Theory via the Energy-Momentum Tensor under Gradient Flow". *Phys. Rev.* D94.11 (2016), p. 114512. arXiv: `1610.07810` [`hep-lat`].

[46] M. A. Stephanov. "QCD phase diagram: An Overview". *PoS* LAT2006 (2006), p. 024. arXiv: `hep-lat/0701002 [hep-lat]`.

[47] G. 't Hooft. "Symmetry Breaking Through Bell-Jackiw Anomalies". *Phys. Rev. Lett.* 37 (1976), pp. 8–11.

[48] G. 't Hooft. "Computation of the Quantum Effects Due to a Four-Dimensional Pseudoparticle". *Phys. Rev.* D14 (1976). [Erratum: Phys. Rev.D18,2199(1978)], pp. 3432–3450.

[49] O. Philipsen. "The QCD equation of state from the lattice". *Prog. Part. Nucl. Phys.* 70 (2013), pp. 55–107. arXiv: `1207.5999 [hep-lat]`.

[50] G. Curci, P. Menotti, and G. Paffuti. "Symanzik's Improved Lagrangian for Lattice Gauge Theory". *Phys. Lett.* 130B (1983). [Erratum: Phys. Lett.135B, 516(1984)], p. 205.

[51] M. Lüscher and P. Weisz. "Computation of the Action for On-Shell Improved Lattice Gauge Theories at Weak Coupling". *Phys. Lett.* 158B (1985), pp. 250–254.

[52] K. G. Wilson. "Quarks and Strings on a Lattice". *New Phenomena in Subnuclear Physics: Proceedings, International School of Subnuclear Physics, Erice, Sicily, Jul 11-Aug 1 1975. Part A.* [,0069(1975)]. 1975, p. 99.

[53] J. Kogut and L. Susskind. "Hamiltonian formulation of Wilson's lattice gauge theories". *Phys. Rev. D* 11 (2 Jan. 1975), pp. 395–408.

[54] L. Susskind. "Lattice fermions". *Phys. Rev. D* 16 (10 Nov. 1977), pp. 3031–3039.

[55] C. Gattringer and C. B. Lang. "Quantum chromodynamics on the lattice". *Lect. Notes Phys.* 788 (2010), pp. 1–343.

[56] T. Umeda et al. "Fixed Scale Approach to Equation of State in Lattice QCD". *Phys. Rev.* D79 (2009), p. 051501. arXiv: `0809.2842 [hep-lat]`.

[57] T. Umeda et al. "Equation of state in 2+1 flavor QCD with improved Wilson quarks by the fixed scale approach". *Phys. Rev.* D85 (2012), p. 094508. arXiv: `1202.4719 [hep-lat]`.

[58] T. Umeda. "Fixed-scale approach to finite-temperature lattice QCD with shifted boundaries". *Phys. Rev.* D90.5 (2014), p. 054511. arXiv: `1408.2328 [hep-lat]`.

[59] J. Engels et al. "Gauge Field Thermodynamics for the SU(2) Yang-Mills System". *Nucl. Phys.* B205 (1982), pp. 545–577.

[60] F. Karsch. "SU(N) Gauge Theory Couplings on Asymmetric Lattices". *Nucl. Phys.* B205 (1982), pp. 285–300.

[61] F. Karsch, J. Engels, and T. Scheideler. "Direct determination of the gauge coupling derivatives for the energy density in lattice QCD". *Nucl. Phys. Proc. Suppl.* 63 (1998), pp. 427–429. arXiv: `hep-lat/9709011 [hep-lat]`.

[62] M. Shirogane et al. "Latent heat at the first order phase transition point of SU(3) gauge theory". *Phys. Rev.* D94.1 (2016), p. 014506. arXiv: `1605.02997 [hep-lat]`.

[63] L. Giusti and H. B. Meyer. "Thermal momentum distribution from path integrals with shifted boundary conditions". *Phys. Rev. Lett.* 106 (2011), p. 131601. arXiv: `1011.2727 [hep-lat]`.

[64] L. Giusti and H. B. Meyer. "Thermodynamic potentials from shifted boundary conditions: the scalar-field theory case". *JHEP* 11 (2011), p. 087. arXiv: `1110.3136 [hep-lat]`.

[65] L. Giusti and H. B. Meyer. "Implications of Poincare symmetry for thermal field theories in finite-volume". *JHEP* 01 (2013), p. 140. arXiv: `1211.6669 [hep-lat]`.

[66] L. Giusti and M. Pepe. "Equation of state of a relativistic theory from a moving frame". *Phys. Rev. Lett.* 113 (2014), p. 031601. arXiv: `1403.0360 [hep-lat]`.

[67] L. Giusti and M. Pepe. "Energy-momentum tensor on the lattice: Nonperturbative renormalization in Yang-Mills theory". *Phys. Rev.* D91 (2015), p. 114504. arXiv: `1503.07042 [hep-lat]`.

[68] S. Caracciolo et al. "The Energy Momentum Tensor for Lattice Gauge Theories". *Annals Phys.* 197 (1990), p. 119.

[69] M. Lüscher. "Properties and uses of the Wilson flow in lattice QCD". *JHEP* 08 (2010). [Erratum: JHEP03,092(2014)], p. 071. arXiv: `1006.4518 [hep-lat]`.

[70] M. Lüscher and P. Weisz. "Perturbative analysis of the gradient flow in non-abelian gauge theories". *JHEP* 02 (2011), p. 051. arXiv: `1101.0963 [hep-th]`.

[71] M. Lüscher. "Future applications of the Yang-Mills gradient flow in lattice QCD". *PoS* LATTICE2013 (2014), p. 016. arXiv: `1308.5598 [hep-lat]`.

[72] H. Suzuki. "Energy–momentum tensor from the Yang–Mills gradient flow". *PTEP* 2013 (2013). [Erratum: PTEP2015,079201(2015)], 083B03. arXiv: `1304.0533 [hep-lat]`.

[73] M. Asakawa et al. "Thermodynamics of SU(3) gauge theory from gradient flow on the lattice". *Phys. Rev.* D90.1 (2014). [Erratum: Phys. Rev.D92, no.5, 059902(2015)], p. 011501. arXiv: `1312.7492 [hep-lat]`.

[74] S. Datta, S. Gupta, and A. Lytle. "Using Wilson flow to study the SU(3) deconfinement transition". *Phys. Rev.* D94.9 (2016), p. 094502. arXiv: `1512.04892 [hep-lat]`.

[75] H. Makino and H. Suzuki. "Lattice energy–momentum tensor from the Yang–Mills gradient flow—inclusion of fermion fields". *PTEP* 2014 (2014). [Erratum: PTEP2015, 079202(2015)], 063B02. arXiv: `1403.4772 [hep-lat]`.

[76] L. Giusti and M. Pepe. "Thermodynamics of strongly interacting plasma with high accuracy". *PoS* LATTICE2016 (2016), p. 061. arXiv: `1612.02337 [hep-lat]`.

[77] A. Bazavov et al. "Equation of state in (2+1)-flavor QCD". *Phys. Rev.* D90 (2014), p. 094503. arXiv: `1407.6387 [hep-lat]`.

[78] S. Borsányi et al. "Calculation of the axion mass based on high-temperature lattice quantum chromodynamics". *Nature* 539.7627 (2016), pp. 69–71. arXiv: `1606.07494 [hep-lat]`.

[79] R. Hagedorn and J. Ranft. "Statistical thermodynamics of strong interactions at high-energies. 2. Momentum spectra of particles produced in pp-collisions". *Nuovo Cim. Suppl.* 6 (1968), pp. 169–354.

[80] R. Hagedorn. "Statistical thermodynamics of strong interactions at high energies. 3. Heavy-pair (quark) production rates". *Nuovo Cim. Suppl.* 6 (1968), pp. 311–354.

[81] R. Hagedorn. "Hadronic matter near the boiling point". *Nuovo Cim.* A56 (1968), pp. 1027–1057.

[82] R. Hagedorn. "Thermodynamics of strong interactions" (1971).

[83] K. Redlich and H. Satz. "The Legacy of Rolf Hagedorn: Statistical Bootstrap and Ultimate Temperature". *Melting Hadrons, Boiling Quarks - From Hagedorn Temperature to Ultra-Relativistic Heavy-Ion Collisions at CERN: With a Tribute to Rolf Hagedorn*. Ed. by J. Rafelski. 2016, pp. 49–68. arXiv: `1501.07523 [hep-ph]`.

[84] W. Nahm. "Analytical solution of the statistical bootstrap model". *Nucl. Phys.* B45 (1972), pp. 525–553.

[85] N. Cabibbo and G. Parisi. "Exponential Hadronic Spectrum and Quark Liberation". *Phys. Lett.* 59B (1975), pp. 67–69.

[86] F. Karsch, K. Redlich, and A. Tawfik. "Hadron resonance mass spectrum and lattice QCD thermodynamics". *Eur. Phys. J.* C29 (2003), pp. 549–556. arXiv: `hep-ph/0303108 [hep-ph]`.

[87] F. Karsch, K. Redlich, and A. Tawfik. "Thermodynamics at nonzero baryon number density: A Comparison of lattice and hadron resonance gas model calculations". *Phys. Lett.* B571 (2003), pp. 67–74. arXiv: `hep-ph/0306208 [hep-ph]`.

[88] A. Tawfik. "QCD phase diagram: A Comparison of lattice and hadron resonance gas model calculations". *Phys. Rev.* D71 (2005), p. 054502. arXiv: `hep-ph/0412336 [hep-ph]`.

[89] M. Cheng et al. "Baryon Number, Strangeness and Electric Charge Fluctuations in QCD at High Temperature". *Phys. Rev.* D79 (2009), p. 074505. arXiv: `0811.1006 [hep-lat]`.

[90] P. Huovinen and P. Petreczky. "QCD Equation of State and Hadron Resonance Gas". *Nucl. Phys.* A837 (2010), pp. 26–53. arXiv: `0912.2541 [hep-ph]`.

[91] S. Borsányi et al. "The QCD equation of state with dynamical quarks". *JHEP* 11 (2010), p. 077. arXiv: `1007.2580 [hep-lat]`.

[92] S. Borsányi et al. "Full result for the QCD equation of state with 2+1 flavors". *Phys. Lett.* B730 (2014), pp. 99–104. arXiv: `1309.5258 [hep-lat]`.

[93]   A. Bazavov et al. "Fluctuations and Correlations of net baryon number, electric charge, and strangeness: A comparison of lattice QCD results with the hadron resonance gas model". *Phys. Rev.* D86 (2012), p. 034509. arXiv: `1203.0784 [hep-lat]`.

[94]   A. Bazavov et al. "Quark number susceptibilities at high temperatures". *Phys. Rev.* D88.9 (2013), p. 094021. arXiv: `1309.2317 [hep-lat]`.

[95]   R. Bellwied et al. "Fluctuations and correlations in high temperature QCD". *Phys. Rev.* D92.11 (2015), p. 114505. arXiv: `1507.04627 [hep-lat]`.

[96]   H.-T. Ding et al. "Diagonal and off-diagonal quark number susceptibilities at high temperatures". *Phys. Rev.* D92.7 (2015), p. 074043. arXiv: `1507.06637 [hep-lat]`.

[97]   W. Broniowski, W. Florkowski, and L. Ya. Glozman. "Update of the Hagedorn mass spectrum". *Phys. Rev.* D70 (2004), p. 117503. arXiv: `hep-ph/0407290 [hep-ph]`.

[98]   J. Noronha-Hostler, J. Noronha, and C. Greiner. "Transport Coefficients of Hadronic Matter near T(c)". *Phys. Rev. Lett.* 103 (2009), p. 172302. arXiv: `0811.1571 [nucl-th]`.

[99]   A. Majumder and B. Müller. "Hadron Mass Spectrum from Lattice QCD". *Phys. Rev. Lett.* 105 (2010), p. 252002. arXiv: `1008.1747 [hep-ph]`.

[100]   A. Bazavov et al. "Additional Strange Hadrons from QCD Thermodynamics and Strangeness Freezeout in Heavy Ion Collisions". *Phys. Rev. Lett.* 113.7 (2014), p. 072001. arXiv: `1404.6511 [hep-lat]`.

[101]   P. M. Lo et al. "Matching the Hagedorn mass spectrum with Lattice QCD results". *Phys. Rev.* C92.5 (2015), p. 055206. arXiv: `1507.06398 [nucl-th]`.

[102]   P. Alba et al. "Constraining the hadronic spectrum through QCD thermodynamics on the lattice" (2017). arXiv: `1702.01113 [hep-lat]`.

[103]   W. Broniowski and W. Florkowski. "Different Hagedorn temperatures for mesons and baryons from experimental mass spectra, compound hadrons, and combinatorial saturation". *Phys. Lett.* B490 (2000), pp. 223–227. arXiv: `hep-ph/0004104 [hep-ph]`.

[104]   J. Cleymans and D. Worku. "The Hagedorn temperature Revisited". *Mod. Phys. Lett.* A26 (2011), pp. 1197–1209. arXiv: `1103.1463 [hep-ph]`.

[105]   F. Buisseret and G. Lacroix. "Comments on Yang–Mills thermodynamics: The Hagedorn spectrum and the gluon gas pictures for a generic gauge algebra". *Phys. Lett.* B705 (2011), pp. 405–409. arXiv: `1105.1092 [hep-ph]`.

[106]   P. Giudice and S. Piemonte. "Improved thermodynamics of SU(2) gauge theory" (2017). arXiv: `1708.01216 [hep-lat]`.

[107]   E. Eichten et al. "Charmonium: The Model". *Phys. Rev.* D17 (1978). [Erratum: Phys. Rev.D21,313(1980)], p. 3090.

[108]   M. Lüscher, K. Symanzik, and P. Weisz. "Anomalies of the Free Loop Wave Equation in the WKB Approximation". *Nucl. Phys.* B173 (1980), p. 365.

[109]   O. Aharony and M. Dodelson. "Effective String Theory and Nonlinear Lorentz Invariance". *JHEP* 02 (2012), p. 008. arXiv: `1111.5758 [hep-th]`.

[110]   O. Aharony and Z. Komargodski. "The Effective Theory of Long Strings". *JHEP* 05 (2013), p. 118. arXiv: `1302.6257 [hep-th]`.

[111]   R. Sommer. "A New way to set the energy scale in lattice gauge theories and its applications to the static force and alpha-s in SU(2) Yang-Mills theory". *Nucl. Phys.* B411 (1994), pp. 839–854. arXiv: `hep-lat/9310022 [hep-lat]`.

[112]   S. Necco and R. Sommer. "The N(f) = 0 heavy quark potential from short to intermediate distances". *Nucl. Phys.* B622 (2002), pp. 328–346. arXiv: `hep-lat/0108008 [hep-lat]`.

[113]   M. Lüscher and P. Weisz. "Coordinate space methods for the evaluation of Feynman diagrams in lattice field theories". *Nucl. Phys.* B445 (1995), pp. 429–450. arXiv: `hep-lat/9502017 [hep-lat]`.

[114]   C. R. Allton. "Lattice Monte Carlo data versus perturbation theory". *Nucl. Phys. Proc. Suppl.* 53 (1997), pp. 867–869. arXiv: `hep-lat/9610014 [hep-lat]`.

[115]   B. Lucini, M. Teper, and U. Wenger. "The High temperature phase transition in SU(N) gauge theories". *JHEP* 01 (2004), p. 061. arXiv: `hep-lat/0307017 [hep-lat]`.

[116]   V. Mathieu, N. Kochelev, and V. Vento. "The Physics of Glueballs". *Int. J. Mod. Phys.* E18 (2009), pp. 1–49. arXiv: `0810.4453 [hep-ph]`.

[117]   V. Crede and C. A. Meyer. "The Experimental Status of Glueballs". *Prog. Part. Nucl. Phys.* 63 (2009), pp. 74–116. arXiv: `0812.0600 [hep-ex]`.

[118]   C. M. Richards et al. "Glueball mass measurements from improved staggered fermion simulations". *Phys. Rev.* D82 (2010), p. 034501. arXiv: `1005.2473 [hep-lat]`.

[119]   E. Gregory et al. "Towards the glueball spectrum from unquenched lattice QCD". *JHEP* 10 (2012), p. 170. arXiv: `1208.1858 [hep-lat]`.

[120]   W. Sun et al. "Glueball spectrum from $N_f = 2$ lattice QCD study on anisotropic lattices" (2017). arXiv: `1702.08174 [hep-lat]`.

[121]   M. J. Teper. "Glueball masses and other physical properties of SU(N) gauge theories in D = (3+1): A Review of lattice results for theorists" (1998). arXiv: `hep-th/9812187 [hep-th]`.

[122]   H. B. Meyer. "Glueball regge trajectories". PhD thesis. Oxford U., 2004. arXiv: `hep-lat/0508002 [hep-lat]`.

[123]   G. Karl and J. E. Paton. "Glue - lump spectrum in the bag model". *Phys. Rev.* D60 (1999), p. 034015. arXiv: `hep-ph/9904407 [hep-ph]`.

[124]   G. Karl and J. E. Paton. "Gluonic states in two space dimensions". *Phys. Rev.* D61 (2000), p. 074002. arXiv: `hep-ph/9910413 [hep-ph]`.

[125]   N. Isgur and J. E. Paton. "A Flux Tube Model for Hadrons in QCD". *Phys. Rev.* D31 (1985), p. 2910.

[126] R. W. Johnson and M. J. Teper. "String models of glueballs and the spectrum of SU(N) gauge theories in (2+1)-dimensions". *Phys. Rev.* D66 (2002), p. 036006. arXiv: `hep-ph/0012287` `[hep-ph]`.

[127] R. W. Johnson and M. Teper. "An Extended Isgur-Paton model: Agreement with the lattice?" *Nucl. Phys. Proc. Suppl.* 63 (1998), pp. 197–199. arXiv: `hep-lat/9709083` `[hep-lat]`.

[128] O. Aharony and E. Karzbrun. "On the effective action of confining strings". *JHEP* 06 (2009), p. 012. arXiv: `0903.1927` `[hep-th]`.

[129] O. Aharony and M. Field. "On the effective theory of long open strings". *JHEP* 01 (2011), p. 065. arXiv: `1008.2636` `[hep-th]`.

[130] M. Billó et al. "The Lorentz-invariant boundary action of the confining string and its universal contribution to the inter-quark potential". *JHEP* 05 (2012), p. 130. arXiv: `1202.1984` `[hep-th]`.

[131] M. Caselle et al. "A different kind of string". *JHEP* 01 (2015), p. 105. arXiv: `1406.5127` `[hep-lat]`.

[132] F. Gliozzi and M. Meineri. "Lorentz completion of effective string (and p-brane) action". *JHEP* 08 (2012), p. 056. arXiv: `1207.2912` `[hep-th]`.

[133] H. B. Meyer. "Poincare invariance in effective string theories". *JHEP* 05 (2006), p. 066. arXiv: `hep-th/0602281` `[hep-th]`.

[134] B. Zwiebach. *A first course in string theory.* Cambridge University Press, 2006. ISBN: 0521831431, 9780521831437, 9780511207570.

[135] G. H. Hardy and S. Ramanujan. "Asymptotic Formulæ in Combinatory Analysis". *Proceedings of the London Mathematical Society* s2-17.1 (1918), pp. 75–115. ISSN: 1460-244X.

[136] Y. Iwasaki et al. "Finite temperature phase transition of SU(3) gauge theory on N(t) = 4 and 6 lattices". *Phys. Rev.* D46 (1992), pp. 4657–4667.

[137] A. Francis et al. "Critical point and scale setting in SU(3) plasma: An update". *Phys. Rev.* D91.9 (2015), p. 096002. arXiv: `1503.05652` `[hep-lat]`.

[138] Y. Chen et al. "Glueball spectrum and matrix elements on anisotropic lattices". *Phys. Rev.* D73 (2006), p. 014516. arXiv: `hep-lat/0510074` `[hep-lat]`.

[139] B. Svetitsky and L. G. Yaffe. "Critical Behavior at Finite Temperature Confinement Transitions". *Nucl. Phys.* B210 (1982), pp. 423–447.

[140] D. H. Rischke et al. "Excluded volume effect for the nuclear matter equation of state". *Zeitschrift für Physik C Particles and Fields* 51.3 (Sept. 1, 1991), pp. 485–489. ISSN: 1431-5858.

[141] G. D. Yen et al. "Excluded volume hadron gas model for particle number ratios in $A + A$ collisions". *Phys. Rev. C* 56 (4 Oct. 1997), pp. 2210–2218.

[142] G. D. Yen and M. I. Gorenstein. "Analysis of particle multiplicities in Pb+Pb collisions at $158A$ GeV$/c$ within hadron gas models". *Phys. Rev. C* 59 (5 May 1999), pp. 2788–2791.

[143] A. Andronic et al. "Interacting hadron resonance gas meets lattice QCD". *Phys. Lett.* B718 (2012), pp. 80–85. arXiv: `1201.0693` `[nucl-th]`.

[144]   M. Albright, J. Kapusta, and C. Young. "Matching Excluded Volume Hadron Resonance Gas Models and Perturbative QCD to Lattice Calculations". *Phys. Rev.* C90.2 (2014), p. 024915. arXiv: `1404.7540 [nucl-th]`.

[145]   V. Vovchenko, D. V. Anchishkin, and M. I. Gorenstein. "Hadron Resonance Gas Equation of State from Lattice QCD". *Phys. Rev.* C91.2 (2015), p. 024905. arXiv: `1412.5478 [nucl-th]`.

[146]   P. Alba et al. "Flavor-dependent eigenvolume interactions in hadron resonance gas and its implications for hadron yields at LHC energies" (2016). arXiv: `1606.06542 [hep-ph]`.

[147]   M. Caselle and M. Hasenbusch. "Universal amplitude ratios in the 3-D Ising model". *J. Phys.* A30 (1997), pp. 4963–4982. arXiv: `hep-lat/9701007 [hep-lat]`.

[148]   M. Lüscher and P. Weisz. "String excitation energies in SU(N) gauge theories beyond the free-string approximation". *JHEP* 07 (2004), p. 014. arXiv: `hep-th/0406205`.

[149]   Y. Nambu. "Strings, Monopoles and Gauge Fields". *Phys. Rev.* D10 (1974), p. 4262.

[150]   T. Goto. "Relativistic quantum mechanics of one-dimensional mechanical continuum and subsidiary condition of dual resonance model". *Prog.Theor.Phys.* 46 (1971), pp. 1560–1569.

[151]   M. Billó and M. Caselle. "Polyakov loop correlators from D0-brane interactions in bosonic string theory". *JHEP* 0507 (2005), p. 038. arXiv: `hep-th/0505201 [hep-th]`.

[152]   C. Jarzynski. "What Is the Microscopic Response of a System Driven Far From Equilibrium?" *Dynamics of Dissipation.* Ed. by P. Garbaczewski and R. Olkiewicz. Berlin, Heidelberg: Springer Berlin Heidelberg, 2002, pp. 63–82.

[153]   C. Bustamante, J. Liphardt, and F. Ritort. "The Nonequilibrium Thermodynamics of Small Systems". *Physics Today* 58.7 (July 2005), pp. 43–48. eprint: `cond-mat/0511629`.

[154]   R. Clausius. "Ueber die bewegende Kraft der Wärme und die Gesetze, welche sich daraus für die Wärmelehre selbst ableiten lassen". *Annalen der Physik* 155.4 (1850), pp. 500–524. ISSN: 1521-3889.

[155]   R. Clausius. "Ueber eine veränderte Form des zweiten Hauptsatzes der mechanischen Wärmetheorie". *Annalen der Physik* 169.12 (1854), pp. 481–506. ISSN: 1521-3889.

[156]   J. Gibbs. *Elementary Principles in Statistical Mechanics: Developed with Especial Reference to the Rational Foundations of Thermodynamics.* C. Scribner's sons, 1902.

[157]   J. L. W. V. Jensen. "Sur les fonctions convexes et les inégalités entre les valeurs moyennes". *Acta Math.* 30 (1906), pp. 175–193.

[158]   H. Híjar, J. Quintana-H., and G. Sutmann. "Non-equilibrium work theorems for the two-dimensional Ising model". *Journal of Statistical Mechanics: Theory and Experiment* 2007.04 (2007), P04010.

[159]   G. E. Crooks. "Nonequilibrium Measurements of Free Energy Differences for Microscopically Reversible Markovian Systems". *Journal of Statistical Physics* 90.5 (Mar. 1, 1998), pp. 1481–1487. ISSN: 1572-9613.

[160]   C. Jarzynski. "Equilibrium Free Energies from Nonequilibrium Processes". *Acta Physica Polonica B* 29 (June 1998), p. 1609. arXiv: `cond-mat/9802155`.

[161]   C. Jarzynski. "Microscopic Analysis of Clausius-Duhem Processes". *Journal of Statistical Physics* 96 (July 1999), pp. 415–427. arXiv: `cond-mat/9802249`.

[162]   G. E. Crooks. "Path-ensemble averages in systems driven far from equilibrium". *Phys. Rev. E* 61 (3 Mar. 2000), pp. 2361–2366.

[163]   S. Yukawa. "A Quantum Analogue of the Jarzynski Equality". *Journal of the Physical Society of Japan* 69.8 (2000), pp. 2367–2370. arXiv: `cond-mat/0007456`.

[164]   R. M. Neal. "Annealed Importance Sampling". *Statistics and Computing* 11.2 (Apr. 2001), pp. 125–139. ISSN: 0960-3174.

[165]   C. Jarzynski. "Rare events and the convergence of exponentially averaged work values". *Phys. Rev. E* 73 (4 Apr. 2006), p. 046105.

[166]   A. Pohorille, C. Jarzynski, and C. Chipot. "Good Practices in Free-Energy Calculations". *J. Phys. Chem.* B114 (32 2010), pp. 10235–10253.

[167]   N. Yunger Halpern and C. Jarzynski. "Number of trials required to estimate a free-energy difference, using fluctuation relations". *Phys. Rev. E* 93.5, 052144 (May 2016), p. 052144. arXiv: `1601.02637 [cond-mat.stat-mech]`.

[168]   K. Kajantie and L. Kärkkäinen. "Surface Energy of the Confined Phase - Nonconfined Phase Interphase in QCD Matter". *Phys. Lett.* B214 (1988), p. 595.

[169]   S. Huang et al. "Surface Tension in Finite Temperature Quantum Chromodynamics". *Phys. Rev.* D42 (1990). [Erratum: Phys. Rev.D43,2056(1991)], p. 2864.

[170]   T. Bhattacharya et al. "Interface tension in an SU(N) gauge theory at high temperature". *Phys. Rev. Lett.* 66 (1991), pp. 998–1000.

[171]   G. 't Hooft. "On the Phase Transition Towards Permanent Quark Confinement". *Nucl. Phys.* B138 (1978), pp. 1–25.

[172]   P. de Forcrand, M. D'Elia, and M. Pepe. "A Study of the 't Hooft loop in SU(2) Yang-Mills theory". *Phys. Rev. Lett.* 86 (2001), p. 1438. arXiv: `hep-lat/0007034 [hep-lat]`.

[173]   C. Chatelain. "Temperature-extended Jarzynski relation: Application to the numerical calculation of the surface tension". *J. Stat. Mech.* 0704 (2007), P04011. arXiv: `cond-mat/0702044 [cond-mat.stat-mech]`.

[174]   H. Híjar and G. Sutmann. "Monte Carlo estimates of interfacial tension in the two-dimensional Ising model from non-equilibrium methods". *Journal of Statistical Mechanics: Theory and Experiment* 2008.07 (2008), P07012.

[175]   Y. Deng and H. W. J. Blöte. "Simultaneous analysis of several models in the three-dimensional Ising universality class". *Phys. Rev.* E68 (2003), p. 036125.

[176] H. Kramers and G. Wannier. "Statistics of the two-dimensional ferromagnet. Part 1." *Phys. Rev.* 60 (1941), pp. 252–262.

[177] F. Wegner. "Duality in Generalized Ising Models and Phase Transitions Without Local Order Parameters". *J. Math. Phys.* 12 (1971), pp. 2259–2272.

[178] M. Caselle, M. Hasenbusch, and M. Panero. "The Interface free energy: Comparison of accurate Monte Carlo results for the 3D Ising model with effective interface models". *JHEP* 0709 (2007), p. 117. arXiv: `0707.0055` `[hep-lat]`.

[179] A. Nada, M. Caselle, and M. Panero. "The equation of state with non-equilibrium methods". 2017. arXiv: `1710.04435 [hep-lat]`.

[180] J. Greensite and R. Höllwieser. "A finite-density transition line for QCD with 695 MeV dynamical fermions" (2017). arXiv: `1708.08031 [hep-lat]`.